Aus dem Institut für Klinische Pharmakologie und Toxikologie
der Medizinischen Fakultät Charité – Universitätsmedizin Berlin

DISSERTATION

Functional analysis of albuminuria candidate genes in zebrafish

zur Erlangung des akademischen Grades
Doctor rerum medicinalium (Dr. rer. medic.)

vorgelegt der Medizinischen Fakultät
Charité – Universitätsmedizin Berlin

von

Nicola Victoria Becker (geb. Müller)

aus Berlin

Datum der Promotion: 26. Juni 2022

Table of contents

Abstract

The Munich Wistar Frömter (MWF) rat is a suitable inbred hypertensive rat model for chronic kidney disease (CKD) with albuminuria of early onset. Here, the MWF rat was used to decipher the genetic basis of albuminuria development in hypertension. Characterization of the genomic architecture of a previously identified CKD *locus* in MWF led to the identification of *transmembrane protein 63c* (*Tmem63c*) as a candidate for albuminuria with differential expression in glomeruli of allele-specific rat models during the onset of albuminuria in MWF. Recent studies identified *Tmem63c* as a potential hyperosmolarity-activated cation channel. Subsequent evaluation of the potential clinical relevance in human kidney biopsies revealed specific loss of TMEM63C in podocytes from patients with focal segmental glomerulosclerosis (FSGS).

To analyze a putative role of *tmem63c* in maintaining glomerular filtration barrier (GFB) functionality, we performed studies in zebrafish as a second vertebrate animal model. We utilized morpholino antisense-oligonucleotides and CRISPR/Cas9-mediated somatic mutagenesis to knockdown *tmem63c* gene function in developing zebrafish embryos. Evaluation of GFB integrity was conducted in *Tg[fabp10a:gc-EGFP]* zebrafish embryos with the fluorescent albumin surrogate gc-EGFP circulating in the vascular system following 48 hours post fertilization (hpf). Leakage of gc-EGFP following GFB damage was assessed using epifluorescence microscopy.

By using both knockdown techniques, *tmem63c*-deficiency resulted in similar mild edema at 48 hpf and an albuminuria-like phenotype showing a significant decrease of gc-EGFP-fluorescence in *Tg[fabp10:gc-EGFP]* at 120 hpf. Specificity of all knockdown systems and conservation of *tmem63c* gene function across species were shown by rescue of the observed albuminuria-like phenotype using zebrafish- or rat- derived mRNA, respectively.

To analyze the ultrastructure of the GFB and the cellular composition of the glomerulus in *Tg[wt1b:EGFP]* embryos with fluorescent podocytes, we deployed electron and confocal microscopy, respectively. Ultrastructural analysis of the GFB upon *tmem63c*-deficiency revealed podocyte foot process effacement with significant increase in foot process width and decrease in the number of slit diaphragms per µm glomerular basement membrane. Quantification of podocyte cell number and density from confocal images revealed a significant increase in glomerular volume with accompanying decrease in podocyte density due to marked dilation of glomerular capillaries. The data suggests a crosstalk between damaged podocytes and vascular endothelium in the manifestation of the observed phenotype in zebrafish.

Together, this study shows a conserved functional role of *Tmem63c* in albuminuria development across species and warrants further translational investigation of *Tmem63c* as a novel therapeutical target.

Zusammenfassung

Die Munich Wistar Frömter (MWF) Ratte stellt ein interessantes genetisches Rattenmodell der chronischen Nierenerkrankung (CKD) dar und entwickelt bereits früh eine spontane Albuminurie. Anhand des MWF Tiermodells ist es möglich die genetische Basis der Entwicklung einer Albuminurie bei gleichzeitigem Vorliegen einer Hypertonie zu untersuchen. Eine tiefergehende Charakterisierung der genetischen Architektur eines zuvor identifizierten CKD-Lokus der MWF-Ratte führte zur Identifizierung von *Transmembran Protein 63c* (*Tmem63c*) als Albuminurie-Kandidatengen. Dieses Gen wurde kürzlich als ein möglicher hyperosmolar-aktivierter Kationenkanal identifiziert. In isolierten Glomeruli allel-spezifischer Rattenmodelle wies *Tmem63c* eine differentielle Expression zum Zeitpunkt des Einsetzens der Albuminurie im MWF-Modell auf. Die darauffolgende Analyse in humanen Nierenbiopsien zeigte einen Verlust von TMEM63C in Podozyten von Patienten mit fokaler segmentaler Glomerulosklerose (FSGS) und unterstützt die mögliche klinische Bedeutung des Kandidatengens.

Untersuchungen im Zebrafischmodell dienten der Analyse der funktionellen Relevanz von *tmem63c* zur Aufrechterhaltung einer intakten glomerulären Filtrationsbarriere (GFB). Anhand von Morpholino Oligonukleotiden und CRISPR/Cas9-vermittelter somatischer Mutagenese wurden Zebrafischembryonen mit herunterregulierter *tmem63c* Genfunktionalität generiert. Mit Hilfe von Larven der Zebrafischlinie *Tg[fabp10a:gc-EGFP]*, in deren vaskulärem System nach 48 Stunden nach der Befruchtung (hpf) das fluoreszierende Albuminsurrogat gc-EGFP zirkuliert, wurde die Integrität der GFB mittels Fluoreszenzmikroskopie untersucht. Dabei führte eine Störung der GFB zur freien Filtration von gc-EGFP und damit zum Fluoreszenzverlust.

Beide verwendeten Knockdown-Techniken führten bei den Zebrafischembryonen gleichermaßen zur Entwicklung milder Ödeme 48 hpf sowie zu einem Albuminurie-ähnlichen Phänotyp mit einem signifikanten Verlust der gc-EGFP-Fluoreszenz in *Tg[fabp10:gc-EGFP]* 120 hpf. Sowohl die Spezifität der verwendeten Knockdown-Techniken als auch die Spezies-übergreifende Konservierung der Genfunktion von *tmem63c* wurde über eine Aufhebung des Albuminurie-ähnlichen Phänotyps nach Co-Injektion von Zebrafisch-bzw. Ratten-*tmem63c*-mRNA bewiesen.

Die Ultrastruktur der GFB und die zelluläre Zusammensetzung des Glomerulus wurden in *Tg[wt1b:EGFP]*-Embryonen mit fluoreszierenden Podozyten mittels Elektronen- beziehungsweise Konfokalmikroskopie evaluiert.

Die ultrastrukturelle Analyse der GFB bei *tmem63c*-Defizienz zeigte eine Ablösung der Podozytenfußfortsätze mit signifikanter Verbreiterung der Zellfortsätze und gleichzeitiger Reduktion der Anzahl von Schlitzdiaphragmata pro µm glomerulärer Basalmembran. Eine Quantifizierung der Podozytenzahl und -dichte mittels Konfokalmikroskopie ergab eine

signifikante Erhöhung des glomerulären Volumens mit gleichzeitiger Erniedrigung der Podozytendichte durch eine deutliche Ektasie glomerulärer Kapillaren. Dies weist auf eine wechselseitige Beteiligung geschädigter Podozyten und des vaskulären Endothels bei der Manifestierung des beobachteten Phänotyps im Zebrafisch hin.

Die hier vorliegende Arbeit identifiziert *Tmem63c* als Gen mit Spezies-übergreifender funktioneller Rolle bei der Entwicklung einer Albuminurie und legt eine weitergehende translationale Erforschung des Gens als potenziellen, neuen therapeutischen Ansatzpunkt nahe.

Synopsis

Part of this work has been previously published in (1): Schulz A, Müller NV, van de Lest NA, Eisenreich A, Schmidbauer M, Barysenka A, Purfurst B, Sporbert A, Lorenzen T, Meyer AM, Herlan L, Witten A, Ruhle F, Zhou W, de Heer E, Scharpfenecker M, Panakova D, Stoll M, Kreutz R. Analysis of the genomic architecture of a complex trait locus in hypertensive rat models links Tmem63c to kidney damage. eLife. 2019;8/ 20.03.2019.

Introduction

In 2016, more than 17 million people died from cardiovascular diseases (CVD) causing over 30% of deaths worldwide (2). Hypertension is a major risk factor for deaths due to CVD and remains the leading cause of premature death accounting for over 200 million disability-adjusted life years (3, 4). An increasing amount of evidence supports an important role of the kidney as a major organ in blood pressure regulation, as well as one of the main targets for hypertension-mediated organ damage (HMOD) leading to chronic kidney disease (CKD) (4-6). CKD is defined as abnormalities of kidney structure or function, present for over 3 months, with implications for health (7) and results mainly in a reduction in glomerular filtration rate and increased urinary albumin excretion (UAE) or albuminuria (5).

Both, hypertension and CKD are complex, multifactorial and polygenetically determined disorders. Recent genome-wide association studies (GWAS) identified more than 100 genetic variants associated with hypertension (8) or CKD (9), respectively. However, finding a biological mechanism underlying the genetic susceptibility of both diseases as well as translation of the findings from GWAS into the clinic has been slow (9-11). Alternatively, translational genomic analysis of inbred hypertensive rat models of HMOD represents a powerful approach in unraveling the genetic basis of hypertension-mediated kidney damage (11, 12). The Munich Wistar Frömter (MWF) rat is an established inbred hypertensive rat model to decipher the genetic basis and pathophysiological mechanisms of CKD in hypertension. This strain develops albuminuria of early onset between 4 and 8 weeks of age as well as mild hypertension and exhibits also an inherited nephron deficit (11).

Previous studies identified a quantitative trait locus (QTL) on rat chromosome 6 (RNO6) of the MWF rat as a major causative genetic locus for the early onset of albuminuria in this rat strain by deploying crosses between the MWF and the contrasting spontaneously hypertensive rat (SHR) strain with low albuminuria-susceptibility (13). Subsequent breeding of the consomic MWF-6^{SHR} rat strain in which MWF-RNO6 was replaced by SHR-RNO6 verified the relevance of the RNO6-QTL as the onset of albuminuria in the MWF rat strain was completely abolished in MWF-6^{SHR} (14).

The zebrafish model is an emerging and particularly relevant vertebrate model in translational genomic studies with high genome conservation towards higher vertebrates and is used as a

straightforward screening tool for gene function in kidney development (15-17). In zebrafish embryos, the functional kidney is formed by the pronephros consisting of two nephrons with glomeruli fused at the embryo midline connecting to the pronephric tubules, which run laterally and drain into the pronephric ducts ultimately joining at the cloaca (17). The pronephric glomerular filtration barrier (GFB) exhibits a similar structure as in higher vertebrates with a fenestrated epithelium followed by the glomerular basement membrane (GBM) and podocytes with their distinctive interdigitating podocyte foot processes (17). Functional analysis of proteins relevant to kidney development and functionality can easily be conducted following gene knockdown using antisense morpholino (MO) oligonucleotides (18) or CRISPR/Cas9-mediated somatic mutagenesis (19, 20). Both methods lead to a reduction in gene expression levels within the first 50 hours post fertilization (hpf), i.e. in the time window of pronephric organogenesis including the onset of organ functionality (17).

The two transgenic zebrafish lines *Tg[fabp10a:gc-EGFP]* and *Tg[wt1b:EGFP]* are used to analyze GFB integrity or glomerular cell composition and development, respectively. The transgenic zebrafish line *Tg[fabp10a:gc-EGFP]* provides a transgene-based assay of GFB integrity and functionality with straightforward analysis of an albuminuria-like phenotype as the hallmark of compromised GFB function (21). Since zebrafish lack the albumin-orthologue, this line expresses vitamin D binding protein (gc) tagged with enhanced green fluorescent protein (EGFP) as a fluorescent tracer protein. gc-EGFP has a similar molecular weight and isoelectric charge as albumin and can thus act as an albumin-surrogate (21). The fluorescent albumin-surrogate gc-EGFP is expressed under the control of the enhancer of liver-specific fatty-acid binding protein (fabp10a) following 48 hpf. After expression gc-EGFP is secreted into the blood to circulate in the vascular system of transgenic zebrafish embryos and is readily observable from this timepoint onwards (21). Damage of the GFB causes leakage of gc-EGFP through the GFB resulting in a decrease of fluorescence in the trunk vasculature of *Tg[fabp10a:gc-EGFP]* zebrafish embryos with an albuminuria-like phenotype.

In embryos of the zebrafish line *Tg[wt1b:EGFP]* EGFP is expressed under the control of the enhancer of the *wt1b* gene as one of two known zebrafish orthologues of the *Wilms tumor suppressor gene Wt1* (22). After 35 hpf, EGFP fluorescence can be observed specifically in podocytes of the pronephric glomeruli, in pronephric tubules and proximal parts of pronephric ducts and other organs including the exocrine pancreas, heart, eyes and gills (22). In this study, these two transgenic zebrafish lines are utilized as useful tools for the translational genomic assessment and functional characterization of albuminuria candidate genes in the zebrafish model.

Aims

The overall aims of the study are as follows:

1) Characterization of the genomic architecture of a previously identified albuminuria-QTL on RNO6 of the MWF rat for identification of albuminuria candidate genes.
2) Evaluation of clinical and pathophysiological relevance of albuminuria candidate genes in human kidney biopsies of FSGS patients and in human cultured podocytes (hPC).
3) Analysis of the functional relevance of albuminuria candidate genes for GFB integrity and assessment of changes in glomerular morphology upon gene-deficiency in transgenic zebrafish embryos.

While the experimental work for aim 1 and 2 was conducted by co-authors, my contribution to the study focused exclusively on aim 3.

Methods

Detailed description of methods is available in (1). Methods described here are those related to work in zebrafish as the relevant animal model of my contribution to the publication (1).

Zebrafish Husbandry

Zebrafish were bred, raised and maintained in accordance with the guidelines of the Max Delbrück Center for Molecular Medicine and the local authority for animal protection (Landesamt für Gesundheit und Soziales, Berlin, Germany) for the use of laboratory animals, and followed the 'Principles of Laboratory Animal Care' (NIH publication no. 86-23, revised 1985) as well as the current version of German Law on the Protection of Animals. Embryos were kept in E3 embryo medium (5 mM NaCl, 0.17 mM KCl, 0.33 mM $CaCl_2$, 0.33 mM $MgSO_4$; pH 7.4) under standard laboratory conditions at 28.5°C. To inhibit melanogenesis, embryos were incubated with 1% 1-phenyl-2-thiourea (PTU) in E3 embryo medium from 24 hours post fertilization onwards, i.e. the timepoint of initial pigmentation (23).

Zebrafish morpholino (MO) and single guide RNA (sgRNA) microinjections

For genetic manipulation, microinjections of zebrafish zygotes using the FemtoJet® 4i microinjector (Eppendorf) together with the M-152 Three-Dimensional Manipulator (Narishge Group) were performed. Prior to microinjection, needle ejection pressure was calibrated using a stage micrometer equipped with halocarbon oil to obtain injection droplets of approximately 1 nl on a M80 dissecting microscope (Leica). Injection droplets were afterwards injected into zygotes of the zebrafish wild type hybrid strain AB/Tülf and the transgenic lines *Tg[fabp10a:gc-EGFP]* (21) and *Tg[wt1b:GFP]* (22). MOs of the following sequences were synthesized by Gene Tools, LLC, Philomath: *tmem63c* ATG-MO 5'-CAGGCCAGGACTCAAACGCCATTGC-3', *tmem63c* ex2-sdMO 5'-TGTTATCATAGATGATGTACCAGCC-3', and a standard control oligo (Control-MO) 5'-CCTCTTACCTCAGTTACAATTTATA-3'. *Tmem63c* ATG-MO was used at a final concentration of 0.3 mM, *tmem63c* ex2-sdMO was used at a final concentration of

0.5 mM. MOs were injected into one-to four-cell stage zebrafish zygotes. As an injection control Control-MO was used at a final concentration of 0.3 mM (Control for *tmem63c* ATG-MO) and 0.5 mM (Control for *tmem63c* ex2-sdMO). *tmem63c* ex2-sgRNA was diluted to a final concentration of 159.6 ng/µl (for functional analysis of the GFB and rescue experiments) or 250 ng/µl (for TEM and confocal microscopy analysis), respectively using water and 1 M KCl (final concentration 300 mM) and co-injected with Cas9-Protein (final concentration 600 ng/µl) into one-cell stage zebrafish zygotes as described (20, 24). As an injection control (Cas9-Control) Cas9-protein was diluted to a final concentration of 600 ng/µl using water and 1 M KCl (final concentration: 300 mM).

CRISPR/Cas9 – mediated somatic mutagenesis

For oligo-based synthesis of sgRNA targeting exon 2 of *tmem63c*, PCR amplification without DNA template was performed using the Phusion High-Fidelity PCR Kit (Thermo Fisher Scientific) as described in (25). Overlapping primers used for amplification were a unique CRISPR-forward oligonucleotide (BioTez, Berlin-Buch GmbH) with the following sequence GAAAT**TAATACGACTCACTATA**GGACGTCAGGAGTTTCCTGAGTTTTAGA GCTAGAAATAGC containing the CRISPR target site (underlined) and the T7 polymerase binding site (bold) and the common CRISPR-reverse oligonucleotide AAAAGCACCGACTCGGTGCCACTTTTTCAAGTTGATAACGGACTAGCCTTATTTTAACTT GCTATTTCTAGCTCTAAAAC containing the remainder of the sgRNA sequence (25). After purification of the resulting PCR product using the GeneJET Gel Extraction Kit (Thermo Fisher Scientific), *in vitro* transcription of 1000 ng DNA template was performed using the MEGAscript T7 Kit (Ambion) according to the manufacturer's protocol with incubation at 37°C overnight. After that, sgRNA was purified with the RNeasy Mini Kit (Qiagen). To determine the efficiency of CRISPR/Cas9-mediated somatic mutagenesis individual embryos were analyzed at 48 hpf as described in (20). In brief, a genomic region flanking the CRISPR target site was amplified from isolated genomic DNA of individual wildtype and sgRNA-injected embryos using the following primers (BioTez, Berlin-Buch GmbH): forward: CAAATGGTGAACACTTGTGAATC, reverse: CTGCGGTTTACTGCGGAGATG and ligated into the pGEM t-easy vector of the pGEM®-T Easy Vector System (Promega) at 4°C overnight as described in the manufacturer's protocol. The resulting vector was transfected into chemically competent DH5α *E.coli* cells and the successful ligation verified using the IPTG/X-Gal-system with readout as white colonies. Subsequent colony PCR of individual white clones was carried out after suspension and 1-hour incubation in 20 µl SOC medium at 37 °C followed by PCR amplification using DreamTaq Polymerase (Thermo Fisher Scientific) and the commonly used T7 forward and SP6 reverse oligonucleotides. After analysis on a 2% agarose gel, samples showing bands of the desired

length were sequenced. Computational sequence analysis was performed using CrispR Variants (26).

Reverse transcriptase (RT)-PCR

For efficiency analysis of *tmem63c* ex2-sdMO, a reverse transcriptase (RT)-PCR was carried out. At 24 hpf, RNA from 50 pooled uninjected, Control-MO- and *tmem63c* ex2-sdMO-injected embryos each was isolated using Trizol Reagent (Invitrogen). DNase I digestion was performed using the RNAse-free DNase set (Qiagen) and samples were purified using the RNeasy Mini Kit (Qiagen) according to the manufacturer's protocol. After determination of RNA quality and quantity using the Nanodrop ND-1000 Spectrophotometer (pegLAB), equal amounts of mRNA for each group analyzed were transcribed to cDNA using the First strand cDNA synthesis kit (Thermo Fisher Scientific) according to the manufacturer's protocol. PCR amplification of the *tmem63c* ex2-sdMO target region from cDNA was carried out with DreamTaq DNA Polymerase (Thermo Fisher) and the following primers flanking the MO target site: forward: CTGATGGAGGAGAACAGCACGG, reverse: ATACAGCAGAGCGAAGATACTGTG. Eukaryotic elongation factor 1 alpha 1, like 1 *(eef1a1l1)* as a well – established housekeeping gene (27) was used as a loading control and amplified using the following primers: forward: TGGAGACAGCAAGAACGACC, reverse: GAGGTTGGGAAGAACACGCC.

Rescue of CRISPR/Cas9-mediated *tmem63c* somatic mutants and *tmem63c* ex2-sdMO-mediated gene knockdown using *tmem63c* mRNA (zebrafish)

Gene knockdown of *tmem63c* using *tmem63c* ex2-sgRNA or *tmem63c* ex2-sdMO, respectively was rescued with zebrafish-derived *tmem63c* mRNA. Zebrafish-derived *tmem63c* cDNA was cloned into the pBluescript II SK(+) vector using the In-Fusion HD Cloning Kit (Takara). Prior to amplification, total cDNA from approximately 50 pooled wildtype embryos was synthesized as described in the preceding paragraph. *tmem63c* cDNA was amplified using Phusion High-Fidelity DNA polymerase (Thermo Fisher Scientific) and the following primers (BioTez, Berlin-Buch GmbH): forward: GCTTGATATCGAATTCATGGCGTTTGAGTCCTGGCCTGC, reverse: CGGGCTGCAGGAATTCTCACTGAAAAGCCACCGGACTG. The pBluescript II SK(+) vector was linearized by digestion using EcoRI FD restriction enzyme (Thermo Fisher Scientific) for 15 minutes at 37°C. The linearized vector and the amplified *tmem63c* cDNA were purified using the GeneJET Gel Extraction Kit (Thermo Fisher Scientific) and the *tmem63c* ORF cloned into the pBluescript II SK(+) vector using the In-Fusion HD Cloning Kit (Takara) according to the manufacturer's protocol. For sequence-verification of the *tmem63c* cDNA insert, the resulting vector of the cloning reaction was amplified by transfection into DH5α *E.coli*

cells and the insert was sequenced using the commonly used T7 forward and M13 reverse primers. For sequencing of the whole ORF, an additional primer was used, GTGCAGAAACTAATGAAGCTGG, located at 822-844 bp starting from the beginning of the ORF. For mRNA synthesis, the *tmem63c* cDNA containing vector was linearized using XbaI FD (Thermo Fisher Scientific) and purified using the GeneJET Gel Extraction Kit (Thermo Fisher Scientific). *In vitro* transcription of capped RNA was performed using the mMessage mMachine T7 Kit (Ambion) with 2 hours incubation time at 37°C followed by DNase treatment using Turbo DNAse provided with the kit. For poly A-tailing, the Poly(A)-tailing Kit (Ambion) was used to the manufacturer's protocol and the resulting *tmem63c* mRNA (zebrafish) extracted using the RNeasy Mini Kit (Qiagen). For *in vivo* rescue experiments of *tmem63c* ex2-sgRNA, the mRNA was diluted to a concentration of 100 ng/µl and co-injected with *tmem63c* ex2-sgRNA of a concentration of 159.5 ng/µl into the same one-cell stage zygotes. For *in vivo* rescue experiments of *tmem63c* ex2-sdMO, *tmem63c* mRNA at a concentration of 100 ng/µl was injected in one-cell stage zygotes followed by *tmem63c* ex2-sdMO, that was co-injected into the same zygote at the one-to four-cell stage at a concentration of 0.5 mM.

Rescue of *tmem63c* ATG-MO-mediated gene knockdown using *Tmem63c* mRNA (Rat)

Rat-derived *Tmem63c* cDNA cloned into pcDNA3.1(+) vector was synthesized and sequence-verified by Thermo Fisher Scientific using their GeneArt Gene synthesis service. For *Tmem63c* mRNA synthesis, the *Tmem63c* cDNA containing vector was linearized using XbaI FD (Thermo Fisher Scientific). The following steps were carried out as described in the preceding section. For *in vivo* rescue experiments of *tmem63c* ATG-MO, *Tmem63c* mRNA at a concentration of 100 ng/µl was injected in one-cell stage zygotes and subsequently *tmem63c* ATG-MO at a concentration of 0.3 mM co-injected into the same zygotes at the one- to four-cell stage.

Functional assessment of the GFB

For functional assessment of the GFB, gc-EGFP fluorescence in the trunk vasculature of *Tg[fabp10a:gc-EGFP]* embryos was evaluated by epifluorescence microscopy using a M165 Fluorescence Microscope (Leica) at 120 hpf following gene knockdown or rescue experiments, respectively. For evaluation of CRISPR/Cas9-mediated *tmem63c* somatic mutants, gene knockdown was carried out with *tmem63c* ex2-sgRNA at a concentration of 159.6 ng/µl. Each embryo was visually associated with the "fluorescent group", the "deficient-fluorescent group" or "crippled/dead" according to their gc-EGFP fluorescence in the trunk vasculature and their number was quantified. The percentage of injected embryos was normalized to the percentage of the control group for each of the three categories. Quantifications were performed for at

least three independent injections, resulting in at least three ratios injected/control for each category with a total number of at least 100 embryos categorized.

Transmission electron microscopy (TEM)

Tg[fabp10a:gc-EGFP] embryos at 120 hpf were fixed in 4% formaldehyde/0.5% glutaraldehyde (EM-grade) in 0.1 M phosphate buffer for 2 hours at room temperature. For knockdown analysis, embryos were injected with *tmem63c* ex2-sgRNA of a concentration of 250 ng/µl to increase mutation rates and enhance the observed phenotype (20). For analysis of CRISPR/Cas9-mediated *tmem63c* somatic mutants, embryos assigned to the "deficient-fluorescent group" displaying a clear knockdown phenotype were evaluated. Samples were stained with 1% OsO_4 for 2 hours, dehydrated in a graded ethanol series and propylene oxide and embedded in Poly/Bed^R 812 (Polysciences, Eppelheim, Germany). Ultrathin sections were contrasted with uranyl acetate and lead citrate. Sections were examined with a FEI Morgagni electron microscope and a Morada CCD camera (EMSIS GmbH, Münster, Germany). Image acquisition and quantification of podocyte foot process width and number of slit diaphragms per µm GBM were performed with the iTEM software (EMSIS GmbH, Münster, Germany). Quantification was done after blinding of group allocations for the pictures quantified to prevent any possible bias.

Confocal microscopy of zebrafish embryos and quantification of podocyte cell number and glomerular volume

Tg[wt1b:EGFP] embryos at 96 hpf were fixed in PEM buffer containing 4% formaldehyde and 0.1% Triton-X 100 for 2 hours at room temperature or overnight at 4°C. For morphological analysis of a knockdown phenotype, embryos were injected with *tmem63c* ex2-sgRNA at a concentration of 250 ng/µl to increase mutation rates and enhance the observed phenotype (20). Nuclei were stained using 4′,6-Diamidin-2-phenylindol (DAPI, Sigma Aldrich, stock solution 1 mg/ml diluted 1:2000 in PBS) overnight at 4°C. After removal of the yolk, head and tail for a minimal distance between specimen and the cover slip of a 35 mm glass bottom dish (Mattek), the specimen was mounted in 0,7% low-melting agarose. The pronephroi of whole-mount fixed embryos were imaged using a Zeiss LSM 710 or LSM 700 microscope with a LD C-Apochromat 40 x NA1.1 water objective and ZEN 2.1 software by sequentially acquiring confocal z-stacks of the GFP (488 nm laser, emission 495-550 nm) and the DAPI signal (405 nm laser, emission 420-480 nm) with a pixel size of 102.4 nm. Care was taken to apply identical settings to all samples and not to oversaturate pixels.

Quantification of podocyte cell number and glomerular volume was done using Imaris version 9.21 software (Bitplane AG, Zürich, Switzerland). A 3D surface covering the total glomerular volume was manually edited by tracing the outlines of EGFP-positive cells for every second

section of the z-stack. EGFP-positive cells of the glomerulus were included, while cells of the pronephric ducts were excluded. Glomerular volume was automatically calculated from this surface. For quantification of podocyte cell number, the DAPI channel was masked with the EGFP channel using Fiji software (28) to include $DAPI^{+}/EGFP^{+}$ cells only, thus representing nuclei of podocyte cells. Then, a spot segmentation of the DAPI channel was performed. Estimated spot diameter was 4 µm. Spots were filtered for a minimum intensity of the EGFP channel and by using the Imaris quality filter algorithm on the DAPI channel. Threshold values were set for each image individually to prevent the occurrence of unspecific spots not matching the DAPI signal. Spots located outside the glomerular surface were manually deleted.

Statistics

Data are presented as mean ± SD. Normal distribution was determined using the Shapiro-Wilk test. For the functional analysis of the GFB in zebrafish, Gaussian distribution was assumed due to the high number of embryos categorized that underlie the analysis. Statistical analysis was done using One-way ANOVA with post-hoc Bonferroni's multiple comparisons test. Statistical analysis was performed using GraphPad Prism 6 software (GraphPad Software, La Jolla California USA). *P* values < 0.05 were considered as statistically significant.

Results

Identification of *Tmem63c* as a positional candidate gene for the onset of albuminuria in MWF and characterization of TMEM63C in FSGS patient biopsies and human podocyte cell culture

The previously identified 55 Mb spanning albuminuria-QTL on RNO6 of the MWF rat strain was narrowed by congenic substitution mapping strategy for both albuminuria and glomerular density phenotypes. For this purpose, 8 congenic rat strains (congenics) were bred with introgression of increasingly larger fragments of the SHR-RNO6 into the MWF genetic background replacing the MWF-RNO6. Deploying a comparison of albuminuria as well as glomerular density phenotypes between congenics and the parental MWF and SHR rat strains allowed to narrow the albuminuria-QTL down to a smaller interval spanning only 4.9 Mb (sub-QTL) that explained 95% of the difference in albuminuria and 89% of the difference of the glomerular density between the MWF strain and the consomic MWF-6^{SHR} strain. The identified sub-QTL was not attributable to blood pressure differences between the parental MWF and SHR rat strains as no changes in blood pressure were detected in the informative congenic strains.

The defined sub-QTL was further analyzed by targeted Next-generation sequencing (NGS) analysis that detected 8 potentially deleterious non-synonymous variants in 5 genes comparing

MWF versus SHR. However, none of the identified genetic variants lead to the identification of a single candidate gene as selective sweeps in the sub-QTL region of the used inbred rat models were detected as a cause for these genetic variants.

In contrast, RNA-sequencing (RNA-seq) of isolated glomeruli, identified a total of 2.454 differentially expressed genes between MWF and SHR. Only 10 genes coding in the sub-QTL were significantly differentially expressed representing potential albuminuria candidate genes. The mRNA expression levels of these genes were further evaluated by quantitative real-time PCR (qPCR) analysis of isolated glomeruli from the parental MWF and SHR as well as the consomic MWF-6^{SHR} strain at 4 and 8 weeks of age.

Of the 10 candidate genes analyzed by qPCR, only *Tmem63c* showed significantly different and allele-dependent differential mRNA expression levels between the parental and consomic rat strains. *Tmem63c* mRNA expression levels were significantly upregulated in isolated glomeruli of the MWF strain, which was completely abolished in the consomic MWF-6^{SHR} strain. In addition, analysis of the two informative congenic strains, that only vary in the identified sub-QTL, confirmed an allelic regulation of *Tmem63c* mRNA expression.

Immunohistochemical analysis of *Tmem63c* in MWF kidneys revealed podocyte-specific localization of *Tmem63c*. However, comparing protein staining patterns of *Tmem63c* between MWF and SHR showed no obvious changes in glomerular protein abundance between these strains at 8 weeks of age.

To evaluate a potential relevance of TMEM63C in human kidney damage, its expression in human kidney biopsies of FSGS patients and healthy controls was analyzed as aging MWF rats develop similar histopathological changes to those observed in FSGS patients (11, 29). TMEM63C was highly abundant in podocytes of healthy controls, while in the majority of FSGS patients a significant decrease in TMEM63C abundance with global loss of glomerular TMEM63C was shown. In addition, marked loss and changes in the glomerular localization of nephrin as a slit diaphraphm core component, which plays an important role in GFB functionality (30), was demonstrated.

Reduction of TMEM63C levels in human cultured podocytes (hPC) using small interfering RNA led to significantly impaired cell viability as demonstrated by a reduction in calcein acetoxymethyl fluorescence intensity. In addition, reduced phosphorylation of protein kinase B combined with an increased transition of cytochrome C from mitochondria to cytoplasm was observed, thus linking TMEM63C to increased apoptosis and decreased pro-survival signaling in hPC.

Functional analysis of *tmem63c* in *Tg[fabp10a:gc-EGFP]* zebrafish embryos

To analyze the functional relevance of *tmem63c* for GFB integrity in a second vertebrate model, gc-EGFP fluorescence in the trunk vasculature of *Tg[fabp10a:gc-EGFP]* zebrafish

embryos at 120 hpf was examined deploying epifluorescence microscopy. Reduction of *tmem63c*-levels in developing zebrafish larvae was achieved using the morpholino (MO) knockdown technology with the use of one translation blocking (*tmem63c* ATG-MO) and one splice blocking (*tmem63c* ex2-sdMO) MO as well as by using CRISPR/Cas9-mediated somatic mutagenesis with the use of *tmem63c* ex2-sgRNA. For *tmem63c* ex2-sdMO, appearance of the double band indicative of a partial *tmem63c* transcript (Figure 1A, arrowheads) as well as reduced abundance of the correctly spliced, 555 bp-long fragment of the *tmem63c* transcript compared to controls confirmed efficiency of the used knockdown system. In the same RT-PCR no changes in the abundance of a Eukaryotic translation elongation factor 1 alpha 1, like 1 transcript, a housekeeping gene that is used as a loading control, were detected (Figure 1A). For *tmem63c* ex2-sgRNA, knockdown-efficiency was determined by subcloning and sequencing of the CRISPR-target site in CRISPR/Cas9-mediated somatic mutants (crispants) showing the presence of insertions and deletions at the CRISPR-target site as a result of non-homologous end-joining repair following efficient generation of DNA double-strand breaks (Figure 1B) (20).

At 48 hpf knockdown of *tmem63c* by both morpholinos as well as in *tmem63c* crispants led to no obvious developmental malformations, but to mild pericardial edema as a first hint linking *tmem63c* to changes in the cardiovascular or renal system, respectively (Figure 1C-G) (31). Evaluation of gc-EGFP fluorescence in the trunk vasculature of *Tg[fabp10a:gc-EGFP]* zebrafish embryos with knockdown of *tmem63c* gene function at 120 hpf revealed leakage of gc-EGFP from the vasculature (Figure 1H-K).

Categorization and counting of *Tg[fabp10a:gc-EGFP]* zebrafish embryos resulted in a significantly increased number of embryos assigned to the “deficient-fluorescent group” upon *tmem63c* knockdown at 120 hpf (Figure 1L). Consequently, reduction of *tmem63c*-levels in developing zebrafish embryos led to an albuminuria-like phenotype for all knockdown-systems analyzed, while the injection of Control-MO or Cas9-protein as injection controls revealed no significant changes compared to uninjected controls (Figure 1L).

To verify the specificity of the respective albuminuria-like phenotypes, rescue experiments by co-injection of zebrafish-derived *tmem63c* mRNA together with *tmem63c* ex2-sdMO and tmem63c ex2-sgRNA or rat-derived *Tmem63c* mRNA together with *tmem63c* ATG-MO, respectively were performed. Rescue of *tmem63c* ATG-MO was conducted using rat-derived *Tmem63c* mRNA due to sequence overlap as well as consequential targeting of zebrafish-derived *tmem63c* mRNA by the translation blocking MO. Sequence identity of *tmem63* mRNA (zebrafish, RefSeq ID NM_001159836) and *Tmem63c* mRNA (rat, RefSeq ID NM_001108045.1) is 65.82% at mRNA level and 53.52% at protein level (32). For all knockdown systems, the albuminuria-like phenotype could be similarly and specifically rescued by co-injection of zebrafish- or rat-derived *tmem63c* mRNA. The data not only shows

the specificity of the observed albuminuria-like phenotype, but also demonstrates the functional conservation of *tmem63c* across species (Figure 1L).

Taken together, these results verify a functional role of *tmem63c* for GFB integrity in zebrafish embryos as a second *in vivo* vertebrate model.

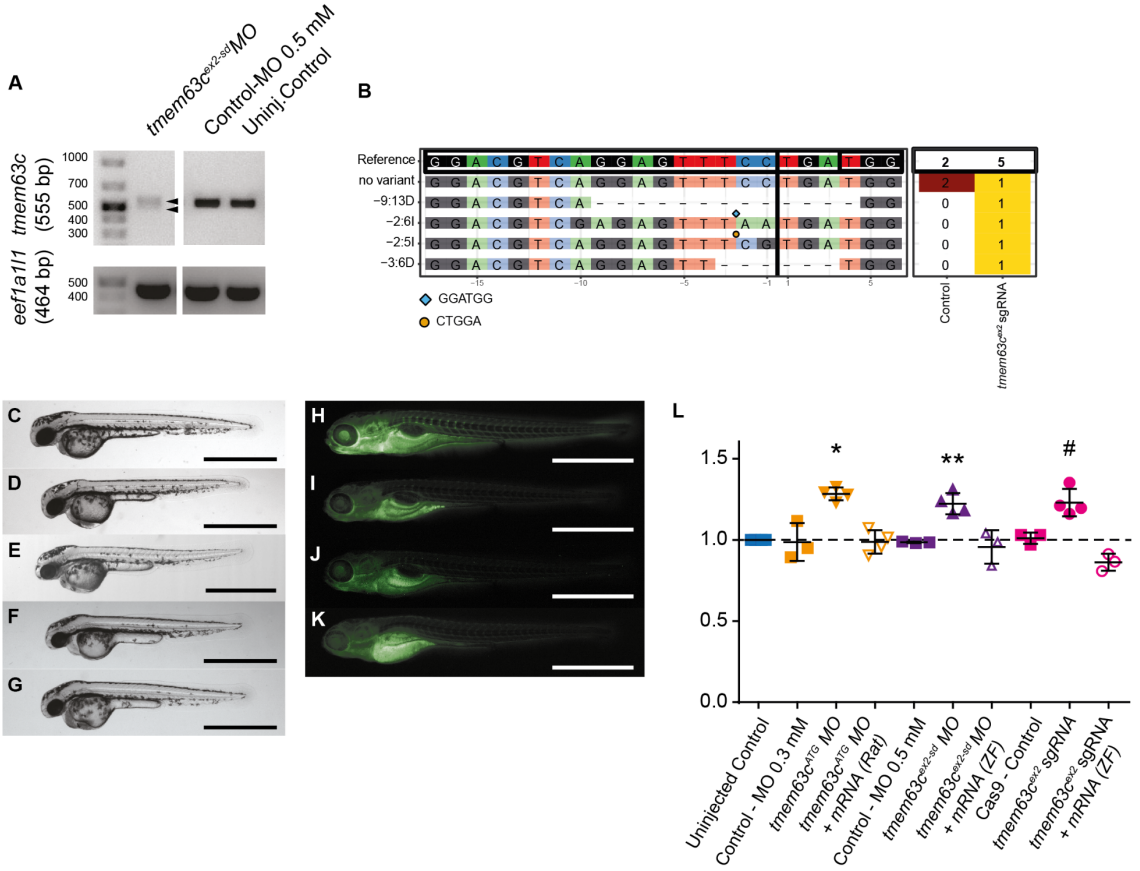

Figure 1. Functional analysis of *tmem63c* in *Tg[fabp10a:gc-EGFP]* zebrafish embryos.

(**A – B**) Analysis of knockdown efficiency. (**A**) RT-PCR showing the appearance of a double band (arrowheads) representing a partial, incorrectly spliced *tmem63c* transcript as well as reduced abundance of the correctly spliced *tmem63c* transcript after injection of *tmem63c* ex2-sdMO, but not in Control-MO injected embryos or uninjected Controls, respectively. Eukaryotic translation elongation factor 1 alpha 1, like 1 *(eef1a1l1)* is used as a loading control. (**B**) Plot of mutagenesis output as created by CrispR Variants Lite analysis of the sequencing data from uninjected control and *tmem63c* crispants. The panel shows the pairwise alignment of each variant to the reference genome proving the presence of genetic mosaicsm with insertions and deletions following the efficient generation of DNA-double strand breaks in *tmem63c* crispants. The 20 bp sgRNA and the 3 bp PAM sequences are indicated in boxes in the reference sequence, the cutting site is indicated by a vertical line. Deletions are indicated by "-" and insertions by symbols with the inserted sequences shown underneath the plot with respect to the cutting site. The right panel demonstrates the frequency of the variants in the embryos analyzed. (**C-G**) Bright field view of wildtype embryos at 48 hours post fertilization (hpf) in uninjected controls (**C**), *tmem63c* ATG-MO injected (**D**), *tmem63c* ex2-sdMO injected (**E**), 159.6 ng/µl *tmem63c* ex2-sgRNA injected (**F**), and 250 ng/µl *tmem63c* ex2-sgRNA injected embryos (**G**). Scale bar = 1 mm. (**H-K**) Epifluorescence microscopy of *Tg[fabp10a:gc-EGFP]* embryos at 120 hpf. Uninjected control with clearly visible gc-EGFP fluorescence in the trunk vasculature ("fluorescent") (**G**). *tmem63c* ATG-MO-injected (**I**), *tmem63c* ex2-sdMO injected (**J**) and *tmem63c* ex2-sgRNA injected (**K**) embryo with partial or complete loss of trunk fluorescence ("deficient-fluorescent"). Scale bar = 1 mm. (**L**) Analysis of gc-EGFP in the trunk vasculature. Shown are embryos categorized as "deficient-fluorescent" (df). Uninjected Control (*n* = 2155); Control-MO 0.3mM (*n* = 189); *tmem63c* ATG-MO (*n* = 227); *tmem63c*

ATG-MO + *Tmem63c* mRNA (Rat) (*n* = 230); Control-MO 0.5 mM (n = 130); *tmem63c* ex2-sdMO (n= 297); *tmem63c* ex2-sdMO + *tmem63c* mRNA (ZF) (n = 137);Cas9-Control (n = 178); *tmem63c* ex2-sgRNA (*n* = 371); *tmem63c* ex2-sgRNA + *tmem63c* mRNA (ZF) (*n* = 111); Dashed line at y = 1 indicates the uninjected control level; * $P < 0.0001$ vs. uninjected Control, Control – MO 0.3 mM, *tmem63c* ATG-MO + *Tmem63c* mRNA (Rat). ** $P < 0.002$ uninjected Control, Control – MO 0.5 mM, *tmem63c* ex2-sdMO + *tmem63c* mRNA (ZF). # $P < 0.004$ vs. uninjected Control, Cas9 – Control, *tmem63c* ex2-sgRNA + *tmem63c* mRNA (ZF). Data points in the graph represent the ratio %(Uninjected Control (df))/%(experimental group (df)) per independent experiment. Data points show the ratio of 3 or 4 independent observations, respectively, in which the above stated number of embryos was categorized.
Part of Figure 1 has been previously published in (1): Schulz A, Müller NV, van de Lest NA, Eisenreich A, Schmidbauer M, Barysenka A, Purfurst B, Sporbert A, Lorenzen T, Meyer AM, Herlan L, Witten A, Ruhle F, Zhou W, de Heer E, Scharpfenecker M, Panakova D, Stoll M, Kreutz R. Analysis of the genomic architecture of a complex trait locus in hypertensive rat models links Tmem63c to kidney damage. eLife. 2019;8. Figure 7, Functional assessment of the glomerular filtration barrier (GFB) after loss of transmembrane protein 63c (tmem63c) in zebrafish; Figure 7-figure supplement 1, Functional assessment of the glomerular filtration barrier (GFB) in Tg[fabp10a:gc-EGFP] zebrafish embryos; p.13.

Assessment of changes in glomerular morphology in *tmem63c* CRISPR/Cas9-mediated somatic mutants

To further analyze the ultrastructural composition of the GFB, we deployed transmission electron microscopy (TEM) in *tmem63c* crispants. Quantification of podocyte foot process width and the total number of slit diaphragms per µm GBM from TEM pictures was used to compare secondary podocyte foot process organization in crispants versus uninjected controls and Cas9-protein-injected *Tg[fabp10a:gc-EGFP]* zebrafish embryos at 120 hpf.

We observed considerable changes in podocyte foot process morphology in *tmem63c* crispants with a loss of the typical interdigitating pattern of podocyte foot processes leading to broadened secondary foot processes (Figure 2 A-C). This pathological finding is commonly described as podocyte foot process effacement (33). Consistent with this, subsequent quantitative image analysis revealed a significant increase in podocyte foot process width (Figure 2D) with accompanying significant decrease in the total number of slit diaphragms per µm glomerular basement membrane (Figure 2E) in *tmem63c* crispants compared to uninjected and Cas9-protein-injected controls, respectively.

This data provides compelling evidence that lack of *tmem63c* in developing zebrafish embryos leads to profound changes in GFB ultrastructure compromising GFB functionality. At the same time, these findings corroborate the previously observed albuminuria-like phenotype evidenced by pathophysiological changes in glomerular ultrastructure.

Since ultrastructural analysis of the GFB suggested detachment of podocytes, confocal microscopy of whole-mount fixed *Tg[wt1b:EGFP]* zebrafish embryos at 96 hpf and subsequent computational 3D reconstruction of the glomerulus was conducted to examine the cellular organization of the glomerulus. For quantification, the 3D reconstruction was used to accurately determine absolute podocyte cell number, glomerular volume and relative podocyte cell number (absolute podocyte cell number normalized to glomerular volume). In this analysis,

the majority of *tmem63c* crispants presented with dilated glomerular capillary loops compared to uninjected and Cas9-protein-injected controls as can be seen in Figure 2H (asterisk). This resulted in a significant increase in total glomerular volume in *tmem63c* crispants compared to uninjected controls (Figure 2J). Quantification of absolute and relative podocyte cell number revealed no changes in absolute podocyte cell number in *tmem63c* crispants (Figure 2I), while relative cell number was significantly decreased compared to uninjected controls indicating a significant reduction in podocyte density (Figure 2K). These findings reveal no absolute detachment of podocytes upon *tmem63c*-deficiency, but rather suggest a role of *tmem63c* in proper development of glomerular capillaries leading to glomerular hypertrophy with decreased podocyte density.

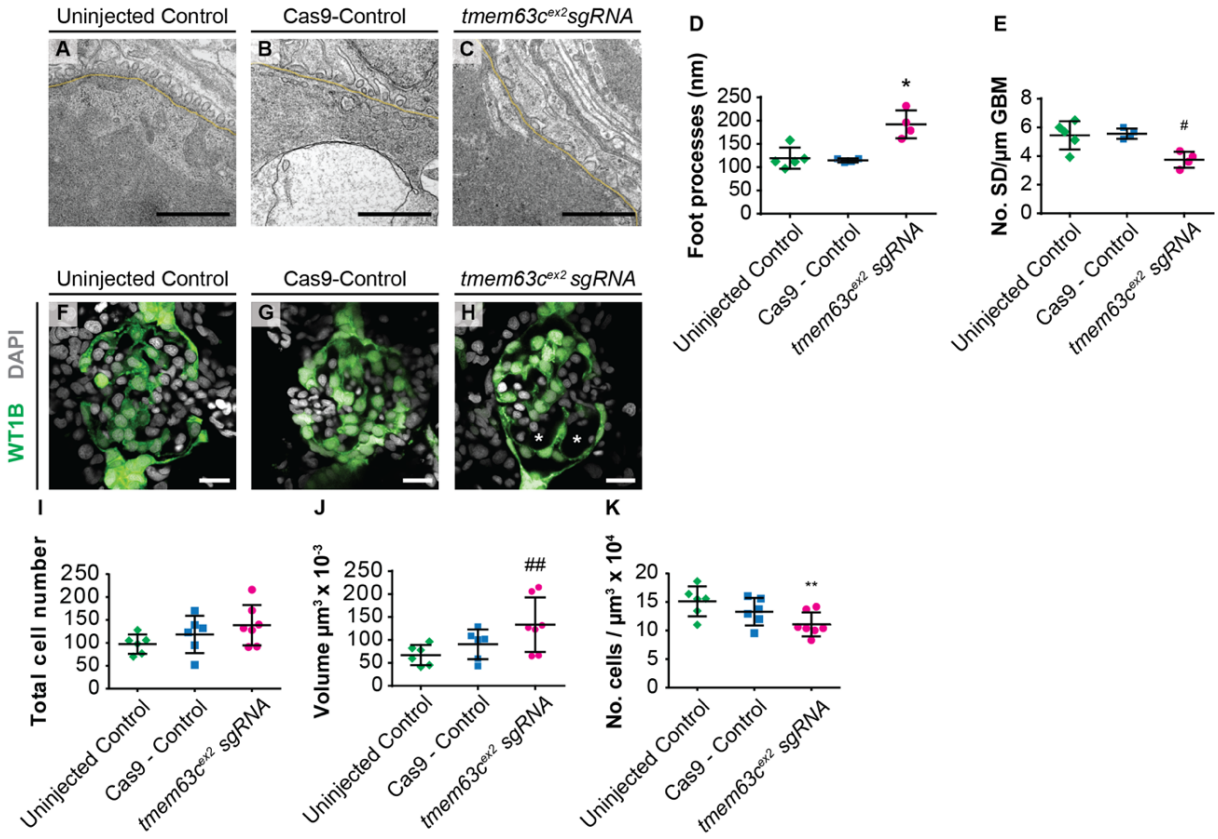

Figure 2. Morphological analysis of glomerular structures in *tmem63c* crispant zebrafish embryos.

(**A-E**) Electron microscopy and quantitative assessment of GFB ultrastructure. (**A-C**) Representative electron microscopy pictures of the GFB in uninjected Controls (**A**), Cas9-Controls (**B**) and after *tmem63c* knockdown (**C**) The GBM is highlighted in yellow. Quantitative analysis of podocyte foot process width (**D**) and number of slit diaphragms per µm GBM (**E**). Uninjected Control (n = 5); Cas9-Control (n = 4); *tmem63c* ex2-sgRNA (n = 4); Scale bar = 1 µm; * P < 0.002 vs. uninjected Control, Cas9-Control; # P < 0.02 vs. uninjected Control, Cas9-Control. (**F-J**) Confocal microscopy and quantification of absolute and relative podocyte cell number in *Tg[wt1b:EGFP]* at 96 hpf. Representative confocal microscopy pictures of glomeruli in uninjected Controls (**F**), Cas9-Controls (**G**) and after *tmem63c* knockdown (**H**). Asterisks indicate dilated glomerular capillaries. Quantitative analysis of absolute podocyte cell number (**I**), total glomerular volume (**J**) and relative podocyte cell number (**K**). Relative podocyte cell number has been obtained after normalization of the absolute cell number to the glomerular volume. Uninjected Control (n = 6); Cas9-Control (n = 6); tmem63c ex2-sgRNA (n = 7); Scale bar = 15 µm; ## P = 0.0381 vs. uninjected Control, ** P = 0.0229 vs. uninjected Control.

Part of Figure 2 has been previously published in (1): Schulz A, Müller NV, van de Lest NA, Eisenreich A, Schmidbauer M, Barysenka A, Purfurst B, Sporbert A, Lorenzen T, Meyer AM, Herlan L, Witten A, Ruhle F, Zhou W, de Heer E, Scharpfenecker M, Panakova D, Stoll M, Kreutz R. Analysis of the genomic architecture of a complex trait locus in hypertensive rat models links Tmem63c to kidney damage. eLife. 2019;8. Figure 8, Ultrastructural and morphological analysis of glomerular structures after loss of tmem63c in zebrafish.; p.15.

Discussion

In this study, the relatively large previously identified albuminuria-QTL on RNO6 of the MWF rat was successfully narrowed to a sub-QTL by congenic substitution mapping strategy for albuminuria and glomerular density phenotypes.

While both, the albuminuria phenotype and the inherited nephron deficit mapped to the identified sub-QTL in MWF, no changes were detected in blood pressure proving that the identified genomic region is responsible for albuminuria development and reduced glomerular density independent from blood pressure changes present in MWF. Since albuminuria is associated with hypertension as well as developmental changes of the kidney and nephron deficit (34) the here identified sub-QTL excludes genes responsible for blood pressure changes in the parental rat strains (11).

Subsequent compartment-specific RNA-seq analysis in isolated glomeruli of MWF and SHR, identified 10 significantly differentially expressed genes coding in the sub-QTL region. Out of these 10, *Tmem63c* was prioritized as a positional candidate gene based on its significantly different and allele-dependent differential mRNA-expression levels between the parental MWF and SHR and the consomic MWF-6^{SHR} rat strain

Immunohistochemical analysis of *Tmem63c* protein expression in MWF and SHR kidneys showed abundance of *Tmem63c* specifically in podocytes, but revealed no obvious changes in protein abundance between the two strains as opposed to significantly increased *Tmem63c* mRNA expression levels in MWF versus SHR.

As stated by Liu et al. (35) transcript levels are not sufficient to predict protein levels as their relationship is influenced by various other factors such as spatial and temporal variation of mRNAs, local availability of resources for protein biosynthesis and the possible buffering of mRNA fluctuations at the protein level, which possibly explains the observed discrepancy.

Clinical relevance of TMEM63C was evaluated in human kidney biopsies of FSGS patients and revealed significantly lower protein abundance in FSGS patients compared to healthy control patients. In addition, this change was associated with a marked decrease and a change in staining pattern of the slit diaphragm core component nephrin. FSGS patients serve as a rational human counterpart as the MWF rat represents a commonly accepted genetic FSGS rat model with the development of glomerulosclerotic lesions (11, 36, 37). While loss of nephrin abundance in FSGS has been shown previously (38, 39), associated loss of TMEM63C provides clinical relevance of the identified candidate gene in human pathology. Furthermore,

siRNA-mediated knockdown of TMEM63C in hPC underlined its pathophysiological relevance by revealing decreased cell viability combined with increased apoptotic and decreased pro-survival signaling in podocytes.

Functional analysis of *tmem63c* in *Tg[fabp10a:gc-EGFP]* zebrafish embryos revealed compromised GFB integrity resulting in an albuminuria-like phenotype upon gene deficiency. Knockdown of *tmem63c* gene function in this study was conducted using Morpholino (MO) antisense oligos as well as CRISPR/Cas9-mediated somatic mutagenesis. While MO-induced gene knockdown efficiency wears off following 72 hours post injection (18), CRISPR/Cas9-mediated somatic mutagenesis induces permanent genomic mutations in developing zebrafish embryos albeit in mosaic manner. The fact that an albuminuria-like phenotype was observed in *tmem63c* morphants may indicate an important role of *tmem63c* in pronephric organogenesis and GFB functionality within the first 72 hpf of embryonic development, which could not be reversed until 120 hpf while *tmem63c* gene function was gradually restored.

Recent reviews discuss the value of loss-of-function studies gained by MO- or transient CRISPR/Cas9-mediated gene knockdown, respectively (40-42). For MO-mediated gene knockdown, major concerns are raised about MO off-target effects that are causing phenotypes independent or only partially caused by the gene analyzed (41). In addition, it has to be taken into account, that for several reasons, including MO-off target effects and lack of genetic compensation in morphants, MO-induced phenotypes are different and often more severe than mutant phenotypes (40). Transient, first generation CRISPR/Cas9-mediated somatic mutants are mosaic somatic mutants with dose-dependent mutation rates (20), in which some cells are carrying the mutation while in others the CRISPR-target site remains unchanged. In these, genetic mosaicism causes a complex, yet unpredictable and difficult to define genetic makeup, that is different for each mosaic animal evaluated (42).

To account for these concerns and ensure specificity of the observed phenotypes, several backup and control experiments were applied as discussed in relevant reviews (40-42): *tmem63c* gene knockdown was conducted using a translation as well as a pre-mRNA splicing blocking MO and was further corroborated by CRISPR/Cas9-mediated somatic mutagenesis as suggested (40, 41). All of these approaches revealed similar phenotypes showing mild pericardial edema at 48 hpf and an albuminuria-like phenotype at 120 hpf. Thus, the here observed phenotype is highly attributable to a knockdown of *tmem63c* function in developing zebrafish embryos.

Specificity of each of the knockdown approaches was successfully verified by rescue of the observed phenotypes with co-injection of mRNA not targeted by the knockdown system used as proposed by Eisen et al. (41). While the pre-mRNA splice-blocking-mediated (*tmem63c* ex2-sdMO) and the CRISPR/Cas9-mediated (*tmem63c* ex2-sgRNA) gene knockdown were rescued by co-injection of zebrafish-derived *tmem63c* mRNA, the translation blocking-

mediated (*tmem63c* ATG-MO) gene knockdown was rescued with rat-derived *Tmem63c* mRNA, that is not targeted by *tmem63c* ATG-MO. Consequently, with rescuing the knockdown of *tmem63c* in zebrafish with rat-derived *Tmem63c* mRNA not only the specificity of the observed knockdown phenotype, but also functional conservation of *tmem63c* function across species was verified. This further supports using the zebrafish as a valuable animal model for further research on a molecular mechanism of *tmem63c* function.

Knockdown-efficiency has been shown for *tmem63c* ex2-sdMO using RT-PCR as suggested (41) with the appearance of a partial, incorrectly spliced *tmem63c* transcript as well as reduced abundance of the correctly spliced *tmem63c* transcript compared to controls and for *tmem63c* ex2-sgRNA by sequencing of the CRISPR target site, which indicated the induced genomic variants.

Control-MOs and a Cas9-Control were used as injection controls to make up for possible phenotypes due to the injection process itself as recommended (41) and showed no significant changes compared to uninjected controls.

Together, the above described knockdown techniques are valuable and easy applicable tools to analyze a gene's functional role in developing zebrafish larvae, but require in-depth knowledge on major drawbacks of these methods and conduction of appropriate control experiments as well as the use of at least two different knockdown systems to corroborate and assure validity of the observed knockdown phenotypes. Further research on a possible molecular mechanism of *tmem63c* should be conducted in zygotic mutants to exclude any possible MO-off-target effects and to ensure the evaluation of genetically identical animals (40, 42).

The observed albuminuria-like phenotype and an important role of *tmem63c* in GFB integrity were corroborated by ultrastructural analysis of *tmem63c* crispants using TEM. This analysis revealed profound changes in podocyte morphology resulting in podocyte foot process effacement, a process that is typically associated with the presence of proteinuria and compromised GFB functionality (33).

Subsequent quantification of absolute and relative podocyte cell number using confocal microscopy of whole-mount fixed *Tg[wt1b:EGFP]* zebrafish embryos revealed no changes in absolute cell number, while glomerular volume was increased with a concomitant decrease in relative podocyte cell number or podocyte density in *tmem63c* crispants compared to uninjected controls. As shown in Figure 2H, this increase in glomerular volume is due to a marked dilation of glomerular capillaries leading to glomerular hypertrophy and possibly attributable to increased podocyte stress as a potential cause of the observed podocyte foot process effacement in TEM (43, 44).

Tmem63c belongs to the TMEM (transmembrane protein) gene family, a family of approximately 310 proteins that are predicted to be components of various cell membranes.

Many TMEMs function as channels, although the exact function of the majority of these proteins including *Tmem63c* remains unknown (45, 46).

Recent studies identified and evaluated *Tmem63c* and its two paralogs *Tmem63a* and *Tmem63b* as mammalian homologues of *AtCSC1* and its close homologue OSCA1, that are responsible for hyperosmolarity-induced Ca^{2+}-signaling in plants and therefore might be putative candidates for osmoreceptor or mechanosensitive channels in mammals (47, 48). While it has been shown, that the *Tmem63c*-family members are able to evoke hyperosmolarity-induced ion currents, if co-expressed (48), mechanosensitivity with the ability to trigger stretch-induced ion currents was shown for *Tmem63a* and *Tmem63b*, but not *Tmem63c* in a more recent study (49). In the same study, the lack of mechanosensitivity of *Tmem63c* was justified with its phylogenetic divergence from *Tmem63a* and *Tmem63b* in mammals (49).

In this study, zebrafish embryos with reduced *tmem63c*-levels presented with glomerular hypertrophy due to ectasia of glomerular capillaries suggesting a role of *tmem63c* in vascular development.

Interestingly, *Tmem63b* has been associated with alterations in *vascular endothelial growth factor A* (*VEGF-A*) levels (50, 51), while it is well-known that podocyte dysfunction and depletion depend on a tightly regulated reciprocal crosstalk between podocytes and endothelial cells including *VEGF-A* as an essential factor for GFB integrity as well as angiogenesis (52, 53).

Since co-expression and thus a tight interplay of the *Tmem63*-family members was identified as an important prerequisite to constitute a hyperosmolarity-activated ion channel (48), a possible relation between the other two *Tmem63*-family members, *Tmem63a* and *Tmem63c*, and alternating *VEGF-A* levels should be further evaluated in future studies.

However, the role of *Tmem63c* as a hyperosmolarity-induced or mechanosensitive ion channel and its interplay with the other *Tmem63*-family members remains currently unclear and has to be evaluated in further studies to elucidate a molecular mechanism of *Tmem63c*-mediated podocyte injury.

This study identifies naturally occurring genetic variants in *Tmem63c* in inbred hypertensive rat models and successfully demonstrates their potential clinical relevance for albuminuria development in humans. Similarly, genetic variants in *RAB38* (54, 55) and *Shroom3* (56) have been identified in the fawn-hooded hypertensive rat strain and have been proven relevant in human pathology later on. This emphasizes the importance of inbred animal models as important tools complementing large-population GWAS.

Altogether, this study indicates a conserved functional role of *Tmem63c* for GFB integrity between rodents, fish and humans and suggests further translational investigation of *Tmem63c* as a novel target for the therapeutic intervention of albuminuria in hypertension.

References

1. Schulz A, Müller NV, van de Lest NA, Eisenreich A, Schmidbauer M, Barysenka A, Purfurst B, Sporbert A, Lorenzen T, Meyer AM, Herlan L, Witten A, Ruhle F, Zhou W, de Heer E, Scharpfenecker M, Panakova D, Stoll M, Kreutz R. Analysis of the genomic architecture of a complex trait locus in hypertensive rat models links Tmem63c to kidney damage. eLife. 2019;8.
2. WHO. Global Health Estimates 2016: Estimated deaths by cause and region, 2000 and 2016. Geneva2018.
3. Global Burden of Metabolic Risk Factors for Chronic Diseases C. Cardiovascular disease, chronic kidney disease, and diabetes mortality burden of cardiometabolic risk factors from 1980 to 2010: a comparative risk assessment. Lancet Diabetes Endocrinol. 2014;2(8):634-47.
4. Williams B, Mancia G, Spiering W, Agabiti Rosei E, Azizi M, Burnier M, Clement DL, Coca A, de Simone G, Dominiczak A, Kahan T, Mahfoud F, Redon J, Ruilope L, Zanchetti A, Kerins M, Kjeldsen SE, Kreutz R, Laurent S, Lip GYH, McManus R, Narkiewicz K, Ruschitzka F, Schmieder RE, Shlyakhto E, Tsioufis C, Aboyans V, Desormais I, Authors/Task Force M. 2018 ESC/ESH Guidelines for the management of arterial hypertension: The Task Force for the management of arterial hypertension of the European Society of Cardiology and the European Society of Hypertension: The Task Force for the management of arterial hypertension of the European Society of Cardiology and the European Society of Hypertension. J Hypertens. 2018;36(10):1953-2041.
5. Eckardt KU, Coresh J, Devuyst O, Johnson RJ, Kottgen A, Levey AS, Levin A. Evolving importance of kidney disease: from subspecialty to global health burden. Lancet. 2013;382(9887):158-69.
6. Coffman TM, Crowley SD. Kidney in hypertension: guyton redux. Hypertension. 2008;51(4):811-6.
7. Group" KDIGOKCW. KDIGO 2012 clinical practice guideline for the evaluation and management of chronic kidney disease. Kidney Int Suppl. 2013;3(1):1-150.
8. Evangelou E, Warren HR, Mosen-Ansorena D, Mifsud B, Pazoki R, Gao H, Ntritsos G, Dimou N, Cabrera CP, Karaman I, Ng FL, Evangelou M, Witkowska K, Tzanis E, Hellwege JN, Giri A, Velez Edwards DR, Sun YV, Cho K, Gaziano JM, Wilson PWF, Tsao PS, Kovesdy CP, Esko T, Magi R, Milani L, Almgren P, Boutin T, Debette S, Ding J, Giulianini F, Holliday EG, Jackson AU, Li-Gao R, Lin WY, Luan J, Mangino M, Oldmeadow C, Prins BP, Qian Y, Sargurupremraj M, Shah N, Surendran P, Theriault S, Verweij N, Willems SM, Zhao JH, Amouyel P, Connell J, de Mutsert R, Doney ASF, Farrall M, Menni C, Morris AD, Noordam R, Pare G, Poulter NR, Shields DC, Stanton A, Thom S, Abecasis G, Amin N, Arking DE, Ayers KL, Barbieri CM, Batini C, Bis JC, Blake T, Bochud M, Boehnke M, Boerwinkle E, Boomsma DI, Bottinger EP, Braund PS, Brumat M, Campbell A, Campbell H, Chakravarti A, Chambers JC, Chauhan G, Ciullo M, Cocca M, Collins F, Cordell HJ, Davies G, de Borst MH, de Geus EJ, Deary IJ, Deelen J, Del Greco MF, Demirkale CY, Dorr M, Ehret GB, Elosua R, Enroth S, Erzurumluoglu AM, Ferreira T, Franberg M, Franco OH, Gandin I, Gasparini P, Giedraitis V, Gieger C, Girotto G, Goel A, Gow AJ, Gudnason V, Guo X, Gyllensten U, Hamsten A, Harris TB, Harris SE, Hartman CA, Havulinna AS, Hicks AA, Hofer E, Hofman A, Hottenga JJ, Huffman JE, Hwang SJ, Ingelsson E, James A, Jansen R, Jarvelin MR, Joehanes R, Johansson A, Johnson AD, Joshi PK, Jousilahti P, Jukema JW, Jula A, Kahonen M, Kathiresan S, Keavney BD, Khaw KT, Knekt P, Knight J, Kolcic I, Kooner JS, Koskinen S, Kristiansson K, Kutalik Z, Laan M, Larson M, Launer LJ, Lehne B, Lehtimaki T, Liewald DCM, Lin L, Lind L, Lindgren CM, Liu Y, Loos RJF, Lopez LM, Lu Y, Lyytikainen LP, Mahajan A, Mamasoula C, Marrugat J, Marten J, Milaneschi Y, Morgan A, Morris AP, Morrison AC, Munson PJ, Nalls MA, Nandakumar P, Nelson CP, Niiranen T, Nolte IM, Nutile T, Oldehinkel AJ, Oostra BA, O'Reilly PF, Org E, Padmanabhan S, Palmas W, Palotie A, Pattie A, Penninx B, Perola M, Peters A, Polasek O, Pramstaller PP, Nguyen QT, Raitakari OT, Ren M, Rettig R, Rice K, Ridker PM, Ried JS, Riese H, Ripatti S, Robino A, Rose LM, Rotter JI, Rudan I, Ruggiero D, Saba Y, Sala CF, Salomaa V, Samani NJ, Sarin AP, Schmidt R, Schmidt H, Shrine N, Siscovick D, Smith AV, Snieder H, Sober S, Sorice R, Starr JM, Stott DJ, Strachan DP, Strawbridge RJ, Sundstrom J, Swertz MA, Taylor KD, Teumer A, Tobin MD, Tomaszewski M, Toniolo D, Traglia M, Trompet S, Tuomilehto J, Tzourio C, Uitterlinden AG, Vaez A, van der Most PJ, van Duijn CM, Vergnaud AC, Verwoert GC, Vitart V, Volker U, Vollenweider P, Vuckovic D,

Watkins H, Wild SH, Willemsen G, Wilson JF, Wright AF, Yao J, Zemunik T, Zhang W, Attia JR, Butterworth AS, Chasman DI, Conen D, Cucca F, Danesh J, Hayward C, Howson JMM, Laakso M, Lakatta EG, Langenberg C, Melander O, Mook-Kanamori DO, Palmer CNA, Risch L, Scott RA, Scott RJ, Sever P, Spector TD, van der Harst P, Wareham NJ, Zeggini E, Levy D, Munroe PB, Newton-Cheh C, Brown MJ, Metspalu A, Hung AM, O'Donnell CJ, Edwards TL, Psaty BM, Tzoulaki I, Barnes MR, Wain LV, Elliott P, Caulfield MJ, Million Veteran P. Genetic analysis of over 1 million people identifies 535 new loci associated with blood pressure traits. Nat Genet. 2018;50(10):1412-25.
9. Xu X, Eales JM, Akbarov A, Guo H, Becker L, Talavera D, Ashraf F, Nawaz J, Pramanik S, Bowes J, Jiang X, Dormer J, Denniff M, Antczak A, Szulinska M, Wise I, Prestes PR, Glyda M, Bogdanski P, Zukowska-Szczechowska E, Berzuini C, Woolf AS, Samani NJ, Charchar FJ, Tomaszewski M. Molecular insights into genome-wide association studies of chronic kidney disease-defining traits. Nat Commun. 2018;9(1):4800.
10. Padmanabhan S, Joe B. Towards Precision Medicine for Hypertension: A Review of Genomic, Epigenomic, and Microbiomic Effects on Blood Pressure in Experimental Rat Models and Humans. Physiol Rev. 2017;97(4):1469-528.
11. Schulz A, Kreutz R. Mapping genetic determinants of kidney damage in rat models. Hypertens Res. 2012;35(7):675-94.
12. Atanur SS, Diaz AG, Maratou K, Sarkis A, Rotival M, Game L, Tschannen MR, Kaisaki PJ, Otto GW, Ma MC, Keane TM, Hummel O, Saar K, Chen W, Guryev V, Gopalakrishnan K, Garrett MR, Joe B, Citterio L, Bianchi G, McBride M, Dominiczak A, Adams DJ, Serikawa T, Flicek P, Cuppen E, Hubner N, Petretto E, Gauguier D, Kwitek A, Jacob H, Aitman TJ. Genome sequencing reveals loci under artificial selection that underlie disease phenotypes in the laboratory rat. Cell. 2013;154(3):691-703.
13. Schulz A, Standke D, Kovacevic L, Mostler M, Kossmehl P, Stoll M, Kreutz R. A major gene locus links early onset albuminuria with renal interstitial fibrosis in the MWF rat with polygenetic albuminuria. J Am Soc Nephrol. 2003;14(12):3081-9.
14. Schulz A, Weiss J, Schlesener M, Hänsch J, Wehland M, Wendt N, Kossmehl P, Sietmann A, Grimm D, Stoll M, Nyengaard JR, Kreutz R. Development of overt proteinuria in the Munich Wistar Fromter rat is suppressed by replacement of chromosome 6 in a consomic rat strain. J Am Soc Nephrol. 2007;18(1):113-21.
15. Poureetezadi SJ, Wingert RA. Little fish, big catch: zebrafish as a model for kidney disease. Kidney Int. 2016;89(6):1204-10.
16. Drummond IA, Majumdar A, Hentschel H, Elger M, Solnica-Krezel L, Schier AF, Neuhauss SC, Stemple DL, Zwartkruis F, Rangini Z, Driever W, Fishman MC. Early development of the zebrafish pronephros and analysis of mutations affecting pronephric function. Development. 1998;125(23):4655-67.
17. Drummond IA. Kidney development and disease in the zebrafish. J Am Soc Nephrol. 2005;16(2):299-304.
18. Timme-Laragy AR, Karchner SI, Hahn ME. Gene knockdown by morpholino-modified oligonucleotides in the zebrafish (Danio rerio) model: applications for developmental toxicology. Methods Mol Biol. 2012;889:51-71.
19. Hwang WY, Fu Y, Reyon D, Maeder ML, Tsai SQ, Sander JD, Peterson RT, Yeh JR, Joung JK. Efficient genome editing in zebrafish using a CRISPR-Cas system. Nat Biotechnol. 2013;31(3):227-9.
20. Burger A, Lindsay H, Felker A, Hess C, Anders C, Chiavacci E, Zaugg J, Weber LM, Catena R, Jinek M, Robinson MD, Mosimann C. Maximizing mutagenesis with solubilized CRISPR-Cas9 ribonucleoprotein complexes. Development. 2016;143(11):2025-37.
21. Zhou W, Hildebrandt F. Inducible podocyte injury and proteinuria in transgenic zebrafish. J Am Soc Nephrol. 2012;23(6):1039-47.
22. Perner B, Englert C, Bollig F. The Wilms tumor genes wt1a and wt1b control different steps during formation of the zebrafish pronephros. Dev Biol. 2007;309(1):87-96.
23. Karlsson J, von Hofsten J, Olsson PE. Generating transparent zebrafish: a refined method to improve detection of gene expression during embryonic development. Mar Biotechnol (N Y). 2001;3(6):522-7.
24. Gagnon JA, Valen E, Thyme SB, Huang P, Akhmetova L, Pauli A, Montague TG, Zimmerman S, Richter C, Schier AF. Efficient mutagenesis by Cas9 protein-mediated

oligonucleotide insertion and large-scale assessment of single-guide RNAs. PLoS One. 2014;9(5):e98186.
25. Bassett AR, Tibbit C, Ponting CP, Liu JL. Highly efficient targeted mutagenesis of Drosophila with the CRISPR/Cas9 system. Cell Rep. 2013;4(1):220-8.
26. Lindsay H, Burger A, Biyong B, Felker A, Hess C, Zaugg J, Chiavacci E, Anders C, Jinek M, Mosimann C, Robinson MD. CrispRVariants charts the mutation spectrum of genome engineering experiments. Nat Biotech. 2016;34(7):701-2.
27. McCurley AT, Callard GV. Characterization of housekeeping genes in zebrafish: male-female differences and effects of tissue type, developmental stage and chemical treatment. BMC Mol Biol. 2008;9:102.
28. Schindelin J, Arganda-Carreras I, Frise E, Kaynig V, Longair M, Pietzsch T, Preibisch S, Rueden C, Saalfeld S, Schmid B, Tinevez JY, White DJ, Hartenstein V, Eliceiri K, Tomancak P, Cardona A. Fiji: an open-source platform for biological-image analysis. Nature methods. 2012;9(7):676-82.
29. Remuzzi A, Puntorieri S, Alfano M, Macconi D, Abbate M, Bertani T, Remuzzi G. Pathophysiologic implications of proteinuria in a rat model of progressive glomerular injury. Lab Invest. 1992;67(5):572-9.
30. Martin CE, Jones N. Nephrin Signaling in the Podocyte: An Updated View of Signal Regulation at the Slit Diaphragm and Beyond. Front Endocrinol (Lausanne). 2018;9:302.
31. Hanke N, Staggs L, Schroder P, Litteral J, Fleig S, Kaufeld J, Pauli C, Haller H, Schiffer M. "Zebrafishing" for novel genes relevant to the glomerular filtration barrier. Biomed Res Int. 2013;2013:658270.
32. Madeira F, Park YM, Lee J, Buso N, Gur T, Madhusoodanan N, Basutkar P, Tivey ARN, Potter SC, Finn RD, Lopez R. The EMBL-EBI search and sequence analysis tools APIs in 2019. Nucleic Acids Res. 2019.
33. Kriz W, Shirato I, Nagata M, LeHir M, Lemley KV. The podocyte's response to stress: the enigma of foot process effacement. Am J Physiol Renal Physiol. 2013;304(4):F333-47.
34. Wang X, Garrett MR. Nephron Number, Hypertension, and CKD: Physiological and Genetic Insight from Humans and Animal Models. Physiol Genomics. 2017;49(3):180-92.
35. Liu Y, Beyer A, Aebersold R. On the Dependency of Cellular Protein Levels on mRNA Abundance. Cell. 2016;165(3):535-50.
36. Lim BJ, Yang JW, Do WS, Fogo AB. Pathogenesis of Focal Segmental Glomerulosclerosis. J Pathol Transl Med. 2016;50(6):405-10.
37. Remuzzi A, Puntorieri S, Mazzoleni A, Remuzzi G. Sex related differences in glomerular ultrafiltration and proteinuria in Munich-Wistar rats. Kidney Int. 1988;34(4):481-6.
38. Doublier S, Ruotsalainen V, Salvidio G, Lupia E, Biancone L, Conaldi PG, Reponen P, Tryggvason K, Camussi G. Nephrin redistribution on podocytes is a potential mechanism for proteinuria in patients with primary acquired nephrotic syndrome. Am J Pathol. 2001;158(5):1723-31.
39. Wernerson A, Duner F, Pettersson E, Widholm SM, Berg U, Ruotsalainen V, Tryggvason K, Hultenby K, Soderberg M. Altered ultrastructural distribution of nephrin in minimal change nephrotic syndrome. Nephrol Dial Transplant. 2003;18(1):70-6.
40. Stainier DYR, Raz E, Lawson ND, Ekker SC, Burdine RD, Eisen JS, Ingham PW, Schulte-Merker S, Yelon D, Weinstein BM, Mullins MC, Wilson SW, Ramakrishnan L, Amacher SL, Neuhauss SCF, Meng A, Mochizuki N, Panula P, Moens CB. Guidelines for morpholino use in zebrafish. PLoS Genet. 2017;13(10):e1007000.
41. Eisen JS, Smith JC. Controlling morpholino experiments: don't stop making antisense. Development. 2008;135(10):1735-43.
42. Teboul L, Murray SA, Nolan PM. Phenotyping first-generation genome editing mutants: a new standard? Mamm Genome. 2017;28(7-8):377-82.
43. Fukuda A, Chowdhury MA, Venkatareddy MP, Wang SQ, Nishizono R, Suzuki T, Wickman LT, Wiggins JE, Muchayi T, Fingar D, Shedden KA, Inoki K, Wiggins RC. Growth-dependent podocyte failure causes glomerulosclerosis. J Am Soc Nephrol. 2012;23(8):1351-63.
44. Nagata M, Scharer K, Kriz W. Glomerular damage after uninephrectomy in young rats. I. Hypertrophy and distortion of capillary architecture. Kidney Int. 1992;42(1):136-47.

45. Wrzesinski T, Szelag M, Cieslikowski WA, Ida A, Giles R, Zodro E, Szumska J, Pozniak J, Kwias Z, Bluyssen HA, Wesoly J. Expression of pre-selected TMEMs with predicted ER localization as potential classifiers of ccRCC tumors. BMC Cancer. 2015;15:518.
46. Schmit K, Michiels C. TMEM Proteins in Cancer: A Review. Front Pharmacol. 2018;9:1345.
47. Hou C, Tian W, Kleist T, He K, Garcia V, Bai F, Hao Y, Luan S, Li L. DUF221 proteins are a family of osmosensitive calcium-permeable cation channels conserved across eukaryotes. Cell Res. 2014;24(5):632-5.
48. Zhao X, Yan X, Liu Y, Zhang P, Ni X. Co-expression of mouse TMEM63A, TMEM63B and TMEM63C confers hyperosmolarity activated ion currents in HEK293 cells. Cell Biochem Funct. 2016;34(4):238-41.
49. Murthy SE, Dubin AE, Whitwam T, Jojoa Cruz S, Cahalan SM, Mosavi SA, Ward AB, Patapoutian A. OSCA/TMEM63 are an evolutionarily conserved family of mechanically activated ion channels. Elife. 2018;7.
50. Chiang DY, Villanueva A, Hoshida Y, Peix J, Newell P, Minguez B, LeBlanc AC, Donovan DJ, Thung SN, Sole M, Tovar V, Alsinet C, Ramos AH, Barretina J, Roayaie S, Schwartz M, Waxman S, Bruix J, Mazzaferro V, Ligon AH, Najfeld V, Friedman SL, Sellers WR, Meyerson M, Llovet JM. Focal gains of VEGFA and molecular classification of hepatocellular carcinoma. Cancer Res. 2008;68(16):6779-88.
51. Lin HJ, Huang YC, Lin JM, Wu JY, Chen LA, Tsai FJ. Association of genes on chromosome 6, GRIK2 , TMEM217 and TMEM63B (linked to MRPL14) with diabetic retinopathy. Ophthalmologica. 2013;229(1):54-60.
52. Garg P. A Review of Podocyte Biology. Am J Nephrol. 2018;47 Suppl 1:3-13.
53. Eremina V, Sood M, Haigh J, Nagy A, Lajoie G, Ferrara N, Gerber HP, Kikkawa Y, Miner JH, Quaggin SE. Glomerular-specific alterations of VEGF-A expression lead to distinct congenital and acquired renal diseases. J Clin Invest. 2003;111(5):707-16.
54. Rangel-Filho A, Lazar J, Moreno C, Geurts A, Jacob HJ. Rab38 modulates proteinuria in model of hypertension-associated renal disease. J Am Soc Nephrol. 2013;24(2):283-92.
55. Teumer A, Tin A, Sorice R, Gorski M, Yeo NC, Chu AY, Li M, Li Y, Mijatovic V, Ko YA, Taliun D, Luciani A, Chen MH, Yang Q, Foster MC, Olden M, Hiraki LT, Tayo BO, Fuchsberger C, Dieffenbach AK, Shuldiner AR, Smith AV, Zappa AM, Lupo A, Kollerits B, Ponte B, Stengel B, Kramer BK, Paulweber B, Mitchell BD, Hayward C, Helmer C, Meisinger C, Gieger C, Shaffer CM, Muller C, Langenberg C, Ackermann D, Siscovick D, Boerwinkle E, Kronenberg F, Ehret GB, Homuth G, Waeber G, Navis G, Gambaro G, Malerba G, Eiriksdottir G, Li G, Wichmann HE, Grallert H, Wallaschofski H, Volzke H, Brenner H, Kramer H, Mateo Leach I, Rudan I, Hillege HL, Beckmann JS, Lambert JC, Luan J, Zhao JH, Chalmers J, Coresh J, Denny JC, Butterbach K, Launer LJ, Ferrucci L, Kedenko L, Haun M, Metzger M, Woodward M, Hoffman MJ, Nauck M, Waldenberger M, Pruijm M, Bochud M, Rheinberger M, Verweij N, Wareham NJ, Endlich N, Soranzo N, Polasek O, van der Harst P, Pramstaller PP, Vollenweider P, Wild PS, Gansevoort RT, Rettig R, Biffar R, Carroll RJ, Katz R, Loos RJ, Hwang SJ, Coassin S, Bergmann S, Rosas SE, Stracke S, Harris TB, Corre T, Zeller T, Illig T, Aspelund T, Tanaka T, Lendeckel U, Volker U, Gudnason V, Chouraki V, Koenig W, Kutalik Z, O'Connell JR, Parsa A, Heid IM, Paterson AD, de Boer IH, Devuyst O, Lazar J, Endlich K, Susztak K, Tremblay J, Hamet P, Jacob HJ, Boger CA, Fox CS, Pattaro C, Kottgen A. Genome-wide Association Studies Identify Genetic Loci Associated With Albuminuria in Diabetes. Diabetes. 2016;65(3):803-17.
56. Yeo NC, O'Meara CC, Bonomo JA, Veth KN, Tomar R, Flister MJ, Drummond IA, Bowden DW, Freedman BI, Lazar J, Link BA, Jacob HJ. Shroom3 contributes to the maintenance of the glomerular filtration barrier integrity. Genome Res. 2015;25(1):57-65.

Eidesstattliche Versicherung

„Ich, Nicola Victoria Müller, versichere an Eides statt durch meine eigenhändige Unterschrift, dass ich die vorgelegte Dissertation mit dem Thema: „Functional analysis of albuminuria candidate genes in zebrafish“ selbstständig und ohne nicht offengelegte Hilfe Dritter verfasst und keine anderen als die angegebenen Quellen und Hilfsmittel genutzt habe.
Alle Stellen, die wörtlich oder dem Sinne nach auf Publikationen oder Vorträgen anderer Autoren beruhen, sind als solche in korrekter Zitierung kenntlich gemacht. Die Abschnitte zu Methodik (insbesondere praktische Arbeiten, Laborbestimmungen, statistische Aufarbeitung) und Resultaten (insbesondere Abbildungen, Graphiken und Tabellen werden von mir verantwortet.

Meine Anteile an etwaigen Publikationen zu dieser Dissertation entsprechen denen, die in der untenstehenden gemeinsamen Erklärung mit dem/der Betreuer/in, angegeben sind. Für sämtliche im Rahmen der Dissertation entstandenen Publikationen wurden die Richtlinien des ICMJE (International Committee of Medical Journal Editors; www.icmje.og) zur Autorenschaft eingehalten. Ich erkläre ferner, dass mir die Satzung der Charité – Universitätsmedizin Berlin zur Sicherung Guter Wissenschaftlicher Praxis bekannt ist und ich mich zur Einhaltung dieser Satzung verpflichte.

Die Bedeutung dieser eidesstattlichen Versicherung und die strafrechtlichen Folgen einer unwahren eidesstattlichen Versicherung (§156,161 des Strafgesetzbuches) sind mir bekannt und bewusst.“

Datum 15.11.2019 _____ Unterschrift

Ausführliche Anteilserklärung an erfolgter Publikation

Die hier angegebene Publikation erfolgte unter Beteiligung von mir, Nicola Victoria Müller, und Dr. Angela Schulz in geteilter Erstautorenschaft im Journal „Elife“.

Publikation: Angela Schulz *, **Nicola Victoria Müller** *, Nina Anne van de Lest, Andreas Eisenreich, Martina Schmidbauer, Andrei Barysenka,, Bettina Purfürst, Anje Sporbert, Theodor Lorenzen, Alexander M. Meyer, Laura Herlan, Anika Witten, Frank Rühle, Weibin Zhou, Emile de Heer, Marion Scharpfenecker, Daniela Panáková, Monika Stoll **, and Reinhold Kreutz **. Analysis of the genomic architecture of a complex trait locus in hypertensive rat models links *Tmem63c* to kidney damage. Elife;8:e42068.
*gleicher Anteil, ** gleicher Anteil

<u>Beitrag im Einzelnen:</u>

- **Projekt**
  - Die Koordination der Zusammenarbeit mit den Core Facilities „Elektronenmikroskopie“ (Leitung Dr. Bettina Purfürst) und „Advanced Light Microscopy“ (Leitung Dr. Anje Sporbert) am Max-Delbrück Centrum für molekulare Medizin zu experimentellen Arbeiten am Zebrafischmodell erfolgte maßgeblich durch mich.

- **Manuskript:**
  - Zebrafisch-bezogene Textpassagen der Einleitung, des Methoden- und Ergebnisteils sowie der Diskussion wurden von mir mitkonzipiert und miterstellt.
  - An der Finalisierung und Korrektur des Manuskripts habe ich mitgewirkt.
  - Die Abbildungskonzeption und Visualisierung für Abb. 7, Abb. 7 – Abb.anhang 1, Abb. 8 und Video 1-3 erfolgten durch mich.
  - Die Abbildungstexte zu Abb. 7, Abb. 7 – Abb.anhang 1 und Abb. 8 und Video 1-3 wurden von mir maßgeblich erstellt.
  - Zur Darstellung der gezeigten Daten als Mittelwert ± SD bzw. Median ± IQR auf Vorgabe eines Gutachters wurden die zugrundeliegenden Primärdaten durch mich auf statistische Normalverteilung getestet und statistisch reevaluiert. Die statistische Anpassung entsprechender graphischer Darstellungen erfolgte

durch mich. Siehe Abb. 1A, J, K, Abb. 2, Abb. 4 A-B, Abb. 5 E, F, I, J, Abb. 6 A-D.

- Die Zusammenstellung aller in der Publikation gezeigten Abbildungen und Abb.anhänge mit Hilfe des Programms „Adobe Illustrator“ erfolgte durch mich.
- Ich war maßgeblich an der Erstellung des *eLife Digest*, einer Zusammenfassung unserer Studie in Laiensprache, in Zusammenarbeit mit der Redaktion des Journals eLife beteiligt.

➢ **Methodenetablierung:**

- In Zusammenarbeit mit Dr. Bettina Purfürst habe ich die elektronenmikroskopische Analyse von Zebrafisch-Nieren etabliert.
- In Zusammenarbeit mit Dr. Anje Sporbert habe ich die konfokalmikroskopische Analyse *wholemount*-eingebetteter Zebrafischlarven etabliert, die im Gegensatz zur allgemein verwendeten Mikroskopie von beispielsweise Paraffin- oder Kryostat-Schnitten eine dreidimensionale Rekonstruktion des Zebrafischglomerulus ermöglichte.
- Zur Quantifizierung der absoluten Podozytenanzahl sowie des glomerulären Volumens habe ich eine teilmanuelle, computerbasierte Auswertung der Mikroskopdaten mit Hilfe des Computerprogramms „Imaris“ eigenständig entwickelt und validiert.

➢ **Methodendurchführung + Ergebniserhebung:**

- Mikroinjektionen der in Abb. 7, Abb.8 und Abb. 7-Abb.anhang 1 dargestellten MO- und CRISPR/Cas9-vermittelten Knockdown-sowie Rescue-Experimente und dazugehörige Kontrollexperimente wurden von mir durchgeführt.
- Die Synthese von *tmem63c* ex2-sgRNA sowie der für Rescue-Experimente verwendeten *tmem63c* mRNA (Zebrafisch) bzw. *Tmem63c* mRNA (Ratte) erfolgte durch mich. Siehe Abb. 7L und Abb. 7-Abb.anhang 1I.
- Die computerbasierte Analyse und graphische Darstellung der Sequenzierungsergebnisse zur Effizienzanalyse der verwendeten *tmem63c* ex2-sgRNA mit Hilfe des Programms „CRISPRVariants lite“ erfolgte durch mich. Siehe Abb. 7-Abb.anhang 1D.
- Die methodische Konzeption, das Primerdesign, die experimentelle Durchführung und Darstellung der RT-PCR zur Effizienzanalyse des *tmem63c* ex2-sdMO erfolgte durch mich. Siehe Abb. 7 – Abb.anhang 1F.

- Alle licht- und fluoreszenzmikroskopischen Aufnahmen von Zebrafischembryonen wurden von mir erstellt, selektiert und graphisch aufgearbeitet. Siehe Abb. 7C – K sowie Abb. 7- Abb.anhang 1A–C, G, H.
- Zur elektronenmikroskopischen Analyse des Pronephros wurden 120 hpf entsprechende Zebrafischembryonen von mir zur Einbettung ausgewählt. Darauffolgend habe ich Semi–Dünnschnitte der in Poly/Bed^{R} 812 eingebetteten Embryonen erstellt, die dem Auffinden des Zebrafisch–Pronephros dienten. Siehe Abb. 8 A-C.
- Die Selektion und graphische Aufarbeitung der gezeigten elektronenmikroskopischen Aufnahmen erfolgte durch mich. Siehe Abb. 8A-C.
- Konfokalmikroskopische Aufnahmen *wholemount*-eingebetteter Zebrafischembryonen wurden von mir erstellt und graphisch aufgearbeitet. Siehe Abb. 8 F-H.
- Die fluoreszenzmikroskopische Analyse der GFB-Integrität inklusive statistischer Analyse (einfaktorielle Varianzanalyse+Bonferroni Post-hoc Test, MW ± SD) wurde von mir durchgeführt. Siehe Abb.7L und Abb.7-Abb.anhang 1I.
- Die Quantifizierung, Auswertung und statistische Analyse (Shapiro-Wilk-Test, einfaktorielle Varianzanalyse+Bonferroni Post-hoc Test, MW ± SD) der Breite der Podozytenfußfortsätze sowie der Anzahl an Schlitzdiaphragmata pro µm glomerulärer Basalmembran anhand elektronenmikroskopischer Aufnahmen erfolgte durch mich. Siehe Abb. 8D – E.
- Die Quantifizierung, Visualisierung, Auswertung und statistische Analyse (Shapiro-Wilk-Test, einfaktorielle Varianzanalyse+Bonferroni Post-hoc Test, MW ± SD) der absoluten und relativen Podozytenanzahl sowie des glomerulären Volumens anhand konfokalmikroskopischer Aufnahmen des Zebrafisch-Pronephros erfolgte durch mich. Siehe Abb. 8I-J und Videos 1-3.

_____

Unterschrift, Datum und Stempel der betreuenden Hochschullehrer/der betreuenden Hochschullehrerinnen

_____

Unterschrift der Doktorandin

Auszug aus der Journal Summary List

Journal Data Filtered By: **Selected JCR Year: 2018** Selected Editions: SCIE,SSCI
Selected Categories: **"BIOLOGY"** Selected Category Scheme: WoS
Gesamtanzahl: 87 Journale

Rank	Full Journal Title	Total Cites	Journal Impact Factor	Eigenfactor Score
1	Physics of Life Reviews	1,514	11.045	0.002650
2	BIOLOGICAL REVIEWS	12,482	10.288	0.019280
3	PLOS BIOLOGY	29,974	8.386	0.057950
4	eLife	37,014	7.551	0.259540
5	BMC BIOLOGY	5,937	6.723	0.017800
6	BIOSCIENCE	18,353	6.591	0.012840
7	PHILOSOPHICAL TRANSACTIONS OF THE ROYAL SOCIETY B-BIOLOGICAL SCIENCES	45,388	6.139	0.071070
8	FASEB JOURNAL	41,854	5.391	0.047670
9	BIOELECTROCHEMISTRY	4,476	4.474	0.004050
10	BIOESSAYS	9,911	4.396	0.016740
11	PROCEEDINGS OF THE ROYAL SOCIETY B-BIOLOGICAL SCIENCES	53,240	4.304	0.079660
12	Geobiology	2,204	4.100	0.004460
13	Current Opinion in Insect Science	1,563	3.784	0.006370
14	ASTROBIOLOGY	3,625	3.768	0.005340
15	Science China-Life Sciences	2,451	3.583	0.006090
16	QUARTERLY REVIEW OF BIOLOGY	4,146	3.519	0.001280
17	Biology Letters	9,783	3.323	0.019530
18	Interface Focus	1,942	3.092	0.004850
19	JOURNAL OF EXPERIMENTAL BIOLOGY	32,933	3.017	0.033230
20	Biology Direct	1,864	3.010	0.003690
21	SAUDI JOURNAL OF BIOLOGICAL SCIENCES	2,746	2.820	0.004410
22	RADIATION RESEARCH	8,561	2.779	0.006480
23	CHRONOBIOLOGY INTERNATIONAL	5,042	2.562	0.006880
24	BIOLOGICAL RESEARCH	1,472	2.482	0.001910
25	JOURNAL OF BIOLOGICAL RHYTHMS	3,069	2.473	0.003570
26	Journal of Biological Research-Thessaloniki	330	2.364	0.000600
27	COMPUTERS IN BIOLOGY AND MEDICINE	5,694	2.286	0.008580
28	INTERNATIONAL JOURNAL OF RADIATION BIOLOGY	4,537	2.266	0.003740
29	CRYOBIOLOGY	4,553	2.141	0.004040
30	Advances in Experimental Medicine and Biology	19,627	2.126	0.033870
31	EXCLI Journal	1,307	2.112	0.002750

eLIFE elifesciences.org

RESEARCH ARTICLE

Analysis of the genomic architecture of a complex trait locus in hypertensive rat models links *Tmem63c* to kidney damage

Angela Schulz[1,2†], Nicola Victoria Müller[1,2,3†], Nina Anne van de Lest[4], Andreas Eisenreich[1,2], Martina Schmidbauer[1,2], Andrei Barysenka[5], Bettina Purfürst[6], Anje Sporbert[7], Theodor Lorenzen[2], Alexander M Meyer, Laura Herlan[2], Anika Witten[5], Frank Rühle[5], Weibin Zhou[8], Emile de Heer[4], Marion Scharpfenecker[4], Daniela Panáková[9]*, Monika Stoll[5,10‡], Reinhold Kreutz[2,9‡]*

[1]Charité - Universitätsmedizin Berlin, corporate member of Freie Universität Berlin, Humboldt-Universität zu Berlin, Berlin, Germany; [2]Institute of Clinical Pharmacology and Toxicology, Berlin Institute of Health, Berlin, Germany; [3]Max Delbrück Center for Molecular Medicine in the Helmholtz Association, Electrochemical Signaling in Development and Disease, Berlin, Germany; [4]Department of Pathology, Leiden University Medical Center (LUMC), Leiden, The Netherlands; [5]Westfälische Wilhelms University, Genetic Epidemiology, Institute for Human Genetics, Münster, Germany; [6]Max Delbrück Center for Molecular Medicine in the Helmholtz Association, Core Facility Electron Microscopy, Berlin, Germany; [7]Max Delbrück Center for Molecular Medicine in the Helmholtz Association, Advanced Light Microscopy, Berlin, Germany; [8]Division of Nephrology, Department of Medicine, Center for Human Disease Modeling, Duke University School of Medicine, Durham, United States; [9]DZHK (German Centre for Cardiovascular Research), Partner site Berlin, Berlin, Germany; [10]Department of Biochemistry, Maastricht University, Genetic Epidemiology and Statistical Genetics, Maastricht, The Netherlands

***For correspondence:** daniela.panakova@mdc-berlin.de (DP); reinhold.kreutz@charite.de (RK)

[†]These authors contributed equally to this work
[‡]These authors also contributed equally to this work

Competing interests: The authors declare that no competing interests exist.

Funding: See page 27

Received: 16 September 2018
Accepted: 20 March 2019
Published: 22 March 2019

Reviewing editor: Tim Aitman, University of Edinburgh, United Kingdom

Abstract Unraveling the genetic susceptibility of complex diseases such as chronic kidney disease remains challenging. Here, we used inbred rat models of kidney damage associated with elevated blood pressure for the comprehensive analysis of a major albuminuria susceptibility locus detected in these models. We characterized its genomic architecture by congenic substitution mapping, targeted next-generation sequencing, and compartment-specific RNA sequencing analysis in isolated glomeruli. This led to prioritization of transmembrane protein *Tmem63c* as a novel potential target. *Tmem63c* is differentially expressed in glomeruli of allele-specific rat models during onset of albuminuria. Patients with focal segmental glomerulosclerosis exhibited specific TMEM63C loss in podocytes. Functional analysis in zebrafish revealed a role for *tmem63c* in mediating the glomerular filtration barrier function. Our data demonstrate that integrative analysis of the genomic architecture of a complex trait locus is a powerful tool for identification of new targets such as *Tmem63c* for further translational investigation.
DOI: https://doi.org/10.7554/eLife.42068.001

Introduction

The analysis of the genetic basis of common diseases remains challenging due to their complex pathogenesis and genetic heterogeneity in human populations (***Deng, 2015***; ***Glazier et al., 2002***;

eLife digest The human kidneys filter the entire volume of the blood about 300 times each day. This ability depends on specialized cells, known as podocytes, which wrap around some of the blood vessels in the kidney. These cells control which molecules leave the blood based on their size. Normally large molecules like proteins are blocked, while smaller molecules including waste products, toxins, excess water and salts pass through into the urine.

If this filtration system is damaged, by high blood pressure, for example, it can lead to chronic kidney disease. A hallmark of this disease, often called CKD for short, is high levels of the protein albumin in the urine. Previous studies involving rats with high blood pressure have found several regions of the genome that contribute to high levels of albumin in the urine, including one on chromosome 6. However, this region contains several genes and it was unclear which genes affected the condition.

Schulz et al. set out to narrow down the list and find specific genes that might contribute to elevated albumin in the urine of rats with high blood pressure. This search identified the gene for a protein called TMEM63c as a likely candidate. This protein spans the outer membrane of podocyte cells. Analysis of kidney biopsies showed that patients with chronic kidney disease also had low levels of this protein in their podocytes. Further experiments, this time in zebrafish, showed that reducing the activity of the gene for *tmem63c* led to damaged podocytes and a leakier filter in the kidneys.

The results suggest that this gene plays an important role in the integrity of the kidneys filtration barrier. It is possible that faulty versions of this gene are behind some cases of chronic kidney disease. If this proves to be the case, a better understanding of the role of this gene may lead to new treatments for the condition.

DOI: https://doi.org/10.7554/eLife.42068.002

McCarthy et al., 2008). This applies also to elevated blood pressure (BP) or hypertension, as recent meta-analyses of genome-wide association studies (GWAS) identified more than 100 gene loci associated with BP (***Hoffmann et al., 2017***; ***Warren et al., 2017***). The effect size of the identified gene loci, however, is in general rather modest and less than 4% of the variance of BP phenotypes can be explained by these loci (***Hoffmann et al., 2017***; ***Warren et al., 2017***), while around 40% to 50% of the variability appears heritable (***Levy et al., 2007***; ***Miall and Oldham, 1963***). Considerable evidence supports a major role of the kidney in BP regulation, and for the renal damage such as albuminuria development as a consequence of long-term BP elevation (***Coffman and Crowley, 2008***; ***Mancia et al., 2013***). Interestingly, genetic risk scores deploying BP genetic variants predict also hypertensive target organ damage in the heart, cerebral vessels, and eye, while only little evidence exists for an effect on kidney damage (***Ehret et al., 2016***). In this regard, several inbred hypertensive rat models provide valuable complementary tools to uncover the genetics of kidney damage in hypertension (***Schulz and Kreutz, 2012***; ***Yeo et al., 2015***). These hypertensive models belong to the large panel of inbred strains that have been generated for a range of physiological and disease phenotypes by selective breeding (***Atanur et al., 2013***). Of interest, compensatory alleles that protect against hypertensive organ damage have also been inadvertently co-selected in this process and explain the impressive resistance of some hypertensive strains against target organ damage (***Jacob, 2010***; ***Jeffs et al., 1997***; ***Rubattu et al., 1996***; ***Schulz and Kreutz, 2012***; ***Yeo et al., 2015***). Quantitative trait loci (QTL) mapping strategies took advantage of these findings by intercrossing hypertensive strains with contrasting kidney damage phenotypes (***Schulz and Kreutz, 2012***). It remains challenging, however, to identify the molecular changes at a complex trait QTL that account for gene-gene or gene-environment interactions, incomplete penetrance, and epigenetic inheritance (***Buchner and Nadeau, 2015***; ***Deng, 2015***).

Here, we successfully overcome the obstacles of QTL mapping in rodents by analyzing two inbred hypertensive rat strains with contrasting kidney damage with albuminuria phenotypes. We used the Munich Wistar Frömter (MWF) rat as a suitable hypertensive model system to target the genetic basis of the albuminuria phenotype in contrast to the spontaneously hypertensive rat (SHR) representing a model that is protected against albuminuria development (***Schulz and Kreutz, 2012***;

G

Figure 1 continued

evaluation (**J**) vs. total glomerular number as previously estimated by the physical fractionator method (**K**). Total glomerular number (n = 7 each); GD (n = 11 each); values plotted: mean ±SD; two-tailed student's t-test; *p<0.0001 vs. SHR; **p=0.0024 vs. SHR.

DOI: https://doi.org/10.7554/eLife.42068.003

The following source data is available for figure 1:

Source data 1. Albuminuria in parental, consomic, and congenic rat strains.

DOI: https://doi.org/10.7554/eLife.42068.004

Source data 2. Glomerular density and total nephron number in parental, consomic, and congenic rat strains.

DOI: https://doi.org/10.7554/eLife.42068.005

van Es et al., 2011). Following initial QTL mapping in intercrosses of contrasting hypertensive strains (***Schulz and Kreutz, 2012***), we successfully combined conventional fine mapping using congenic strains with characterization of the genomic architecture in sub-QTLs by targeted next-generation sequencing (NGS), and compartment-specific RNA sequencing (RNA-Seq) analysis. This comprehensive approach allowed us to prioritize transmembrane protein *Tmem63c* as a novel positional target for albuminuria development among several candidates. Functional relevance of *Tmem63c* was supported by allele-specific and BP-independent differential glomerular expression during onset of albuminuria in allele-specific minimal congenic rat lines derived from the contrasting rat models. Loss of glomerular TMEM63C expression in podocytes of patients with focal segmental glomerulosclerosis (FSGS) provided strong evidence for translational relevance. Loss-of-function studies in zebrafish induced a glomerular filtration barrier (GFB) defect compatible with the albuminuria phenotype, which was rescued upon co-injection of zebrafish *tmem63c* mRNA or rat *Tmem63c* mRNA, showing not only the specificity of the observed knockdown phenotype, but also conservation of the gene's function across species. Ultrastructural analysis by electron microscopy, demonstrated severe morphological defects including podocyte damage with foot process effacement in *tmem63c*-

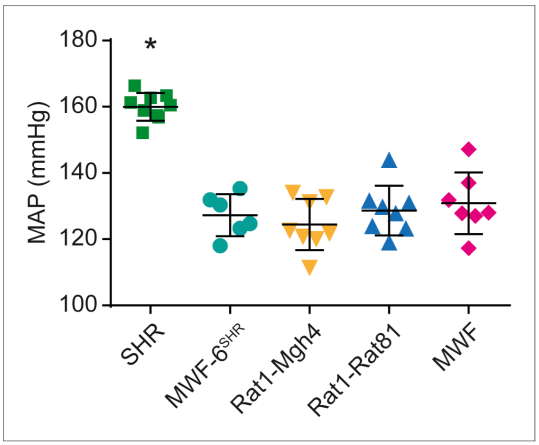

Figure 2. Mean arterial blood pressure (MAP) in consomic and congenic rat strains. Measurement of MAP is shown for SHR (n = 9), MWF-6^{SHR} (n = 6), congenic MWF.SHR-(*D6Rat1-D6Mgh4*) (Rat1-Mgh4, n = 8) and congenic MWF.SHR-(*D6Rat1-D6Rat81*) (Rat1-Rat81, n = 8) and MWF (n = 7) at week 14; values plotted: mean ±SD; one-way ANOVA with Bonferroni's post hoc analysis; *p<0.0001 vs. other strains, respectively.

DOI: https://doi.org/10.7554/eLife.42068.006

The following source data is available for figure 2:

Source data 1. Mean Arterial Pressure in parental, consomic, and congenic rat strains.

DOI: https://doi.org/10.7554/eLife.42068.007

H

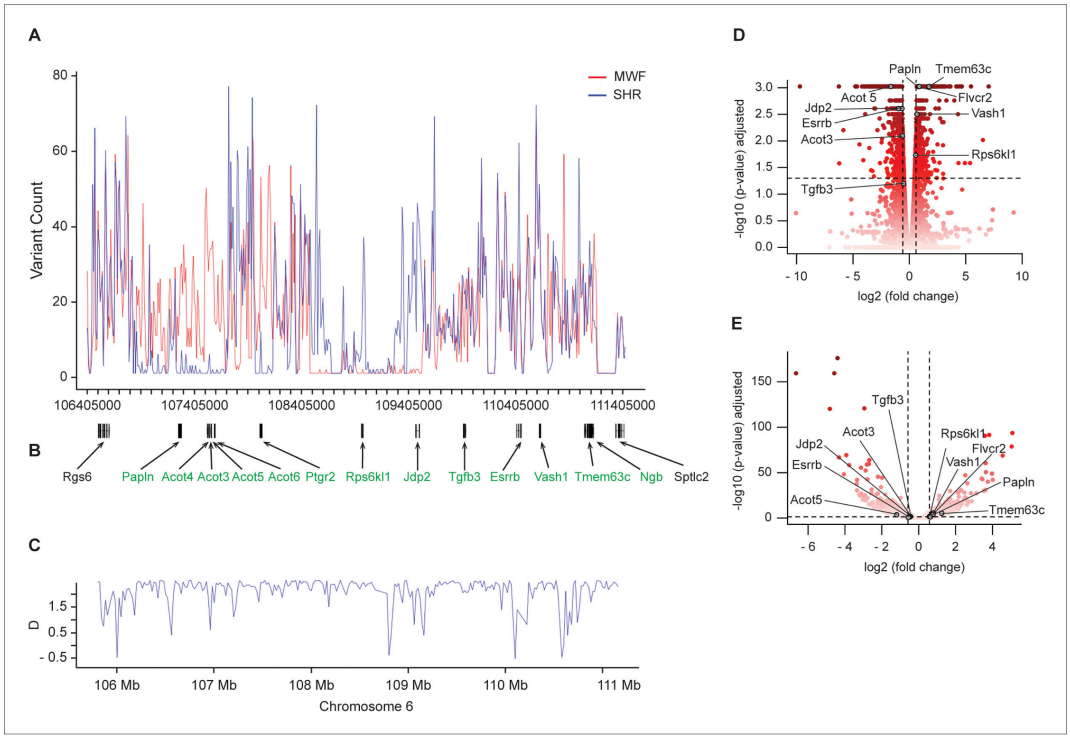

Figure 3. Next-generation sequencing (NGS) analysis of the kidney damage region on rat chromosome 6 and RNA sequencing (RNA-Seq) analysis in isolated glomeruli. (**A–B**) DNA sequencing (DNA-Seq) analysis revealed the numbers of DNA variants in comparison to the reference genome across the sequenced region for the Munich Wistar Frömter (MWF) and spontaneously hypertensive rat (SHR) strains (*n* = 3, each) (**A**). The physical map between nucleotide position 106,405,000 and 111,405,000 is shown together with positions of potential candidate genes (in green) (**B**); in addition, the two genes at the 5'-position and 3'-position of the candidate region are visualized in black. (**C**) The Tajima's D variation across the sequenced region. (**D–E**) Volcano plots illustrating the differential expression results (MWF vs. SHR) in RNA-Seq analysis in isolated glomeruli using the Cuffdiff (**D**) and DESeq2 (**E**) analysis tools. For each gene, the log10 transformed differential expression *P*-value adjusted for false discovery rate is plotted against the log2 transformed expression fold change. The color gradient refers to the P-values given on the y-axis. The applied significance threshold of adjusted p-value<0.05 is indicated as dashed horizontal line. Dashed vertical lines indicate fold changes > 1.5. Genes of interest are highlighted in grey and are annotated with gene symbols. (See ***Figure 3—figure supplement 1***).

DOI: https://doi.org/10.7554/eLife.42068.008

The following source data and figure supplement are available for figure 3:

Source data 1. Predicted effects of variants identified by NGS in the candidate region on rat chromosome 6 in human.

DOI: https://doi.org/10.7554/eLife.42068.010

Figure supplement 1. Venn diagram of NGS analysis.

DOI: https://doi.org/10.7554/eLife.42068.009

deficient embryos. Altogether, our findings reveal TMEM63C being integral to podocyte physiology, and identified its potential role in glomerular renal damage in patients with chronic kidney disease. Our data demonstrate, despite the difficulties of QTL analysis in experimental models such as inbred strains, the feasibility to identify novel targets by combining conventional congenic substitution mapping with integrative analysis of genomic architecture of identified susceptibility loci and functional studies.

Table 1. Significant variants in the candidate kidney damage region on rat chromosome 6.

Gene	Gene coordinates		Variant position	Variant type	Allelic variants		Amino acid exchange	Effect of sequence variant	PROVEAN score
	Start position (bp)	Stop position (bp)			MWF	SHR			
Acot4	107,517,668	107,522,952	107,518,131	exonic	A	G	Gly → Arg	non-synonymous	−5.660
Acot5	107,550,904	107,557,688	107,551,446	exonic	A	C	Arg → Ser	non-synonymous	−2.842
			107,551,528	exonic	A	G	Arg → His	non-synonymous	−2.646
			107,551,717	exonic	G	C	Pro → Arg	non-synonymous	−5.314
			107,557,092	exonic	A	T	Leu → Gln	non-synonymous	−5.291
Acot6	107,581,608	107,590,373	107,590,006	exonic	C	T	Leu → Pro	non-synonymous	−5.091
Ptgr2	108,009,251	108,029,859	108,029,833	exonic	T	C	Arg → Cys	non-synonymous	−3.672
Ngb	111,126,261	111,132,320	111,128,730	exonic	G	A	Leu → Pro	non-synonymous	−3.000
			111,131,291	exonic	ACT	A	NA	frameshift deletion	NA

MWF, Munich Wistar Frömter; SHR, spontaneously hypertensive rat. NA, not applicable.

DOI: https://doi.org/10.7554/eLife.42068.011

Results

Congenic substitution mapping in the MWF rat model refines the albuminuria QTL to a chromosomal region linked to both albuminuria and nephron deficit

We previously confirmed the pivotal role of a major albuminuria QTL on rat chromosome 6 (RNO6) in the MWF model by generating a consomic MWF-6^{SHR} strain, which carries RNO6 from the contrasting albuminuria-resistant SHR strain in the MWF genetic background (***Figure 1A–D***) (***Schulz et al., 2007***). In addition, MWF rats inherit a deficit in nephron (and glomeruli) number, which represents a predisposition for the development of both hypertension and kidney damage (***Wang and Garrett, 2017***). We performed congenic substitution mapping for both albuminuria and glomerular density phenotypes by generating eight congenic lines by introgression of nested chromosomal fragments from SHR onto the MWF genetic background, and compared the renal

Table 2. Presence of the frameshift deletion in inbred rat strains in neuroglobin (*Ngb*) at 111,131,291 bp.

Strain	Presence of deletion	Strain	Presence of deletion
ACI	no	MHS	no
BBDP	no	MNS	no
BN.Lx	no	SBH	no
EVE	no	SBN	no
F344/Ncrl	no	**SHR**	**yes**
FHH	no	**SHR/NHsd**	**yes**
FHL	no	**SHRSP/Gla**	**yes**
GK	**yes**	SR/Jr	no
LE/Stm	no	SS/Jr	no
LEW	no	SS_JRHSDMCWI	no
LEW/NcrlBR	no	WAG	no
LH	no	**WKY**	**yes**
LL	no	**WKY/Gla**	**yes**
LN	no	**WKY_NHSD**	**yes**

The inbred rat strains with presence of the *Ngb* frame shift deletion in bold belong to a clade of Wistar rat derived strains from Japan.

DOI: https://doi.org/10.7554/eLife.42068.012

J

Table 3. Genes in the candidate kidney damage region with differential expression in RNA-Seq analysis.

Gene	Start (bp position)	End (bp position)	ID	P(DeSeq2)	P(Cuffdiff)	Strain[a]
Acot3	107,531,528	107,536,789	ENSRNOG00000053460	0.09426742	0.00799931	SHR
Rps6kl1	108,961,994	108,976,489	ENSRNOG00000005530	0.024515465	0.0186294	MWF
Acot5	107,550,904	107,557,688	ENSRNOG00000032508	0.000234652	0.000948356	SHR
Papln	107,245,820	107,276,755	ENSRNOG00000009448	8.82E-05	0.000948356	MWF
Tmem63c	111,049,559	111,120,799	ENSRNOG00000011334	6.26E-06	0.000948356	MWF
Flvcr2	109,617,355	109,681,495	ENSRNOG00000008754	2.06E-06	0.000948356	MWF
Jdp2	109,466,060	109,505,161	ENSRNOG00000008224	0.052146312	0.00245615	SHR
Esrrb	110,410,141	110,455,906	ENSRNOG00000010259	0.278291584	0.00245615	SHR
Tgfb3	109,913,757	109,935,533	ENSRNOG00000009867	0.019914732	0.0632265	SHR
Vash1	110,624,856	110,637,382	ENSRNOG00000010457	0.070552875	0.00314268	MWF

MWF, Munich Wistar Frömter; RNA-Seq, RNA sequencing; SHR, spontaneously hypertensive rat. Genes shown in bold were found to be significantly differentially expressed using both CuffDiff and DeSeq2 analysis. [a] The strain name is given for upregulation of mRNA expression.

DOI: https://doi.org/10.7554/eLife.42068.016

phenotypes between congenic lines and the parental MWF strain (***Figure 1E,F***). We successfully narrowed the original region identified by QTL mapping, spanning about 55 Mb between genetic markers *D6Rat106* and *D6Rat9* (***Schulz et al., 2003***), to a smaller interval comprising 4.9 Mb between *D6Mgh4* and *D6Rat81* (***Figure 1E,F***). The comparison between the two informative congenic lines MWF.SHR-(*D6Rat1-D6Mgh4*) and MWF.SHR-(*D6Rat1-D6Rat81*) revealed that 95% of the difference in albuminuria and 89% of the difference in glomerular density observed between the MWF and consomic MWF-6^{SHR} strains is attributable to this interval (***Figure 1E,F***). Subsequently, we set out to analyze the BP phenotype by direct intra-arterial measurements in the two congenic lines in comparison to the MWF and SHR strains. This analysis revealed similar mean arterial BP values in the two congenic lines and parental MWF strain (***Figure 2***). This findings clearly indicate the UAE difference between MWF.SHR-(*D6Rat1-D6Mgh4*) and MWF.SHR-(*D6Rat1-D6Rat81*) are not attributable to BP differences (***Figure 2***). Thus, we dissected away a role of this region for BP regulation and show that both the albuminuria and glomerular density phenotype co-localize in the same refined locus (sub-QTL), supporting further exploration of this region as an independent candidate region for kidney damage. Direct comparison of glomerular density (***Figure 1G–J***) with the total glomerular number as previously estimated by the physical fractionator method (***Figure 1K***) (***Schulz et al., 2007***) confirmed the nephron deficit in MWF compared to SHR (***Figure 1J***, $p<0.0001$). We further demonstrated that this phenotype maps also to RNO6 (***Figure 1F***) when determined by glomerular density analysis in kidney sections (***Figure 1G–J***).

Targeted NGS analysis of the identified kidney damage candidate region

We employed targeted NGS on the region ranging from nucleotide positions 105,780,000 to 111,425,000 on RNO6. After genotype calling and comparing genotypes of consomic and congenic rats, we refined coordinates of the kidney damage locus from 106,400,000 bp to 111,360,000 bp (***Figure 3A,B***). This region contains 75 predicted protein-coding genes. In comparison to the reference genome (Rattus norvegicus, ENSEMBL rn6.0) (***Yates et al., 2016***), we identified 5,158 SNPs and 1893 small insertions and deletions (INDELs) in MWF, and 5326 single nucleotide polymorphisms (SNPs) and 1804 INDELs in SHR (***Figure 3—figure supplement 1***). Direct comparison between MWF and SHR revealed that both strains differ for 5376 SNPs and for 1613 INDELs (***Figure 3—figure supplement 1***), showing a remarkable pattern of stretches of variants either coming from the MWF or the contrasting SHR strain (***Figure 3A***). As selective sweeps have recently been reported as a consequence of inbreeding in rats (***Atanur et al., 2013***), we performed a formal analysis of selective processes such as directional selection or balancing selection, genetic hitchhiking, or introgression using the Tajima's D statistics (***Tajima, 1989***). We observe such traces of selection with the majority of Tajima's D values exceeding the generally accepted threshold of $D > 2$ (***Figure 3C***).

K

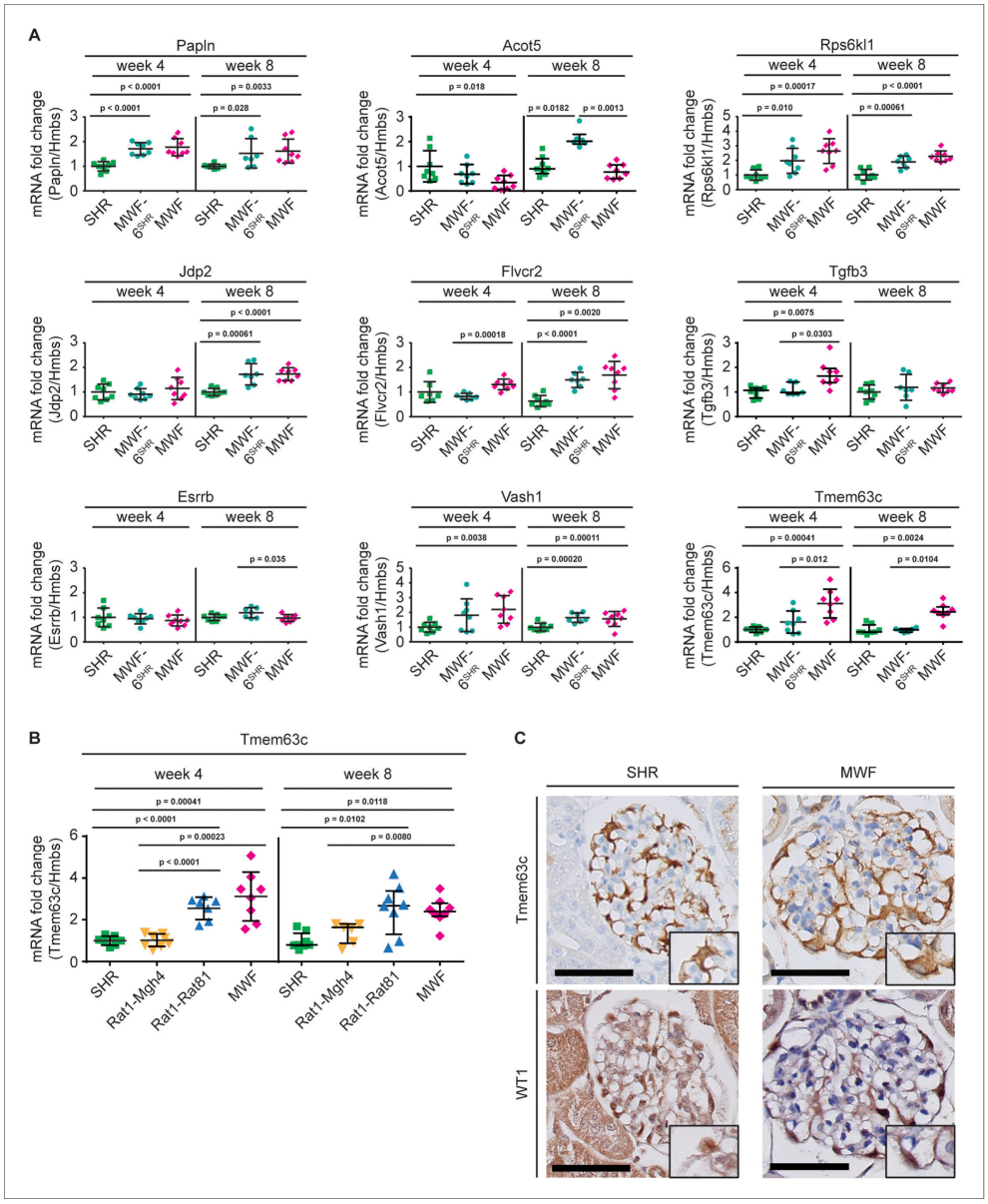

Figure 4. Validation of differentially expressed genes in isolated glomeruli by quantitative real-time PCR (qPCR) analysis. (**A**) qPCR analysis showed no consistent differential expression for eight genes from overall 10 genes identified with differential expression in RNA sequencing (RNA-Seq) analysis (***Table 3***) between parental Munich Wistar Frömter (MWF), spontaneously hypertensive rats (SHR), and consomic MWF-6^{SHR} during the crucial time window for onset of albuminuria between weeks 4 and 8. Only transmembrane protein 63c (*Tmem63c*) demonstrated differential mRNA expression at

Figure 4 continued on next page

Figure 4 continued

both time points. Acyl-CoA thioesterase 3 (*Acot3*) (***Table 3***) showed very low mRNA expression in qPCR analysis precluding quantitative analysis. Consequently, *Acot3* and the genes shown were excluded from and *Tmem63c* was included for further functional analysis. Rats per strain (n = 7–8, each); values for *Acot5* (week 8),*Tgfb3* (week 4) and *Tmem63c* (week 8) are plotted as median ±IQR, while the rest of data are plotted as mean ±SD; data for *Acot5* (week 8), *Tgfb3* (week 4) and *Tmem63c* (week 8) were analyzed using Kruskal-Wallis test with Dunn's post-hoc analysis and Mann-Whitney U test, while the rest of data was analyzed by one-way ANOVA with Bonferroni's post hoc analysis and Mann-Whitney U test. (**B**) mRNA expression analysis for *Tmem63c* in isolated glomeruli by qPCR analysis is shown for MWF, SHR, congenic MWF.SHR-(*D6Rat1-D6Mgh4*) (Rat1-Mgh4) and congenic MWF.SHR-(*D6Rat1-D6Rat81*) (Rat1-Rat81), at week 4 and week 8. Rats per strain (n = 6–8, each); data for week 8 are plotted as median ±IQR and analyzed using Kruskal-Wallis test with Dunn's post hoc analysis and Mann-Whitney U test; the other data are plotted as mean ±SD and analyzed by one-way ANOVA with Bonferroni's post hoc analysis and Mann-Whitney U test (**C**) Representative immunohistochemical stainings of TMEM63C and Wilms tumor 1 (WT1) on kidney sections from SHR and MWF at 8 weeks of age; the insert indicates expression in podocytes. Scale bar = 50 µm. Quantitative analysis of TMEM63C intensity in podocytes using one-way ANOVA revealed lower intensity in MWF (n = 7) vs. SHR (n = 6) at 8 weeks (p=0.0032).

DOI: https://doi.org/10.7554/eLife.42068.013

The following source data is available for figure 4:

Source data 1. Quantitative real-time PCR analysis of differentially expressed genes in isolated glomeruli between rat strains.

DOI: https://doi.org/10.7554/eLife.42068.014

Source data 2. Primer list for quantitative real-time PCR analysis.

DOI: https://doi.org/10.7554/eLife.42068.015

Functional annotation using PROVEAN scores identified eight potentially deleterious non-synonymous variants in five genes (***Table 1***). In addition, in the contrasting SHR reference strain one frameshift deletion was detected in the gene encoding neuroglobin (*Ngb*). However, this deletion is also present in the entire clade of SHR-related rat strains derived from one ancestor including other strains with normal urinary albumin excretion and normal kidney function (***Table 2***) (***Atanur et al., 2013***). Consequently, this frameshift deletion is not to be considered involved in the kidney damage phenotype and was not further pursued. Thus, we identified no obvious single candidate by NGS analysis in the sub-QTL.

Positional candidate gene identification by transcriptome analysis in isolated glomerular tissue by RNA-Seq

In order to identify other positional candidates at the sub-QTL on RNO6, we next embarked on RNA-Seq analysis in isolated glomeruli from MWF and SHR to assess global mRNA transcription patterns in the target compartment. We performed gene-based differential expression analysis using *Cuffdiff* and *DESeq2* software tools (***Figure 3D,E***). After correcting for multiple testing, 1838 genes were assigned a p-value<0.05 for *Cuffdiff* analysis and 1841 genes for *DESeq2*, respectively, yielding a total set of 2454 unique differentially expressed genes. When filtering the results for those genes residing in the candidate region, we identified a total of 10 genes to be significantly differentially expressed between MWF and SHR (***Table 3***, ***Figure 3D,E***) at significant p-values. These genes were taken forward to validation by quantitative real-time PCR (qPCR) analysis in isolated glomeruli obtained from the two parental and MWF-6^{SHR} consomic animals during onset of albuminuria occurring between 4 and 8 weeks of age (***Figure 4A***). This analysis revealed that from the nine genes, which could be analyzed, only *Tmem63c*, showed consistent and allele-dependent differential expression during the crucial time window (***Figure 4A,B***).

Tmem63c represents a positional candidate gene in MWF with differential glomerular expression

RNA-Seq and qPCR analysis indicated a significant 2.5- to 3-fold upregulation of *Tmem63c* mRNA expression in isolated glomeruli in the MWF model, which was abolished by transfer of RNO6 from SHR onto the MWF genetic background in the corresponding MWF-6^{SHR} consomic line (***Figure 4A***). Moreover, comparison of *Tmem63c* mRNA expression between the two informative congenic lines MWF.SHR-(*D6Rat1-D6Rat81*) and MWF.SHR-(*D6Rat1-D6Mgh4*) confirmed an allelic (cis) regulation of *Tmem63c* mRNA expression in MWF and SHR, and its association with albuminuria (***Figure 4B***). Further evaluation of the NGS data for *Tmem63c* in MWF and SHR revealed no significant sequence variants, with the exception of one detected variant in intron 18 (ENSRNOT00000015571) at

M

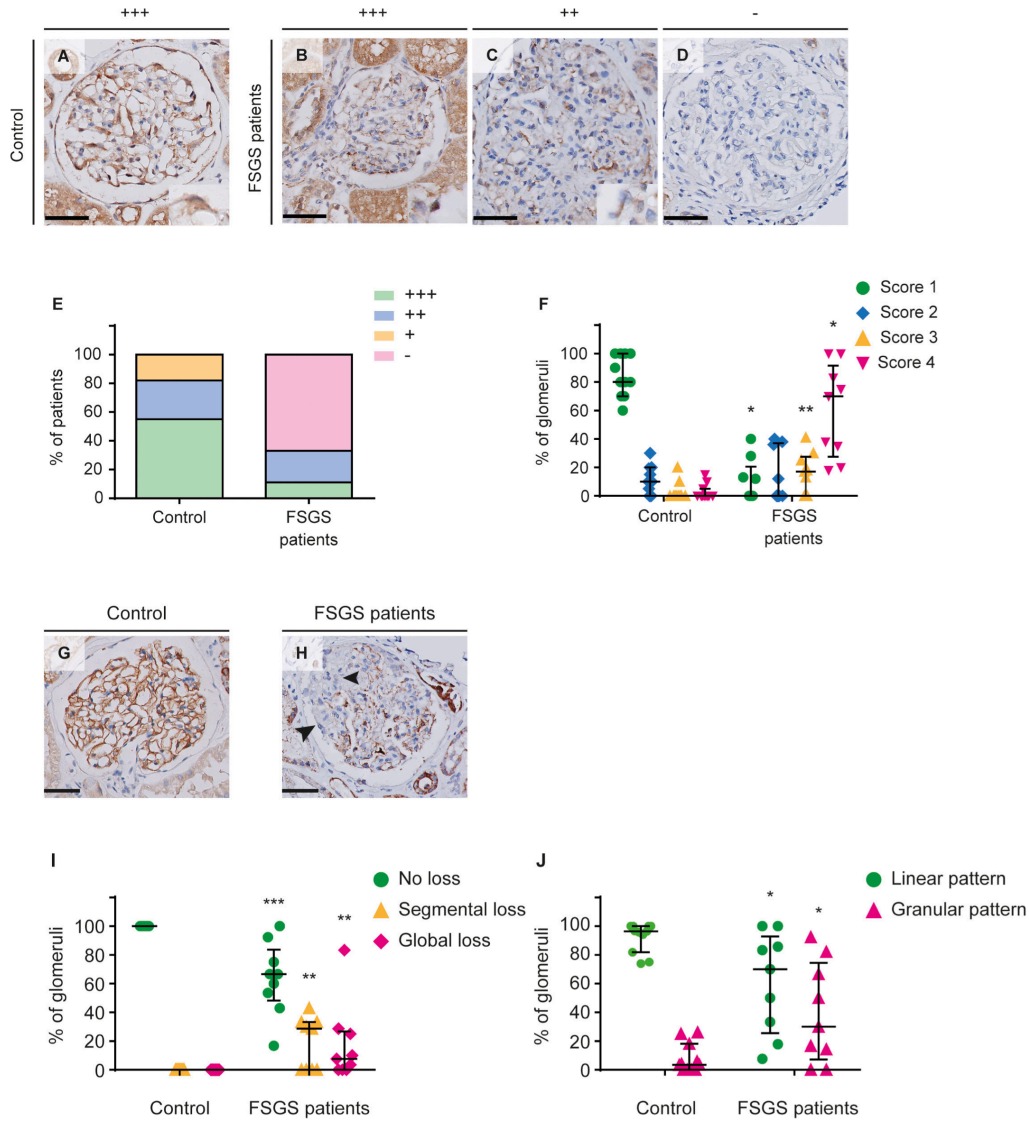

Figure 5. Transmembrane protein 63c (TMEM63C) protein and Nephrin expression deficiency in patients with focal segmental glomerulosclerosis (FSGS). (**A–D**) High-intensity TMEM63C staining in a glomerulus of a healthy human control subject (**A**) and representative glomeruli of FSGS patients with high (+++) (**B**), intermediate (+) TMEM63C staining intensity (**C**), or loss (-) of TMEM63C protein expression (**D**). The inserts indicate TMEM63C-positive podocytes. Scale bar = 50 µm. (**E**) Scoring of the TMEM63C staining intensity in controls (n = 11) and FSGS patients (n = 9). Percentage of cases with high intensity (green); intermediate intensity (blue); low intensity (yellow) and no TMEM63C staining (magenta). Linear-by-Linear association; p=0.005. (**F**) Scoring of the percentage of TMEM63C positivity in glomeruli. Green: no loss; blue:<25% loss; yellow: 25–50% loss; magenta:>50% loss of

Figure 5 continued on next page

N

Figure 5 continued

TMEM63C expression. Controls (n = 11) and FSGS patients (n = 9); values plotted: median ±IQR; Mann-Whitney U test; *p<0.0001 vs. control; **p=0.021 vs. control. (**G–J**) Linear nephrin staining in a glomerulus of a healthy human control subject (**G**) and segmental loss of nephrin staining in a glomerulus of a patient with FSGS (**H**), indicated by arrowheads. Nephrin expression was significantly reduced in patients with FSGS compared to healthy controls (**I**). Moreover, we observed a shift from a normal linear staining pattern, following the glomerular capillary wall, to a granular staining pattern (**H and J**). values plotted: median ±IQR; Mann-Whitney U test; *p=0.05 vs. control; **p<*0.01* vs. control; ***p<0.001 vs. controls.

DOI: https://doi.org/10.7554/eLife.42068.017

The following source data is available for figure 5:

Source data 1. TMEM63C intensity score and percentage of TMEM63C positivity in glomeruli in FSGS patients.

DOI: https://doi.org/10.7554/eLife.42068.018

Source data 2. Nephrin staining in FSGS patients.

DOI: https://doi.org/10.7554/eLife.42068.019

111,101,251 bp at a potential splice site position. However, when analyzing our RNA-Seq data concerning differential exon usage in *Tmem63c*, we found no significant difference in exon usage between both parental strains.

We then set out to perform immunohistochemistry analysis of TMEM63C in MWF kidney. This revealed TMEM63C expression in a podocyte-specific pattern (***Figure 4C***). In contrast to the clearly elevated mRNA expression in isolated glomeruli, this analysis indicated no elevated glomerular protein expression in MWF, and only somewhat lower TMEM63C protein expression in podocytes in MWF compared to SHR at onset of albuminuria at 8 weeks of age (***Figure 4C***).

Patients with focal segmental glomerulosclerosis exhibit loss of glomerular TMEM63C expression

Aging MWF rats develop histopathological changes similar to those observed in patients with FSGS (***Remuzzi et al., 1992***; ***Schulz and Kreutz, 2012***). Podocyte injury with the development of glomerular proteinuria represents a pivotal hallmark of FSGS (***D'Agati et al., 2011***; ***Lim et al., 2016***). Thus, we explored TMEM63C expression in patients with FSGS and healthy controls to evaluate its potential role for human kidney damage (***Yu et al., 2016***). This analysis demonstrated that TMEM63C is expressed in podocytes of all glomeruli in healthy controls (***Figure 5A,E***), while patients with FSGS exhibit a significant decrease of TMEM63C expression (***Figure 5B–E***) with a global loss of glomerular TMEM63C in the majority of patients analyzed (***Figure 5D–F***). In addition to TMEM63C expression, we analyzed the expression of nephrin protein as a pivotal component of the slit diaphragm of the GFB (***Figure 5G–J***) (***Kestilä et al., 1998***). Nephrin expression was also significantly reduced in patients with FSGS (***Figure 5H,I***), which is in accordance with previously published results (***Kim et al., 2002***). Moreover, we observed a shift from the normal linear staining pattern to a granular staining pattern as reported (***Figure 5H,J***) (***Doublier et al., 2001***; ***Wernerson et al., 2003***).

Knockdown of TMEM63C expression in human podocytes impairs cell viability and survival signaling

We further analyzed the effect of reduced *TMEM63C* expression in human podocytes in culture using small interfering RNA (siRNA) methodology (***Figure 6A***). We found significantly impaired cell viability in response to TMEM63C downregulation (***Figure 6B***). In addition, reduction of TMEM63C expression by siRNA decreased pro-survival signaling in human podocytes as indicated by reduced levels of pAKT (***Figure 6C***), and increased pro-apoptotic transition of cytochrome C from mitochondria to the cytoplasm (***Figure 6D***).

Functional analysis of *tmem63c* in zebrafish

To assess the functional role of *tmem63c* for albuminuria development, we utilized the transgenic zebrafish line *Tg[fabp10a:gc-EGFP]* (***Zhou and Hildebrandt, 2012***). This model expresses a vitamin D binding protein tagged with enhanced green fluorescent protein (gc-EGFP) in the liver, from which it is released into the blood stream and circulates under the normal conditions in the blood (***Figure 7A,G***). Upon GFB damage, gc-EGFP leaks through the glomerular filtration barrier, indicated by a marked decrease in fluorescence in the trunk vasculature of *Tg[fabp10a:gc-EGFP]* embryos

O

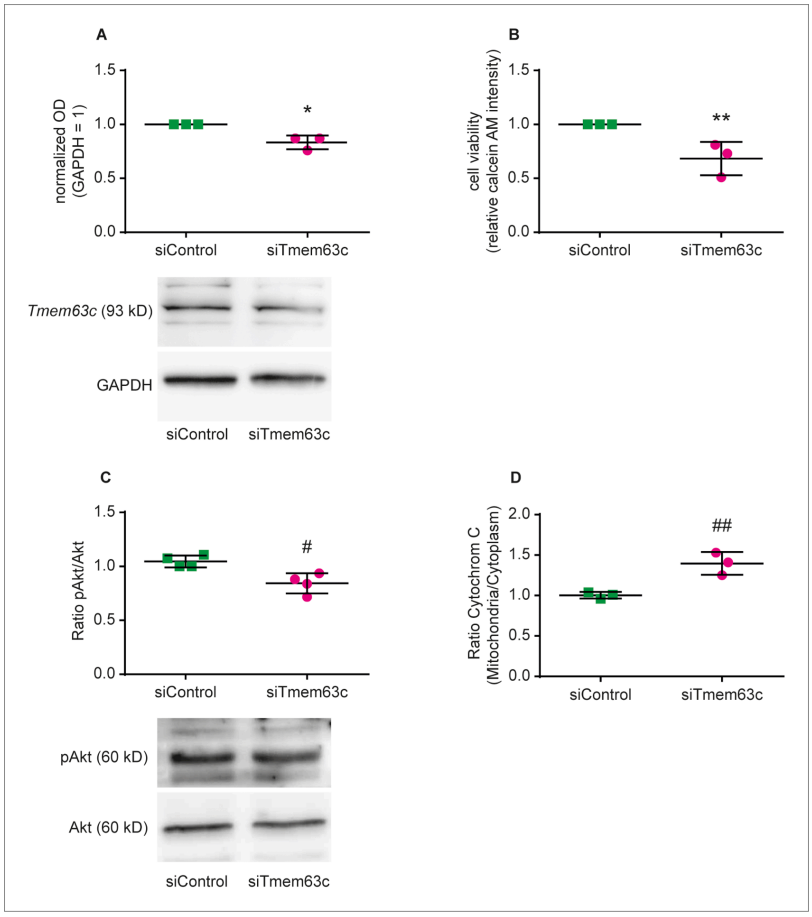

Figure 6. Functional role of TMEM63C in human podocytes (hPC) in vitro. Shown is the impact of siRNA-mediated inhibition of TMEM63C (siTMEM63C) or treatment of hPC with a corresponding nonsense negative control (siControl). (**A**) TMEM63C protein expression normalized against GAPDH as a loading control (*p=0.011). Shown is a representative Western blot. (**B**) Cell viability determined via measurement of calcein acetoxymethyl (AM) fluorescence intensity in hPC (**p=0.024). (**C**) Phosphorylation state of protein kinase B (pAKT) normalized against the expression of total AKT (AKT) ($^{\#}$p=0.0094). Shown is a representative Western blot, GAPDH is used as a loading control. (**D**) Pro-apoptotic cytochrome C transition from mitochondria to the cytoplasm of hPC ($^{\#\#}$p=0.0096). The mean ±SD of at least three independent experiments is shown, respectively. Two-tailed Student´s *t*-test was performed for all experiments.

DOI: https://doi.org/10.7554/eLife.42068.020

The following source data is available for figure 6:

Source data 1. TMEM63C expression in human podocytes using small interfering RNA (siRNA) methodology.

DOI: https://doi.org/10.7554/eLife.42068.021

mimicking an albuminuria-like phenotype (***Figure 7A***). To reduce *tmem63c* levels in developing zebrafish embryos, we used the morpholino knockdown technology as well as CRISPR/Cas9-mediated somatic mutagenesis (***Bassett et al., 2013***; ***Burger et al., 2016***) (***Figure 7B***). In both morpholino-injected embryos and crispants (CRISPR/Cas9-mediated somatic mutants), loss of *tmem63c* did

P

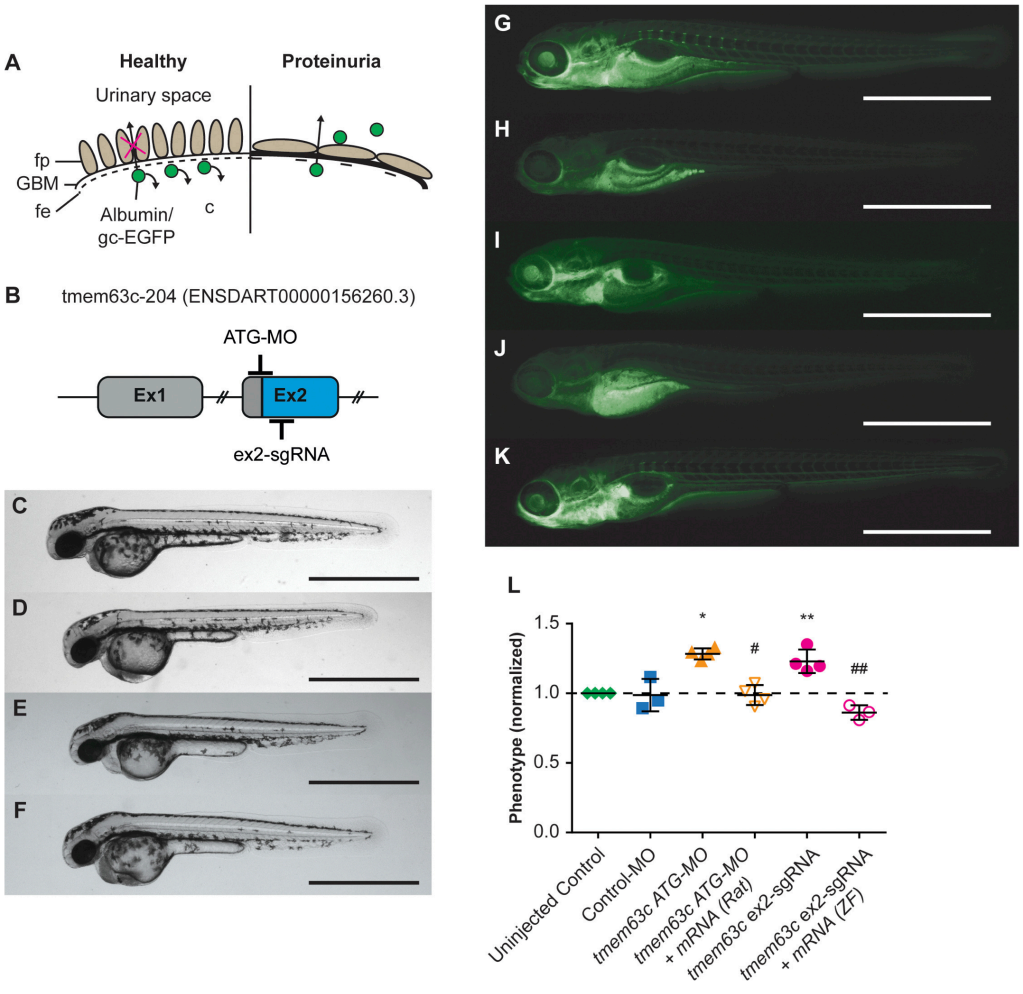

Figure 7. Functional assessment of the glomerular filtration barrier (GFB) after loss of transmembrane protein 63c (*tmem63c*) in zebrafish. (**A**) Scheme of the GFB in healthy and albuminuric zebrafish embryos. Green fluorescent protein (gc-EGFP) represents an albumin surrogate and is filtrated after impairment of the GFB. fe, fenestrated endothelium; fp, foot processes of podocytes; GBM, glomerular basement membrane. (**B**) Schematic of *tmem63c* showing the target regions in Exon 2 (ex2) used for Morpholino (MO)- and CRISPR/Cas9-mediated somatic mutagenesis. (**C–F**) Bright field view of wildtype embryos at 48 hr post-fertilization (hpf) in uninjected controls (**C**), ATG-MO injected (**D**), 159.6 ng/µl ex2-sgRNA injected (**E**), and 250 ng/µl ex2-sgRNA injected embryos (**F**). Scale bar = 1 mm. (**G–K**) Fluorescence microscopy of *Tg[fabp10a:gc-EGFP]* embryos at 120 hpf. Uninjected control with clearly visible gc-EGFP fluorescence in the trunk vasculature ('fluorescent') (**G**). *tmem63c* ATG-MO-injected embryo with partial or a complete loss of trunk fluorescence ('deficient-fluorescent') (**H**) and *tmem63c* ATG-MO +*Tmem63c* mRNA (Rat) co-injected embryo (**I**) showing rescue of the phenotype. *Tmem63c* ex2-sgRNA-injected embryo with partial or a complete loss of trunk fluorescence ('deficient-fluorescent') (**J**) and *tmem63c* ex2-sgRNA + *tmem63c* mRNA (ZF) co-injected embryo (**K**) showing rescue of the phenotype. Scale bar = 1 mm. (**L**) Analysis of gc-EGFP in the trunk vasculature. Shown are embryos categorized as 'deficient-fluorescent' (df), see Materials and method section and ***Figure 7—figure supplement 2*** for details. Experimental groups are normalized to the corresponding uninjected control group per experiment. Uninjected Control (n = 1198); Control-MO

Figure 7 continued on next page

Figure 7 continued

(*n* = 189); *tmem63c* ATG-MO (*n* = 227); tmem63c ATG-MO +Tmem63c mRNA (Rat) (*n* = 230); *tmem63c* ex2-sgRNA (*n* = 371); *tmem63c* ex2-sgRNA + *tmem63c* mRNA (ZF) (*n* = 126); One-way ANOVA with Bonferroni's multiple comparisons test. Values plottet: mean ±SD, dashed line at y = 1 indicates the uninjected control level; *p=0.0002 vs. uninjected Control, #p<0.0001 vs. *tmem63c* ATG-MO. **p=0.0014 vs. uninjected Control, ##p<0.0001 vs. *tmem63c* ex2-sgRNA. Data points in the graph represent the ratio per independent experiment, %(Uninjected Control (df)) / % (experimental group (df)), N ≥ 3. (See ***Figure 7—figure supplement 1*** and ***Figure 7—figure supplement 2***).

DOI: https://doi.org/10.7554/eLife.42068.022

The following source data and figure supplements are available for figure 7:

Source data 1. Functional assessment of the GFB after tmem63c-knockdown using tmem63c ex2-sgRNA and ex2-sgRNA and tmem63c ATG-MO.

DOI: https://doi.org/10.7554/eLife.42068.026

Figure supplement 1. Functional assessment of the glomerular filtration barrier (GFB) in *Tg[fabp10a:gc-EGFP]* zebrafish embryos.

DOI: https://doi.org/10.7554/eLife.42068.023

Figure supplement 1—source data 1. Functional assessment of the GFB after tmem63c-knockdown using tmem63c ex2-sdMO.

DOI: https://doi.org/10.7554/eLife.42068.024

Figure supplement 2. Excerpt from sequence alignment of *tmem63c* mRNA zebrafish (NM_001159836) vs *Tmem63c* mRNA rat (NM_001108045.1).

DOI: https://doi.org/10.7554/eLife.42068.025

not result in any visible developmental malformations apart from mild pericardial edema (***Figure 7C–F***). Knockdown of *tmem63c* using morpholino technology resulted in a significant decrease in gc-EGFP fluorescence in the trunk vasculature at 120 hr post fertilization (hpf) (***Figure 7H***). We corroborated this finding in *tmem63c* crispants (***Figure 7J***, ***Figure 7—figure supplement 1D***) as well as by using another splice-blocking morpholino (***Figure 7—figure supplement 1E–I***); both experiments showed a similar albuminuria-like phenotype. To verify the specificity of the observed phenotype rescue experiments were carried out by co-injection of zebrafish *tmem63c* mRNA with *tmem63c* sgRNA/Cas9 complexes and rat *Tmem63c* mRNA (mRNA sequence identity vs. zebrafish = 65.82% (Clustal 2.1), ***Figure 7—figure supplement 2***) with *tmem63c* ATG-MO, respectively. For both cases similarly, the albuminuria-like phenotype could be specifically rescued proving knockdown specificity on the one hand and functional conservation of *tmem63c* across species on the other hand (***Figure 7I,K and L***). Our data indicate that *tmem63c* may regulate the GFB integrity.

To understand the possible functional changes in GFB in more detail, we deployed electron microscopy to visualize the GFB ultrastructure in embryos with reduced *tmem63c* levels. We observed significant changes in podocyte foot process morphology manifested by foot process effacement (***Figure 8A–C***). Quantitative analysis in *tmem63c* crispants revealed a significant increase in the foot process width compared to uninjected controls and Cas9-controls (***Figure 8D***) with concomitant significant decrease of the number of slit diaphragms per µm glomerular basement membrane (GBM) (***Figure 8E***). To analyze, whether the observed albuminuria-like phenotype upon *tmem63c*-deficiency is associated with the loss of podocytes, we utilized confocal microscopy to image glomeruli of *Tg(wt1b:EGFP)* embryos. In this analysis, *tmem63c* crispants (*tmem63c* ex2-sgRNA) showed a widened Bowman's space and increased glomerular volumes compared to uninjected controls (133457 ± 59547 μm^3 vs 67067 ± 21933 μm^3, p=0.04) as quantified by 3D surface reconstruction. In addition, we observed dilated capillary loops in the crispants (***Figure 8F–H***). Quantification of podocyte cell number in embryos with reduced *tmem63c* levels revealed no changes in absolute cell number (***Figure 8I***, ***Videos 1–3***), while relative podocyte cell number normalized to the total glomerular volume was significantly decreased compared to uninjected controls (***Figure 8J***, ***Videos 1–3***). Collectively, our data indicate the conserved role for *tmem63c* in GFB function between fish, rodents, and humans.

Discussion

Previous genetic analysis in the fawn-hooded hypertensive (FHH) rat model led to the identification of naturally occurring genetic variants in RAB38, member RAS oncogene family (*Rab38*), and shroom family member 3 (*Shroom3)* that successfully complemented studies in humans supporting their role for albuminuria (***Rangel-Filho et al., 2013***; ***Yeo et al., 2015***). Interestingly, the genetic variant in *Rab38* was linked to altered tubular (***Rangel-Filho et al., 2013***; ***Teumer et al., 2016***), and the variant

R

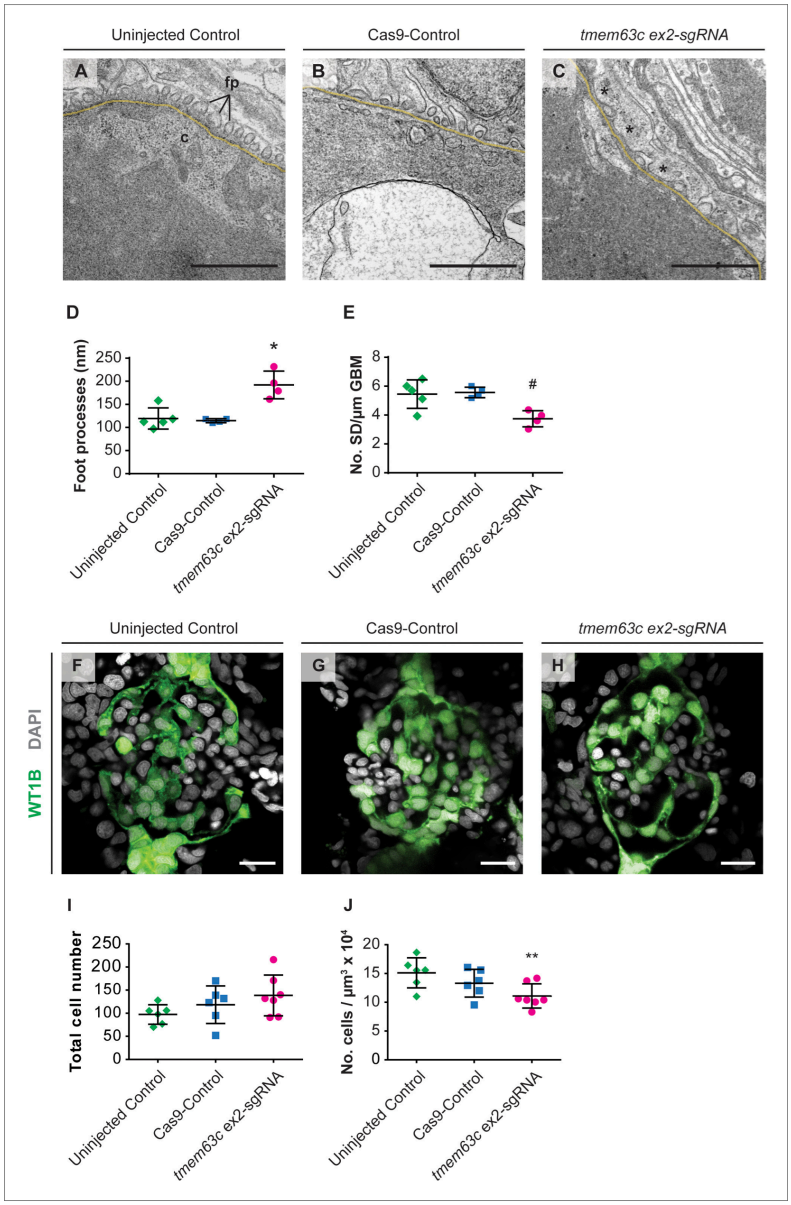

Figure 8. Ultrastructural and morphological analysis of glomerular structures after loss of *tmem63c* in zebrafish. (**A–E**) Electron microscopy and quantitative assessment of GFB ultrastructure. Representative electron microscopy pictures of the GFB in uninjected Controls (**A**), Cas9-Controls (**B**) and after *tmem63c* knockdown (**C**), asterisks indicate effaced podocyte foot processes). Quantitative analysis of podocyte foot process width (**D**) and number of slit diaphragms per µm GBM (**E**). Uninjected Control (n = 5); Cas9-Control (n = 4); *tmem63c* ex2-sgRNA (n = 4); Scale bar = 1 µm; values

Figure 8 continued on next page

S

Figure 8 continued

plottet: mean ±SD; One-way ANOVA with Bonferroni's multiple comparisons test; *p=0.0019 vs. uninjected Control, *p=0.0017 vs Cas9-Control; # p=0.0171 vs. uninjected Control, # p=0.0148 vs. Cas9-Control. (**F–J**) Confocal microscopy and analysis of absolute and relative podocyte cell number in *Tg(wt1b:EGFP)* at 96 hpf. Representative confocal microscopy pictures of glomeruli in uninjected Controls (**F**), Cas9-Controls (**G**) and after *tmem63c* knockdown (**H**). Quantitative analysis of absolute (**I**) and relative (**J**) podocyte cell number. Relative podocyte cell number has been obtained after normalization to the glomerular volume. Uninjected Control (*n* = 6); Cas9-Control (*n* = 6); tmem63c ex2-sgRNA (*n* = 7); Scale bar = 15 µm; values plottet: mean ±SD; One-way ANOVA with Bonferroni's multiple comparisons test; **p=0.0421 vs. uninjected Control.

DOI: https://doi.org/10.7554/eLife.42068.027

The following source data is available for figure 8:

Source data 1. Tables and legends.

DOI: https://doi.org/10.7554/eLife.42068.028

in *Shroom3* to altered glomerular (***Yeo et al., 2015***) albumin handling. Thus, animal models have been proven useful not only for the explanation of missing heritability (***Chatterjee et al., 2013***), but also for the elucidation of the differences between glomerular and tubular origins of albuminuria (***Rangel-Filho et al., 2013***; ***Yeo et al., 2015***). Currently, in GWAS meta-analyses in general population cohorts, only cubilin (*CUBN*) has been significantly associated with albuminuria (***Böger et al., 2011***). In addition, variants in *HS6ST1* and near *RAB38/CTSC* were implicated in albuminuria in patients with diabetes (***Teumer et al., 2016***). Nevertheless, in parallel to the findings obtained in BP GWAS (***Hoffmann et al., 2017***; ***Warren et al., 2017***), only a small fraction of the estimated heritability of albuminuria can be attributed to the identified genes (***Langefeld et al., 2004***; ***Teumer et al., 2016***). The MWF rat, in which we identified at least 11 albuminuria QTL, highlights the polygenic nature of complex traits such as kidney damage with albuminuria in hypertension (***Schulz and Kreutz, 2012***). Here, we focused on a major albuminuria QTL (***Schulz and Kreutz, 2012***; ***Schulz et al., 2003***) and refined the candidate region to a sub-QTL comprising 4.9 Mb. We confirmed that both the albuminuria and the nephron deficit phenotype map to the same genomic region supporting a genetic link between albuminuria and embryonic/fetal nephron development (***Wang and Garrett, 2017***). In addition, the informative congenic lines with differential albuminuria development showed similar BP values by which we showed that this genomic region affects albuminuria development independently from BP changes. In the targeted NGS analysis, multiple non-deleterious variants but no clear candidate was identified. However, significant signs of selective sweeps in this region, potentially leading to an enrichment of multiple non-deleterious alleles due to genetic hitchhiking, were detected. This is in agreement with a recent systematic genome sequencing study of laboratory inbred rat strains indicating that private single-nucleotide variants are highly concentrated in a small number of discrete regions of the genome (***Atanur et al., 2013***). The authors of this report hypothesized that variants that are unique to a single strain reside within these regions because many of these regions were positively selected in the initial phenotype-driven derivation of these strains. Surprising - and challenging however - remains our observation that no obvious causative variant for the kidney damage phenotype was observed in our targeted NGS analysis. Notwithstanding, complex traits

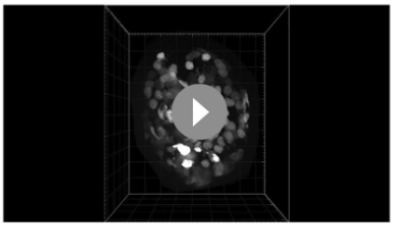

Video 1. Representative spot segmentation of podocyte nuclei and 3D surface reconstruction of glomeruli in uninjected controls of *Tg(wt1b:EGFP)* zebrafish embryos. The videos show a maximum intensity projection of the masked DAPI channel acquired by confocal microscopy of *Tg(wt1b:EGFP)* zebrafish embryos at 96 hpf. The DAPI channel of $DAPI^+/EGFP^+$-cells visualized here represents podocyte nuclei. Blue spots show the podocyte nuclei identified by software-based spot segmentation. Spots were counted for quantification of the absolute podocyte cell number. The grey surface represents the 3D surface reconstruction of glomeruli containing all $DAPI^+/EGFP^+$ nuclei, which was used for quantification of the total glomerular volume. Shown here are representative analysis results of uninjected controls (***Video 1***), Cas9-Controls (***Video 2***) and *tmem63c* ex2-sgRNA-injected embryos (***Video 3***).

DOI: https://doi.org/10.7554/eLife.42068.029

T

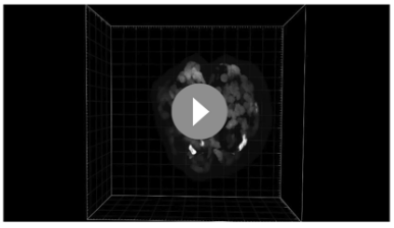

Video 2. Representative spot segmentation of podocyte nuclei and 3D surface reconstruction of glomeruli in Cas9 - injected controls (Cas9 - controls) of Tg(wt1b:EGFP) zebrafish embryos.
DOI: https://doi.org/10.7554/eLife.42068.030

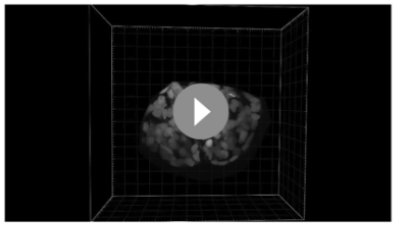

Video 3. Representative spot segmentation of podocyte nuclei and 3D surface reconstruction of glomeruli in *tmem63c* ex2-sgRNA - injected Tg(wt1b:EGFP) zebrafish embryos
DOI: https://doi.org/10.7554/eLife.42068.031

can also be a consequence of gene expression changes resulting in dysregulation of physiological pathways, a concept which becomes increasingly recognized as RNA sequencing is employed to distinguish tissue-specific gene expression patterns in a variety of complex diseases (***Joehanes et al., 2017***; ***Kirsten et al., 2015***).

We therefore complemented the DNA re-sequencing by compartment-specific RNA-Seq analysis which is rational, because MWF rats develop early glomerular changes that precede albuminuria development and show early podocyte injury in parallel with the onset of albuminuria (***Ijpelaar et al., 2008***). We identified *Tmem63c* as a positional candidate based on its mRNA expression pattern with differential glomerular expression in allele-specific rat models. Immunohistochemistry analysis in MWF kidneys identified TMEM63C protein in podocytes, and in contrast to the observed marked glomerular mRNA upregulation only a modest downregulation. Bioinformatics analysis of our NGS and RNA-Seq data has not yet provided a potential explanation for this discrepancy, for example interstrain differences related to exon usage or other events shown to mediate protein expression control on the post-transcriptional level. The relationship between protein levels and their coding transcripts is, however, rather complex and factors such as spatial and temporal variations of mRNAs, as well as the local availability of resources for protein biosynthesis, strongly influence this relationship (***Liu et al., 2016***). Spatial variation in expression regulation during renal injury development could be specifically important in podocytes due to their unique ultrastructural and molecular anatomy (***Endlich et al., 2017***). To explore the potential clinical relevance of TMEM63C for kidney damage, we selected patients with FSGS because they mirror the disease pattern observed in the MWF model (***D'Agati et al., 2011***; ***Lim et al., 2016***; ***Yu et al., 2016***). Importantly, patients with FSGS exhibit a significant decrease of TMEM63C protein levels in podocytes with a global loss of glomerular expression in the majority of patients. Furthermore, the loss of TMEM63C was associated with a decrease and altered granular staining pattern of nephrin protein in glomeruli of FSGS patients as previously reported (***Doublier et al., 2001***; ***Wernerson et al., 2003***). The latter has been previously shown to correspond to the degree of foot process effacement (***Wernerson et al., 2003***). While our data cannot establish a functional link between changes in nephrin and TMEM63c in FSGS, they nonetheless demonstrate a concomitant deficiency of both proteins in this setting.

To further validate *Tmem63c*, we tested its functional relevance for albuminuria development in zebrafish (*Danio rerio*). Our data confirm that in both *tmem63c* morphants and crispants, loss of *tmem63c* leads to a phenotype indicative of a GFB defect. Importantly, rescue of the observed phenotypes in zebrafish with rat *Tmem63c* mRNA pointed to the functional conservation across species. Ultrastructural analysis in zebrafish embryos demonstrated the role of *tmem63c* for the GFB integrity by revealing overt effacement of podocyte foot processes upon gene deficiency. Further structural analysis by confocal microscopy revealed dilated capillary loops and enlarged glomerular volumes with a reduction of relative podocyte number in relation to glomerular volume (podocyte density) in *tmem63c*-deficient embryos. Thus, our data reveal an important role of *tmem63c* for normal development of capillary structure and podocyte function of the glomerulus in zebrafish.

U

Tmem63c belongs to the TMEM (transmembrane protein) gene family comprising more than 300 different proteins with about 580 transcript variants (**Wrzesiński et al., 2015**). These proteins are predicted components of cellular membranes. However, the function of the majority of TMEM proteins - including *Tmem63c* - is currently unclear. There are no previous reports that demonstrate TMEM63C expression in the kidney, while assessment of the human protein atlas database indicates TMEM63C expression in human kidney in both the glomerular and tubular compartments (**Lundberg et al., 2010**); 'Tissue expression of TMEM63C - Staining in kidney' - **The Human Protein Atlas, 2019**; **Uhlén et al., 2015**). T*mem234*, another member of the TMEM family, may represent a component of the basal membrane of podocytes and has recently been associated with proteinuria development in zebrafish (**Rodriguez et al., 2015**). The mechanism by which changes in *Tmem63c* expression cause podocyte damage and thus contribute to the final common pathway of injury in FSGS (**De Vriese et al., 2018**) remains however unclear and cannot be elucidated by our current analysis. Accordingly, our data do not allow to describe possible interactions between TMEM63c and the heterogeneous group of known causative FSGS genes. Nevertheless, previous reports suggested that T*mem63c* and two other genes of the tmem63-family, i.e. *Tmem63a* and *Tmem63b*, are mammalian homologues of the hyperosmolarity-activated cation channel proteins AtCSC1 and its paralogue OSCA1 in plants (**Hou et al., 2014**; **Zhao et al., 2016**). Based on these reports, it appeared tempting to speculate that Tmem63c may be involved in mechanosensing in podocytes providing thus a functional basis for interactions with cytoskeleton genes or slit pore proteins, for example nephrin, in podocytes. However, the potential role of Tmem63c as a hyperosmolarity-activated cation channel remains controversial, since the activation by hyperosmolarity was not confirmed in a more recent study (**Murthy et al., 2018**). Moreover, the latter report indicated that *Tmem63c* is phylogenetically divergent from *Tmem63a* and *Tmem63b* and lacks their function to induce stretch-activated ion currents. Consequently, further studies are needed to characterize the functional role of *Tmem63c* and to explore its potential to influence podocyte function as a novel target for therapeutic intervention (**Endlich et al., 2017**; **Forst et al., 2016**; **Wieder and Greka, 2016**). In contrast to our experiments in zebrafish, in the explorative analysis in biopsies of FSGS patients we cannot differentiate between a primary (causative) or secondary effect of TMEM63C expression loss in patients. Nevertheless, taken together with our experimental analysis, the data clearly support *Tmem63c* as a novel candidate for further translational research on kidney damage.

Materials and methods

Key resources table

Reagent type (species) or resource	Designation	Source or reference	Identifiers	Additional information
Antibody	anti-TMEM63C	Perbio Science Germany; this paper	epitope: GLRGFAREL DPAQFQEGLE	1:1600 for rat tissue, 1:800 for human biopsies
Antibody	rabbit anti-WT1	Santa Cruz	RRID:AB_632611	1:500
Antibody	rabbit anti-nephrin	Abcam	RRID:AB_944400	1:750
Antibody	Goat anti-rabbit EnVision HRP conjugate	Dako		
Antibody	GAPDH	Calbiochem		
Antibody	AKT	Merck Chemicals GmbH		
Antibody	phospho-AKT Ser_{473}	Merck Chemicals GmbH		
Biological sample (*Homo sapiens*)	Renal biopsy samples of patients with FSGS	archive of the Department of Pathology of the Leiden University Medical Center (LUMC)		For patient information see Table 4

Continued on next page

Continued

Reagent type (species) or resource	Designation	Source or reference	Identifiers	Additional information
ell line (*Homo sapiens*)	hPC	***Saleem et al., 2002***	RRID:CVCL_W186	
Gene (*Danio rerio*)	*tmem63c*	NA	ZFIN: ZDB-GENE-120928–2	
Gene (*Homo sapiens*)	*TMEM63C*	NA	Ensembl: ENST00000298351.4	
Gene (*Rattus norvegicus*)	*Tmem63c*	NA	Ensembl: ENSRNOT00 000015571.6	
Other	DAPI stain	Sigma Aldrich		stock solution 1 mg/ml diluted 1:2000 in PBS
Other	DNA-Seq database	this paper	GEO and SRA: Submission ID: SUB2950675 and BioProject ID: PRJNA398197	See Data availability
Other	RNA-Seq database	this paper	GEO and SRA: accession GSE102546	See Data availability
Recombinant DNA reagent	*tmem63c* (cDNA) zebrafish	this paper		Infusion cloning primer sequences for cDNA synthesis: forward: GCTTGATATC GAATTCATG GCGTTTGAGTCCT GGCCTGC; reverse: CGGGCTGCAGGA ATTCTCACTGAA AAGCCACCGGACTG; Sequence additional primer for amplification of ORF: GTGCAGAAAC TAATGAAGCTGG; Progenitors: *tmem63c* (cDNA); pBluescript II SK(+)
Sequence-based reagent	*tmem63c* ATG-MO	Gene Tools LLC Philomath		sequence: 5'-CAGGCCAGGAC TCAAACGCCATTGC-3'
Sequence-based reagent	*tmem63c* ex2-sdMO	Gene Tools LLC Philomath		sequence: 5'-TGTTATCATAGATGA TGTACCAGCC-3'
Sequence-based reagent	*tmem63c* ex2-sgRNA	this paper		Sequence synthesis forward primer with CRISPR target site underlined: GAAATTAATACGACT CACTATAGGACGTC AGGAGTTTCCTGAGTT TTAGAGCTAGAAATAGC
Sequence-based reagent	*tmem63c* ex2-sgRNA primers flanking CRISPR target site	BioTez Berlin-Buch GmbH		Sequences: forward: CAAATGGTGAAC ACTTGTGAATC, reverse: CTGCGGTT TACTGCGGAGATG
Sequence-based reagent	siTMEM63C	Sigma-Aldrich Chemie GmbH		
Strain, strain background (*Danio rerio*)	*Tg(fabp10a:gc-EGFP)*	***Zhou and Hildebrandt, 2012***		

Continued on next page

W

Continued

Reagent type (species) or resource	Designation	Source or reference	Identifiers	Additional information
Strain, strain background (*Danio rerio*)	*Tg(wt1b:GFP)*	***Perner et al., 2007***		
Strain, strain background (*Rattus norvegicus*)	MWF/Rkb	Own colony Charité – Universitätsmedizin Berlin, Germany	http://dels.nas.edu/ilar/ (laboratory code Rkb); ***Schulz and Kreutz, 2012***; RRID:RGD_724569	
Strain, strain background (*Rattus norvegicus*)	SHR/Rkb	Own colony Charité – Universitätsmedizin Berlin, Germany	http://dels.nas.edu/ilar/ (laboratory code Rkb); ***Schulz and Kreutz, 2012***; RRID:RGD_631696	
Strain, strain background (*Rattus norvegicus*)	MWF-6^{SHR}	Own colony Charité – Universitätsmedizin Berlin, Germany	http://dels.nas.edu/ilar/ (laboratory code Rkb); ***Schulz and Kreutz, 2012***; RRID:RGD_1641831	
Strain, strain background (*Rattus norvegicus*)	Congenic strains see ***Figure 1***	Own colony Charité – Universitätsmedizin Berlin, Germany; this paper		For generation of congenic strains see Materials and method section

Rat animals

Male rats were obtained from our MWF/Rkb (RRID:RGD_724569, laboratory code Rkb, http://dels.nas.edu/ilar/) and SHR/Rkb (RRID:RGD_631696, laboratory code Rkb, http://dels.nas.edu/ilar/) colonies at the Charité – Universitätsmedizin Berlin, Germany. The consomic MWF-6^{SHR} (RRID:RGD_1641831) was previously described (***Schulz et al., 2007***). Rats were grouped under conditions of regular 12 hr diurnal cycles with an automated light switching device and climate-controlled conditions at a room temperature of 22°C. The rats were fed a normal diet containing 0.2% NaCl and had free access to food and water.

A panel of eight congenic rat lines MWF.SHR-(*D6Rat1-D6Rat30*), MWF.SHR-(*D6Rat1-D6Rat106*), MWF.SHR-(*D6Rat1-D6Mit8*), MWF.SHR-(*D6Rat1-D6Rat121*), MWF.SHR-(*D6Rat1-D6Mgh4*), MWF.SHR-(*D6Rat1-D6Rat81*), MWF.SHR-(*D6Rat1-D6Rat115*), and MWF.SHR-(*D6Rat1-D6Rat184*) was generated by transfer of different nested SHR segments onto the MWF background. For this procedure, male and female rats of the MWF-6^{SHR} breeding, that were homozygous for all MWF chromosomes except RNO6 and heterozygous for RNO6, were intercrossed (***Schulz et al., 2003***). All experimental work in rat models was performed in accordance with the guidelines of the Charité-Universitätsmedizin Berlin and the local authority for animal protection (Landesamt für Gesundheit und Soziales, Berlin, Germany) for the use of laboratory animals. The registration numbers for the rat experiments are G 0255/09 and T 0189/02.

Determination of albuminuria, direct BP and glomerular density in rats

Urinary albumin excretion was measured as reported (***Kreutz et al., 2000***). Direct intra-arterial BP measurements were performed in awake male rats at 14 weeks of age as previously described (***Kreutz et al., 1995***; ***Schulz et al., 2010***). For determination of glomerular density, animals were sacrificed under ketamine-xylazine anesthesia (87 and 13 mg/kg body wt, respectively) at week 4. The right kidney was fixed in methacarn and embedded in paraffin. Tissue samples were cut into 5-µm-thick histological sections (***Figure 1G–I***) and stained with the periodic acid-Schiff (PAS) technique. Section analysis was performed by a photomicroscope Axiophot (Zeiss) and a digital camera system AxioCam MRc Rev. 3 FireWire (Zeiss) at a 10x magnification. Glomerular density was calculated using the formula n = G/FA(D + T) as reported (***ELIAS et al., 1961***; ***Lucas et al., 1997***). Glomeruli in 20–25 fields for each sample were counted in the outer cortex zone (***Figure 1H,I***). Glomerular diameter was calculated by the AxioVision release 4.8.2 software program (Zeiss). This method was validated by comparison with the absolute nephron numbers as determined by the physical fractionator method in rat strains as previously reported (***Gundersen, 1986***; ***Schulz et al., 2007***).

X

NGS of the candidate region on RNO6

Based on the fine mapping results of the congenic MWF strains, a target candidate region of about 5.63 Mbp (chr6:105.8–111.43 Mb, R. norvegicus, ENSEMBL rn6.0) (**Yates et al., 2016**) was defined for subsequent next-generation resequencing analysis. The solution-based SureSelectXT (Agilent Technologies) capture method was applied for custom target enrichment of the defined region according to the manufacturer's instructions starting with 3 µg genomic rat DNA of MWF, SHR, MWF-6^{SHR}, MWF.SHR-(*D6Rat1-D6Mgh4*), and MWF.SHR-(*D6Rat1-D6Rat81*) (n = 3, each), uniquely labelled by index tags.

Library quality control and final quantification for subsequent pooling of the 16 sequencing libraries was performed using the 2100 Bioanalyzer instrument (Agilent Technologies). The pooled library was paired end sequenced (2 × 76 cycles plus index read) on a MiSeq system (Illumina) using the MiSeq reagent kit v3 (Illumina). The CASAVA software package v1.8.2 (Illumina) was used for demultiplexing of the sequencing reads and conversion to fastq data for further analysis. The resulting high-quality reads for identification of SNPs and short INDELs were mapped to the reference genome according to the annotation release Rat Genome Sequencing Consortium (RGSC) genome assembly v6.0 using BWA software, version 0.6.2 (**Li and Durbin, 2009**). Mapped reads were processed and calling of SNPs and short INDELs were performed by the GATK pipeline, version 2.8 (**Van der Auwera et al., 2013**). Effects of the genomic variations were evaluated with the SnpEff software tool, version 3.3 (**Cingolani et al., 2012**). Impairment of protein function by common exonic variants in MWF and SHR were analysed using the PROVEAN algorithm (**Choi et al., 2012**). A PROVEAN Score <2.5 was considered significant for genes.

The Tajima's D statistic (**Tajima, 1989**) was used to test for signatures of selection in the region of interest utilizing the vcftools software (Vs. 0.1.13) (**Danecek et al., 2011**).

Rat glomeruli isolation

Different protocols were used for isolation of glomeruli from male rats at 4 and 8 weeks of age, due to the different body size. Rats were anesthetized with ketamine-xylazine (87 and 13 mg/kg body weight, respectively). In 4-week-old rats, the abdominal artery was catheterized and kidneys were perfused with 10 ml 1x phosphate buffered saline (PBS) and subsequently with 20 ml ferrous solution (12.5 g ferric oxide (Iron(II/III) powder <5 micron, 98%; Sigma- Aldrich Chemie GmbH) suspended in 1000 ml 1x PBS. Kidneys were removed, decapsulated and passed through a 125 µm steel sieve (Retsch GmbH) with 1x PBS. The glomeruli containing ferrous particles were gathered by a magnet, snap-frozen and stored at −80°C. Kidneys of 8-week-old rats were removed, decapsulated and passed through a 125 µm steel sieve with 1x PBS. The filtrate was put on a 71 µm steel sieve (Retsch GmbH) to separate glomeruli from the flow-through. Glomeruli were washed off the sieve with 1x PBS, centrifuged, immediately snap-frozen and stored at −80°C.

Transcriptome analysis

RNA sequencing (RNA-Seq) was performed in glomerular RNA of male MWF and SHR rats at week 4 (n = 3, each). The NEBNext Poly(A) mRNA magnetic isolation module followed by library preparation using NEBNext Ultra RNA Library Prep Kit for Illumina (New England BioLabs) was applied on 1 µg total RNA to generate a cDNA library for subsequent paired end (80 cycles) sequencing on the NextSeq 500 system (Illumina) using v2 chemistry yielding in about 415M single reads. RNA and library quality control was performed using the Bioanalyzer RNA 600 Nano and High-Sensitivity DNA Analysis Kit (Agilent Technologies), respectively. The KAPA Library Quantification Kit (Kapa Biosystems) was used for library quantification.

Initial quality control of the raw data was performed using Cutadapt version 1.9 (**Martin, 2012**) program. Raw reads were quality trimmed (minimal base quality: 25, minimal read length after trimming: 70 nt), adapter sequences were removed from reads 3' ends. TopHat2 version 2.1.0 (**Trapnell et al., 2009**; **Trapnell et al., 2010**) software tool together with Bowtie2 aligner version 2.2.3 (**Langmead and Salzberg, 2012**) was used for read mapping against ENSEMBL rn6.0 reference assembly (**Yates et al., 2016**). After the reads have been mapped to the reference genome, the Cufflinks version 2.2.1 (**Trapnell et al., 2010**) program together with Ensembl (release 81) gene annotation (**Aken et al., 2016**), baw093) were used to assemble transcripts and estimate their abundances. Differential expression analysis was performed using both Cuffdiff version 2.2.1 software package

Y

(*Trapnell et al., 2010*) and DESeq2 R package version 1.12.4 (*Love et al., 2014*). Genes having absolute fold change value <1.5 were excluded from further analysis. Genes were considered significantly differentially expressed if the corresponding adjusted p-value was less than 0.05.

Reverse transcription and qPCR

First-strand cDNA synthesis was carried out on 2 µg of total RNA using the First Strand cDNA Synthesis Kit (Fermentas Life Sciences) following the manufacturer's protocol. Isolated glomeruli preparations of rat strains were analyzed at week 4 and week 8. qPCR of each gene was performed in a 7000 Real-Time PCR System (Applied Biosystems) with version 1.2.3 software or a 7500 Fast Real-Time PCR System with version 2.0.6 software (Applied Biosystems) using the comparative quantification cycle method as reported (Fast SYBRGreen Master Mix or Power SYBR Green PCR Master Mix; Applied Biosystems) (*Schulz et al., 2008*). Primers are listed in *Figure 4—source data 2*. Normalization of expression data was done by the reference gene hydroxymethylbilane synthase (*Hmbs*) (*Schulz et al., 2008*). For all analyses, three technical replicates of each animal/experiment were performed. Genes with low mRNA expression levels were only considered when the quantification cycles (Cqs) were ≥30 and the Cqs of the no-template controls were at least 5 Cqs delayed. Acyl-CoA thioesterase 3 (Acot3) demonstrated low expression levels and was therefore not analyzed.

Immunohistochemistry of TMEM63C in rat and human kidneys

For determination of protein expression of TMEM63C an anti-TMEM63C antibody (epitope: G LRGFARELDPAQFQEGLE, custom antibody production: Perbio Science Germany) was generated. The epitope does not cross react with TMEM63A or TMEM63B or other genes. For Wilms tumor 1 (WT1) protein expression analysis, we used a rabbit anti-WT1 antibody (Santa Cruz). For nephrin protein expression analysis, we used a rabbit anti-nephrin antibody (Abcam). Paraffin embedded rat kidney sections and human biopsy samples were cut at 4 µm and incubated with the anti-TMEM63C antibody (1:1600 for rat tissue, 1:800 for human biopsies), the anti-WT1 antibody (1:500) or the anti-nephrin antibody (1:750). Rabbit IgG negative control fraction was used as a negative control in the same concentration as the primary antibody. Goat anti-rabbit EnVision HRP conjugate (Dako) was used as secondary antibody. The staining was visualized using diaminobenzidine as the chromogen and counterstained with haematoxylin.

Evaluation of TMEM63C staining in MWF and SHR rats

Consecutive slides of MWF and SHR kidney sections stained for TMEM63C and WT1 were evaluated to determine TMEM63C co-localization with podocytes. TMEM63C protein level in glomeruli was analyzed using ImageJ analysis.

Table 4. Characteristics of focal segmental glomerulosclerosis patients.

Patient-specific features	Values[‡]
Number of patients	9
Age, years	36 ± 23
Sex, male	5 (55%)
SBP, mmHg[*]	167 ± 38
DBP, mmHg[†]	106 ± 25
Hypertension	7 (88%)
Proteinuria, g/day[†]	9.2 ± 4.4
Serum creatinine, µmol/l[†]	150 ± 43
eGFR, ml/min/1.73 m^{2}[*]	51 (42–66)
Nephrotic syndrome	8 (89%)

[*]$n = 7$; [†]$n = 6$; [‡] values are reported as number (%), mean ±SD or as median (interquartile range) for eGFR.

DOI: https://doi.org/10.7554/eLife.42068.032

Z

FSGS patients

Renal biopsy samples of patients with FSGS (*Table 4*) were collected from the archive of the Department of Pathology of the Leiden University Medical Center (LUMC). Demographic data and laboratory data at time of biopsy were retrospectively retrieved from the patients' medical records or pathology reports following the good practice guidelines of the LUMC. All biopsy samples were handled and analyzed anonymously in accordance with the Dutch National Ethics Guidelines (Code for Proper Secondary Use of Human Tissue, Dutch Federation of Medical Scientific Societies). This study is in agreement with the Declaration of Helsinki and the Department of Health and Human Services Belmont Report and the use of the patient biopsies was approved by the medical ethical committee of the LUMC (registration number G16.110). Samples obtained from Eurotransplant donors that were unsuited for transplantation because of technical problems, were used as healthy controls. All sections were scored separately by two observers for TMEM63C intensity as well as for percentage of glomeruli with loss of TMEM63C staining. Each case was given a score for TMEM63C staining intensity: high intensity in >50% of glomeruli, intermediate intensity in >50% of glomeruli, low intensity in >50% of glomeruli or no TMEM63C staining present in >50% of glomeruli. Secondly, sections were scored based on the percentage of glomeruli with loss of TMEM63C expression in podocytes. Per case, the percentage of glomeruli with 1) no loss 2) <25% loss 3) 25–50% loss or 4) >50% loss of TMEM63C expression in podocytes was determined. For nephrin staining analysis, each glomerulus was scored based on staining pattern (linear or granular) and loss of staining (no loss, segmental loss or global loss).

All biopsy samples were handled and analyzed anonymously in accordance with the Dutch National Ethics Guidelines (Code for Proper Secondary Use of Human Tissue, Dutch Federation of Medical Scientific Societies) and in agreement with the Declaration of Helsinki and the Department of Health and Human Services Belmont Report. The use of the patient biopsies was approved by the medical ethical committee of the LUMC.

Cell lines

Immortalized human podocytes (RRID:CVCL_W186, a kind gift from Professor Moin Saleem, MA, Academic and Children's Renal Unit, University of Bristol, Bristol, UK) (*Saleem et al., 2002*) were used as described (*Eisenreich et al., 2016*). The cell line has previously been authenticated (*Saleem et al., 2002*) and we have confirmed this by expression of podocyte specific markers such as podocin and synaptopodin as recently reported (*Eisenreich et al., 2016*). The cell line tested negative for mycoplasma contamination. Before transfection, human podocytes were starved with FBS-free RPMI 1640 medium overnight. Transfection of cells was performed using 200 nM of TMEM63C-specific siRNAs (siTMEM63C; Sigma-Aldrich Chemie GmbH) or non-sense control siRNAs (siControl; Sigma-Aldrich Chemie GmbH) as well as Lipofectamine 2000 (Life Technologies GmbH). The transfection efficacy of 25% in human podocytes was experimentally determined earlier (*Eisenreich et al., 2016*).

Western blotting

Western blot analyses were done as described earlier (*Eisenreich et al., 2016*; *Langer et al., 2016*). For detection, specific antibodies against TMEM63C (Thermo Fisher Scientific), GAPDH (Calbiochem), protein kinase B (AKT; Merck Chemicals GmbH), and phospho-AKT (Ser_{473}, pAKT; Merck Chemicals GmbH) were used. Quantification of Western blot analyses were done using Gel-Pro Analyzer software version 4.0.00.001 (Media Cybernetics).

Cytochrome C releasing apoptosis assay

The cytochrome C releasing apoptosis assay kit (BioVision Inc) was used following the manufacturer's protocol as described previously (*Eisenreich et al., 2016*). In brief, 1×10^4 cells per well were transfected for 48 hr with siTMEM63C or siControl, respectively. After that, cells were lysed and the cytosolic fraction was separated from the mitochondrial fraction. Comparative Western blot analyses of these fractions using a cytochrome C-specific antibody were performed to determine pro-apoptotic translocation of cytochrome C from mitochondria into cytosol.

AA

Cell viability assay

The calcein AM (acetoxymethyl) cell viability kit (Trevigen Inc) was used as earlier described following the manufacturer's protocol (**Eisenreich et al., 2016**). In brief, 1×10^4 cells per well were transfected for 48 hr with siTMEM63C or siControl, respectively. Then, human podocytes were washed and incubated with calcein AM working solution for 30 min. Fluorescence was measured at 490 nm excitation and 520 nm emission.

Zebrafish animals

Zebrafish were bred, raised and maintained in accordance with the guidelines of the Max Delbrück Center for Molecular Medicine and the local authority for animal protection (Landesamt für Gesundheit und Soziales, Berlin, Germany) for the use of laboratory animals, and followed the 'Principles of Laboratory Animal Care' (NIH publication no. 86–23, revised 1985) as well as the current version of German Law on the Protection of Animals.

Zebrafish morpholino and single guide RNA (sgRNA) microinjections

Injection droplets of approximately 1 nl were injected into one-cell stage zygotes of the zebrafish wild type hybrid strain AB/Tülf and the transgenic lines *Tg(fabp10a:gc-EGFP)* (**Zhou and Hildebrandt, 2012**) and *Tg(wt1b:GFP)* (**Bollig et al., 2009**; **Perner et al., 2007**). Morpholinos (MO) of the following sequences were synthesized by Gene Tools LLC Philomath: *tmem63c* ATG-MO 5'-CAGGCCAGGACTCAAACGCCATTGC-3', *tmem63c* ex2-sdMO 5'-TGTTATCATAGATGATGTACCAGCC-3', and standard control oligo (Control-MO) 5'-CCTCTTACCTCAGTTACAATTTATA-3'. *Tmem63c* ATG-MO was used at a final concentration of 0.3 mM (**Figure 7B**), *tmem63c* ex2-sdMO was used at a final concentration of 0.5 mM (**Figure 7—figure supplement 1**). sgRNA targeting exon 2 (**Figure 7B**) was generated as described (**Bassett et al., 2013**; **Burger et al., 2016**) using the ex2-sgRNA forward primer with CRISPR target site underlined: GAAATTAATACGACTCACTATAGGACGTCAGGAGTTTCCTGAGTTTTAGAGCTAGAAATAGC and the invariant reverse primer: AAAAGCACCGACTCGGTGCCACTTTTTCAAGTTGATAACGGACTAGCCTTATTTTAACTTGCTATTTCTAGCTCTAAAAC. PCR product was purified with GeneJET Gel Extraction Kit (Thermo Fisher Scientific, respectively). sgRNA was transcribed using the MEGAscript T7 Kit (Ambion) and extracted with RNeasy Mini Kit (Qiagen) according to the manufacturer's protocol. sgRNA was diluted to a final concentration of 159.6 ng/µl or 250 ng/µl, respectively using water and 1 M KCl (final concentration: 300 mM) and co-injected with Cas9-Protein of 600 ng/µl final concentration as described (**Burger et al., 2016**; **Gagnon et al., 2014**). To determine the efficiency of sgRNA-mediated mutagenesis crispants alleles were analyzed as described (**Figure 7—figure supplement 1D**) (**Burger et al., 2016**). The following primers (BioTez Berlin-Buch GmbH) were used to amplify the genomic region flanking the CRISPR target site; forward: CAAATGGTGAACACTTGTGAATC, reverse: CTGCGGTTTACTGCGGAGATG. Computational sequence analysis was performed using CrispR Variants (**Lindsay et al., 2016**). For an injection control Cas9 was diluted to a final concentration of 600 ng/µl using water and 1 M KCl (final concentration: 300 mM; Cas9-Control).

Reverse transcriptase (RT)-PCR in zebrafish embryos

For efficiency analysis of the *tmem63c* ex2-sdMO a reverse transcriptase (RT)-PCR was carried out (**Figure 7—figure supplement 1F**). At 24 hpf, RNA from 50 pooled embryos was isolated using Trizol Reagent (Invitrogen); DNase I digestion was performed using the RNAse-free DNase set (Qiagen) and samples were purified using the RNeasy Mini Kit (Qiagen) according to the manufacturer's protocol. After determination of RNA quality and quantity, equal amounts of mRNA for each group analyzed were transcribed to cDNA using First strand cDNA synthesis kit (Thermo Fisher) according to the manufacturer's protocol.

We amplified *tmem63c* from cDNA using DreamTaq DNA Polymerase (Thermo Fisher) with the following primers: forward: CTGATGGAGGAGAACAGCACGG, reverse: ATACAGCAGAGCGAAGATACTGTG. Eucaryotic elongation factor 1 alpha 1, like 1 (*eef1a1l1*) was used as a loading control and amplified using the following primers: forward: TGGAGACAGCAAGAACGACC, reverse: GAGGTTGGGAAGAACACGCC.

BB

Cloning of *tmem63c* cDNA (*Danio rerio*)

Primers (BioTez Berlin-Buch GmbH) for the In-Fusion HD Cloning Kit (Takara) were designed using the web tool provided by TaKaRa (TaKaRa) (***TaKaRa, 2018***); forward: GCTTGATATCGAATTCA TGGCGTTTGAGTCCTGGCCTGC, reverse: CGGGCTGCAGGAATTCTCACTGAAAAGCCACCGGAC TG. *tmem63c* cDNA was amplified using Phusion High-Fidelity DNA polymerase (Thermo Fisher Scientific). The pBluescript II SK(+) vector was linearized using EcoRI FD enzyme. The *tmem63c* ORF was cloned into the pBluescript II SK (+) vector using the In-Fusion HD Cloning Kit (Takara). The *tmem63c* cDNA was sequence-verified using the common T7 forward and M13 reverse primers. For sequencing of the whole ORF, an additional primer was used, GTGCAGAAACTAATGAAGCTGG, located at 822–844 bp starting from the beginning of the ORF.

Rescue of CRISPR/Cas9-mediated *tmem63c* somatic mutants and *tmem63c* ex2-sdMO-mediated gene knockdown

For in vivo rescue experiments *tmem63c* cDNA (*Danio rerio*) was linearized using ApaI FD (Thermo Fisher Scientific) and purified using GeneJET Gel Extraction Kit (Thermo Fisher Scientific). In vitro transcription of capped RNA and following TurboDNase treatment were performed using mMessage mMachine T7 Kit (Ambion). For poly-A-tailing, the Poly(A)-tailing Kit (Ambion) was used, followed by RNA extraction using RNeasy Mini Kit (Qiagen). The mRNA was diluted to a concentration of 100 ng/µl and injected into one-cell stage zygotes. For in vivo rescue experiments, mRNA of a concentration of 100 ng/µl and ex2-sgRNA of a concentration of 159.6 ng/µl were subsequently injected into the same one-cell stage zygotes. For in vivo rescue of the *tmem63c* ex2-sdMO-mediated knockdown, mRNA with a concentration of 100 ng/µl and ex2-sdMO with a concentration of 0.5 mM were subsequently injected into the same zygote at one- or one-to-four cell stage, respectively.

Rescue of *tmem63c* ATG-MO-mediated gene knockdown

Tmem63c cDNA (Rattus norvegicus) was synthesized by Thermo Fisher Scientific using their GeneArt Gene synthesis service. For in vivo rescue experiments, *Tmem63c* cDNA was linearized using XbaI FD (Thermo Fisher Scientific) and purified using GeneJET Gel Extraction Kit (Thermo Fisher Scientific). In vitro transcription of capped RNA followed by TurboDNase treatment were performed using mMessage mMachine T7 Kit (Ambion). For poly-A-tailing, the Poly(A)-tailing Kit (Ambion) was used, followed by RNA extraction by RNeasy Mini Kit (Qiagen). The mRNA was diluted to a concentration of 100 ng/µl and injected into one-cell stage zygotes. For in vivo rescue of the *tmem63c* ATG-MO-mediated knockdown, mRNA with a concentration of 100 ng/µl and ATG-MO with a concentration of 0.3 mM were subsequently injected into the same zygote at one- or one to four cell-stage, respectively.

Functional assessment of the GFB

To assess the functionality of the GFB, the gc-EGFP fluorescence in the trunk vasculature *of Tg (fabp10a:gc-EGFP)* embryos were evaluated at 120 hpf by epifluorescence microscopy. For CRISPR-Cas9-mediated somatogenesis of *tmem63c* the above described sgRNA was used in a concentration of 159.6 ng/µl. Each embryo was visually assigned to the 'fluorescent group', 'deficient-fluorescent group', or 'crippled/dead' and their number quantified. Due to the heterogeneous genotype of the used transgenic *Tg(fabp10a:gc-EGFP)* zebrafish families, the 'deficient-fluorescent group' included the embryos with reduced fluorescence in the trunk as well as embryos that did not carry the transgene (***Figure 7—figure supplement 1A–C***). The percentage of injected embryos was normalized to the percentage of the control group for each category. Quantifications were performed for at least three individual injections.

Electron microscopy in zebrafish embryos

Tg(fabp10a:gc-EGFP) embryos at 120 hpf were fixed in 4% formaldehyde/0.5% glutaraldehyde (EM-grade) in 0.1 M phosphate buffer for 2 hr at RT. For knockdown analysis embryos were injected with *tmem63c* ex2-sgRNA of a concentration of 250 ng/µl to enhance the observed phenotype (***Figure 7E,F***). Prior to analysis embryos were sorted for a clear knockdown phenotype. Samples were stained with 1% OsO_4 for 2 hr, dehydrated in a graded ethanol series and propylene oxide and embedded in Poly/Bed^R 812 (Polysciences, Eppelheim, Germany). Ultrathin sections were contrasted

with uranyl acetate and lead citrate. Sections were examined with a FEI Morgagni electron microscope and a Morada CCD camera (EMSIS GmbH, Münster, Germany). Image acquisition and quantification of podocyte foot process width and number of slit diaphragms per µm GBM was performed with the iTEM software (EMSIS GmbH, Münster, Germany).

Confocal microscopy of zebrafish embryos and quantification of podocyte cell number and glomerular volume

Tg(wt1b:EGFP) embryos at 96 hpf were fixed in PEM buffer containing 4% formaldehyde and 0.1% Triton-X 100 for 2 hr at RT or overnight at 4˚C. For knockdown analysis embryos were injected with *tmem63c* ex2-sgRNA with a concentration of 250 ng/µl to enhance the observed phenotype. Nuclei were stained using 4',6-Diamidin-2-phenylindol (DAPI, Sigma Aldrich, stock solution 1 mg/ml diluted 1:2000 in PBS) overnight at 4˚C. After removal of the yolk and mounting in 0,7% low-melting agarose, the kidneys of whole-mount fixed embryos were imaged using a Zeiss LSM 710 or LSM 700 microscope with a LD C-Apochromat 40 x NA1.1 water objective and ZEN 2.1 software by sequentially acquiring confocal z-stacks of the GFP (488 nm laser, emission 495–550 nm) and the DAPI signal (405 nm laser, emission 420–480 nm) with a pixel size of 102.4 nm. Care was taken to apply identical settings to all samples and not to oversaturate pixels.

Quantification of podocyte cell number and glomerular volume was done using Imaris version 9.21 software (RRID:SCR_007370, Bitplane AG, Zurich, Switzerland). A 3D surface covering the total glomerular volume was manually edited by tracing the outlines of EGFP-positive cells for every second section of the z-stack. EGFP-positive cells of the glomerulus were included, while cells of the pronephric ducts were excluded. For quantification of podocyte cell number, the DAPI channel was masked with the EGFP channel using Fiji software (RRID:SCR_002285) (***Schindelin et al., 2012***) to include $DAPI^+/EGFP^+$ cells only, thus representing nuclei of podocyte cells. Subsequently, a spot segmentation of the DAPI channel was performed. Estimated spot diameter was 4 µm. Spots were filtered for a minimum intensity of the EGFP channel and by using the Imaris quality filter for the occurrence of unspecific spots not matching the EGFP signal. Spots located outside the glomerular surface were manually deleted.

Statistics

Data are presented as mean ±SD for normally distributed data or median (25% percentile – 75% percentile, that is interquartile range [IQR]) for non-normally distributed data with the indicated number of experiments. Normal distribution was determined using the Shapiro-Wilk test. For identification of outliers, Grubbs' outliers test ($\alpha = 0.05$) was performed. Where appropriate, sample size calculations were performed by the power analyses program G*Power according to Cohen (***Cohen, 1988***; ***Faul et al., 2009***). Differences between experimental rat and zebrafish groups were analyzed using One-way ANOVA with post-hoc Bonferroni's multiple comparisons test and non-parametric Mann-Whitney-U or Kruskall-Wallis test with Dunn's multiple comparisons post-hoc test, when appropriate. For the analysis shown in ***Figure 7L*** and ***Figure 7—figure supplement 1I*** Gaussian distribution was assumed due to the number of embryos categorized. Differences between FSGS patients and controls were analyzed using the Linear-by-Linear association test and the Mann-Whitney U test. Differences in human cultured podocytes were analyzed using two-tailed Student's t-test. Statistical analysis was performed using SPSS and GraphPad Prism 6 software 6.00 (RRID:SCR_002798, GraphPad Software, La Jolla, CA). p values < 0.05 were considered as statistically significant.

Data availability

The genomic and transcriptomic data from this publication have been deposited to the NCBI (https://www.ncbi.nlm.nih.gov/) curated repositories, GEO, and SRA, and assigned the identifier SubmissionID: SUB2950675 and BioProject ID: PRJNA398197 (DNA-Seq) and accession GSE102546 (RNA-Seq).

Acknowledgements

We acknowledge the contributions of Karen Böhme, Bettina Bublath, Marianne Jansen-Rust, Claudia Plum, Christiane Priebsch, Christina Schiel, Sabine Wunderlich†, and Malu Zandbergen for excellent laboratory or animal assistance. *Tg(wt1b:GFP)* line was kindly provided by Christoph Englert. This

DD

study was supported by the Deutsche Hochdruckliga (DHL) Hypertensiologie Professur to RK, by the grants from the Deutsche Forschungsgemeinschaft (DFG) KR 1152-3-1 (RK) and SCHU 2604/1–1 (ASch), by the DFG (German Research Foundation) – Project number 394046635 – SFB 1365 (RK, DP), and by the grants from the Helmholtz Young Investigator Program VH-NG-736, and Marie Curie CIG from the European Commission (WNT/CALCIUM IN HEART-322189) (DP).

Additional information

Funding

Funder	Grant reference number	Author
Deutsche Forschungsgemeinschaft	DFG KR 1152-3-1	Reinhold Kreutz
Helmholtz-Gemeinschaft	VH-NG-736	Daniela Panáková
European Commission	WNT/CALCIUM IN HEART-322189	Daniela Panáková
Deutsche Forschungsgemeinschaft	SCHU 2604/1-1	Angela Schulz
Deutsche Forschungsgemeinschaft	Project number 394046635 - SFB 1365	Reinhold Kreutz
Deutsche Hochdrckliga (DHL)	Stiftungsprofessur Hypertensiologie	Reinhold Kreutz

The funders had no role in study design, data collection and interpretation, or the decision to submit the work for publication.

Author contributions

Angela Schulz, Conceptualization, Resources, Data curation, Formal analysis, Supervision, Funding acquisition, Validation, Investigation, Visualization, Methodology, Writing—original draft, Project administration, Writing—review and editing; Nicola Victoria Müller, Nina Anne van de Lest, Conceptualization, Data curation, Formal analysis, Supervision, Validation, Investigation, Visualization, Methodology, Writing—original draft, Writing—review and editing; Andreas Eisenreich, Conceptualization, Data curation, Formal analysis, Supervision, Validation, Investigation, Visualization, Methodology, Writing—original draft, Project administration, Writing—review and editing; Martina Schmidbauer, Conceptualization, Data curation, Formal analysis, Validation, Investigation, Visualization, Methodology, Writing—original draft, Writing—review and editing; Andrei Barysenka, Resources, Data curation, Formal analysis, Validation, Investigation, Visualization, Writing—review and editing; Bettina Purfürst, Resources, Data curation, Formal analysis, Validation, Methodology, Writing—original draft, Writing—review and editing; Anje Sporbert, Resources, Methodology, Writing—review and editing; Theodor Lorenzen, Investigation, Writing—review and editing; Alexander M Meyer, Laura Herlan, Investigation, Methodology, Writing—review and editing; Anika Witten, Formal analysis, Validation, Investigation, Methodology, Writing—review and editing; Frank Rühle, Resources, Formal analysis, Validation, Investigation, Visualization, Writing—original draft, Writing—review and editing; Weibin Zhou, Resources, Writing—review and editing; Emile de Heer, Conceptualization, Resources, Validation, Writing—review and editing; Marion Scharpfenecker, Conceptualization, Supervision, Validation, Methodology, Writing—original draft, Project administration, Writing—review and editing; Daniela Panáková, Reinhold Kreutz, Conceptualization, Resources, Data curation, Supervision, Funding acquisition, Validation, Methodology, Writing—original draft, Project administration, Writing—review and editing; Monika Stoll, Conceptualization, Data curation, Software, Supervision, Validation, Methodology, Writing—original draft, Project administration, Writing—review and editing

Author ORCIDs

Angela Schulz http://orcid.org/0000-0002-4576-8035
Nicola Victoria Müller http://orcid.org/0000-0001-7261-830X

EE

Daniela Panáková https://orcid.org/0000-0002-8739-6225
Reinhold Kreutz http://orcid.org/0000-0002-4818-211X

Ethics

Human subjects: All biopsy samples were handled and analyzed anonymously in accordance with the Dutch National Ethics Guidelines (Code for Proper Secondary Use of Human Tissue, Dutch Federation of Medical Scientific Societies). Because this study concerned retrospectively collected anonymized material, no informed consent was necessary following the Dutch National Ethics Guidelines. This study is in agreement with the Declaration of Helsinki and the Department of Health and Human Services Belmont Report and the use of the patient biopsies was approved by the medical ethical committee of the LUMC (registration number G16.110).
Animal experimentation: All experimental work in rat models was performed in accordance with the guidelines of the Charité-Universitätsmedizin Berlin and the local authority for animal protection (Landesamt für Gesundheit und Soziales, Berlin, Germany) for the use of laboratory animals. The registration numbers for the rat experiments are G 0255/09 and T 0189/02. Zebrafish were bred, raised and maintained in accordance with the guidelines of the Max Delbrück Center for Molecular Medicine and the local authority for animal protection (Landesamt für Gesundheit und Soziales, Berlin, Germany) for the use of laboratory animals, and followed the 'Principles of Laboratory Animal Care' (NIH publication no. 86-23, revised 1985) as well as the current version of German Law on the Protection of Animals.

Decision letter and Author response

Decision letter https://doi.org/10.7554/eLife.42068.039
Author response https://doi.org/10.7554/eLife.42068.040

Additional files

Supplementary files

- Transparent reporting form

DOI: https://doi.org/10.7554/eLife.42068.033

Data availability

The genomic and transcriptomic data from this publication have been deposited to the NCBI curated repositories, GEO, and SRA, and assigned the identifier SubmissionID: SUB2950675 and BioProject ID: PRJNA398197 (DNA-Seq) and accession GSE102546 (RNA-Seq).

The following datasets were generated:

Author(s)	Year	Dataset title	Dataset URL	Database and Identifier
Barysenka A, Schulz A, van de Lest NA, Eisenreich A, Schmidbauer M, Müller N, Lorenzen T, Meyer A, Herlan L, Witten A, Rühle F, Zhou W, de Heer E, Scharpfenecker M, Panakova D, Stoll M, Kreutz R	2017	Integrative analysis of the genomic architecture of a complex kidney damage QTL in inbred hypertensive rats implies Tmem63c for translational research	https://www.ncbi.nlm.nih.gov/bioproject/?term=PRJNA398197	NCBI BioProject, PRJNA398197
Barysenka A, Schulz A, van de Lest NA, Eisenreich A, Schmidbauer M, Müller N, Lorenzen T, Meyer A, Herlan L, Witten A, Rühle F, Zhou W, de Heer E, Scharpfenecker M, Panakova D,	2017	Integrative analysis of the genomic architecture of a complex kidney damage QTL in inbred hypertensive rats implies Tmem63c for translational research	https://www.ncbi.nlm.nih.gov/geo/query/acc.cgi?acc=GSE102546	NCBI Gene Expression Omnibus, GSE102546

FF

References

Aken BL, Ayling S, Barrell D, Clarke L, Curwen V, Fairley S, Fernandez Banet J, Billis K, García Girón C, Hourlier T, Howe K, Kähäri A, Kokocinski F, Martin FJ, Murphy DN, Nag R, Ruffier M, Schuster M, Tang YA, Vogel JH, et al. 2016. The ensembl gene annotation system. *Database* **2016**:baw093. DOI: https://doi.org/10.1093/database/baw093, PMID: 27337980

Atanur SS, Diaz AG, Maratou K, Sarkis A, Rotival M, Game L, Tschannen MR, Kaisaki PJ, Otto GW, Ma MC, Keane TM, Hummel O, Saar K, Chen W, Guryev V, Gopalakrishnan K, Garrett MR, Joe B, Citterio L, Bianchi G, et al. 2013. Genome sequencing reveals loci under artificial selection that underlie disease phenotypes in the laboratory rat. *Cell* **154**:691–703. DOI: https://doi.org/10.1016/j.cell.2013.06.040, PMID: 23890820

Bassett AR, Tibbit C, Ponting CP, Liu JL. 2013. Highly efficient targeted mutagenesis of *Drosophila* with the CRISPR/Cas9 system. *Cell Reports* **4**:220–228. DOI: https://doi.org/10.1016/j.celrep.2013.06.020, PMID: 23827738

Böger CA, Chen MH, Tin A, Olden M, Köttgen A, de Boer IH, Fuchsberger C, O'Seaghdha CM, Pattaro C, Teumer A, Liu CT, Glazer NL, Li M, O'Connell JR, Tanaka T, Peralta CA, Kutalik Z, Luan J, Zhao JH, Hwang SJ, et al. 2011. CUBN is a gene locus for albuminuria. *Journal of the American Society of Nephrology : JASN* **22**:555–570. DOI: https://doi.org/10.1681/ASN.2010060598, PMID: 21355061

Bollig F, Perner B, Besenbeck B, Köthe S, Ebert C, Taudien S, Englert C. 2009. A highly conserved retinoic acid responsive element controls wt1a expression in the zebrafish pronephros. *Development* **136**:2883–2892. DOI: https://doi.org/10.1242/dev.031773, PMID: 19666820

Buchner DA, Nadeau JH. 2015. Contrasting genetic architectures in different mouse reference populations used for studying complex traits. *Genome Research* **25**:775–791. DOI: https://doi.org/10.1101/gr.187450.114, PMID: 25953951

Burger A, Lindsay H, Felker A, Hess C, Anders C, Chiavacci E, Zaugg J, Weber LM, Catena R, Jinek M, Robinson MD, Mosimann C. 2016. Maximizing mutagenesis with solubilized CRISPR-Cas9 ribonucleoprotein complexes. *Development* **143**:2025–2037. DOI: https://doi.org/10.1242/dev.134809, PMID: 27130213

Chatterjee N, Wheeler B, Sampson J, Hartge P, Chanock SJ, Park JH. 2013. Projecting the performance of risk prediction based on polygenic analyses of genome-wide association studies. *Nature Genetics* **45**:400–405. DOI: https://doi.org/10.1038/ng.2579, PMID: 23455638

Choi Y, Sims GE, Murphy S, Miller JR, Chan AP. 2012. Predicting the functional effect of amino acid substitutions and indels. *PLoS ONE* **7**:e46688. DOI: https://doi.org/10.1371/journal.pone.0046688, PMID: 23056405

Cingolani P, Platts A, Wang LL, Coon M, Nguyen T, Wang L, Land SJ, Lu X, Ruden DM. 2012. A program for annotating and predicting the effects of single nucleotide polymorphisms, SnpEff. *Fly* **6**:80–92. DOI: https://doi.org/10.4161/fly.19695

Coffman TM, Crowley SD. 2008. Kidney in hypertension: guyton redux. *Hypertension* **51**:811–816. DOI: https://doi.org/10.1161/HYPERTENSIONAHA.105.063636, PMID: 18332286

Cohen J. 1988. *Statistical Power Analysis for the Behavioral Sciences*. Second Edition. Hillsdale: Lawrence Erlbaum.

D'Agati VD, Kaskel FJ, Falk RJ. 2011. Focal segmental glomerulosclerosis. *New England Journal of Medicine* **365**:2398–2411. DOI: https://doi.org/10.1056/NEJMra1106556, PMID: 22187987

Danecek P, Auton A, Abecasis G, Albers CA, Banks E, DePristo MA, Handsaker RE, Lunter G, Marth GT, Sherry ST, McVean G, Durbin R, 1000 Genomes Project Analysis Group. 2011. The variant call format and VCFtools. *Bioinformatics* **27**:2156–2158. DOI: https://doi.org/10.1093/bioinformatics/btr330, PMID: 21653522

De Vriese AS, Sethi S, Nath KA, Glassock RJ, Fervenza FC. 2018. Differentiating primary, genetic, and secondary FSGS in adults: a clinicopathologic approach. *Journal of the American Society of Nephrology* **29**:–774. DOI: https://doi.org/10.1681/ASN.2017090958

Deng AY. 2015. Genetic mechanisms of polygenic hypertension: fundamental insights from experimental models. *Journal of Hypertension* **33**:669–680. DOI: https://doi.org/10.1097/HJH.0000000000000479, PMID: 25915868

Doublier S, Ruotsalainen V, Salvidio G, Lupia E, Biancone L, Conaldi PG, Reponen P, Tryggvason K, Camussi G. 2001. Nephrin redistribution on podocytes is a potential mechanism for proteinuria in patients with primary acquired nephrotic syndrome. *The American Journal of Pathology* **158**:1723–1731. DOI: https://doi.org/10.1016/S0002-9440(10)64128-4, PMID: 11337370

Ehret GB, Ferreira T, Chasman DI, Jackson AU, Schmidt EM, Johnson T, Thorleifsson G, Luan J, Donnelly LA, Kanoni S, Petersen AK, Pihur V, Strawbridge RJ, Shungin D, Hughes MF, Meirelles O, Kaakinen M, Bouatia-Naji N, Kristiansson K, Shah S, et al. 2016. The genetics of blood pressure regulation and its target organs from association studies in 342,415 individuals. *Nature Genetics* **48**:1171–1184. DOI: https://doi.org/10.1038/ng.3667, PMID: 27618452

Eisenreich A, Langer S, Herlan L, Kreutz R. 2016. Regulation of podoplanin expression by microRNA-29b associates with its antiapoptotic effect in angiotensin II-induced injury of human podocytes. *Journal of Hypertension* **34**:323–331. DOI: https://doi.org/10.1097/HJH.0000000000000799, PMID: 26867059

ELIAS H, HENNIG A, ELIAS PM. 1961. Some methods for the study of kidney structure. *Zeitschrift Fur Wissenschaftliche Mikroskopie Und Mikroskopische Technik* **65**:70–82. PMID: 13889833

GG

Endlich K, Kliewe F, Endlich N. 2017. Stressed podocytes—mechanical forces, sensors, signaling and response. *Pflügers Archiv - European Journal of Physiology* **469**:937–949. DOI: https://doi.org/10.1007/s00424-017-2025-8

Faul F, Erdfelder E, Buchner A, Lang AG. 2009. Statistical power analyses using G*power 3.1: tests for correlation and regression analyses. *Behavior Research Methods* **41**:1149–1160. DOI: https://doi.org/10.3758/BRM.41.4.1149, PMID: 19897823

Forst AL, Olteanu VS, Mollet G, Wlodkowski T, Schaefer F, Dietrich A, Reiser J, Gudermann T, Mederos y Schnitzler M, Storch U. 2016. Podocyte purinergic P2X4 channels are mechanotransducers that mediate cytoskeletal disorganization. *Journal of the American Society of Nephrology* **27**:848–862. DOI: https://doi.org/10.1681/ASN.2014111144, PMID: 26160898

Gagnon JA, Valen E, Thyme SB, Huang P, Akhmetova L, Ahkmetova L, Pauli A, Montague TG, Zimmerman S, Richter C, Schier AF. 2014. Efficient mutagenesis by Cas9 protein-mediated oligonucleotide insertion and large-scale assessment of single-guide RNAs. *PLoS ONE* **9**:e98186. DOI: https://doi.org/10.1371/journal.pone.0098186, PMID: 24873830

Glazier AM, Nadeau JH, Aitman TJ. 2002. Finding genes that underlie complex traits. *Science* **298**:2345–2349. DOI: https://doi.org/10.1126/science.1076641, PMID: 12493905

Gundersen HJG. 1986. Stereology of arbitrary particles*. *Journal of Microscopy* **143**:3–45. DOI: https://doi.org/10.1111/j.1365-2818.1986.tb02764.x

Hoffmann TJ, Ehret GB, Nandakumar P, Ranatunga D, Schaefer C, Kwok PY, Iribarren C, Chakravarti A, Risch N. 2017. Genome-wide association analyses using electronic health records identify new loci influencing blood pressure variation. *Nature Genetics* **49**:54–64. DOI: https://doi.org/10.1038/ng.3715, PMID: 27841878

Hou C, Tian W, Kleist T, He K, Garcia V, Bai F, Hao Y, Luan S, Li L. 2014. DUF221 proteins are a family of osmosensitive calcium-permeable cation channels conserved across eukaryotes. *Cell Research* **24**:632–635. DOI: https://doi.org/10.1038/cr.2014.14, PMID: 24503647

Ijpelaar DH, Schulz A, Koop K, Schlesener M, Bruijn JA, Kerjaschki D, Kreutz R, de Heer E. 2008. Glomerular hypertrophy precedes albuminuria and segmental loss of podoplanin in podocytes in Munich-Wistar-Frömter rats. *American Journal of Physiology-Renal Physiology* **294**:F758–F767. DOI: https://doi.org/10.1152/ajprenal.00457.2007, PMID: 18199599

Jacob HJ. 2010. The rat: a model used in biomedical research. *Methods in Molecular Biology* **597**:1–11. DOI: https://doi.org/10.1007/978-1-60327-389-3_1, PMID: 20013222

Jeffs B, Clark JS, Anderson NH, Gratton J, Brosnan MJ, Gauguier D, Reid JL, Macrae IM, Dominiczak AF. 1997. Sensitivity to cerebral ischaemic insult in a rat model of stroke is determined by a single genetic locus. *Nature Genetics* **16**:364–367. DOI: https://doi.org/10.1038/ng0897-364, PMID: 9241273

Joehanes R, Zhang X, Huan T, Yao C, Ying SX, Nguyen QT, Demirkale CY, Feolo ML, Sharopova NR, Sturcke A, Schäffer AA, Heard-Costa N, Chen H, Liu PC, Wang R, Woodhouse KA, Tanriverdi K, Freedman JE, Raghavachari N, Dupuis J, et al. 2017. Integrated genome-wide analysis of expression quantitative trait loci aids interpretation of genomic association studies. *Genome Biology* **18**:16. DOI: https://doi.org/10.1186/s13059-016-1142-6, PMID: 28122634

Kestilä M, Lenkkeri U, Männikkö M, Lamerdin J, McCready P, Putaala H, Ruotsalainen V, Morita T, Nissinen M, Herva R, Kashtan CE, Peltonen L, Holmberg C, Olsen A, Tryggvason K. 1998. Positionally cloned gene for a novel glomerular protein–nephrin–is mutated in congenital nephrotic syndrome. *Molecular Cell* **1**:575–582. DOI: https://doi.org/10.1016/S1097-2765(00)80057-X, PMID: 9660941

Kim BK, Hong HK, Kim JH, Lee HS. 2002. Differential expression of nephrin in acquired human proteinuric diseases. *American Journal of Kidney Diseases* **40**:964–973. DOI: https://doi.org/10.1053/ajkd.2002.36328, PMID: 12407641

Kirsten H, Al-Hasani H, Holdt L, Gross A, Beutner F, Krohn K, Horn K, Ahnert P, Burkhardt R, Reiche K, Hackermüller J, Löffler M, Teupser D, Thiery J, Scholz M. 2015. Dissecting the genetics of the human transcriptome identifies novel trait-related trans-eQTLs and corroborates the regulatory relevance of non-protein coding loci†. *Human Molecular Genetics* **24**:4746–4763. DOI: https://doi.org/10.1093/hmg/ddv194, PMID: 26019233

Kreutz R, Hübner N, James MR, Bihoreau MT, Gauguier D, Lathrop GM, Ganten D, Lindpaintner K. 1995. Dissection of a quantitative trait locus for genetic hypertension on rat chromosome 10. *PNAS* **92**:8778–8782. DOI: https://doi.org/10.1073/pnas.92.19.8778, PMID: 7568016

Kreutz R, Kovacevic L, Schulz A, Rothermund L, Ketteler M, Paul M. 2000. Effect of high NaCl diet on spontaneous hypertension in a genetic rat model with reduced nephron number. *Journal of Hypertension* **18**:777–782. DOI: https://doi.org/10.1097/00004872-200018060-00017, PMID: 10872564

Langefeld CD, Beck SR, Bowden DW, Rich SS, Wagenknecht LE, Freedman BI. 2004. Heritability of GFR and albuminuria in caucasians with type 2 diabetes mellitus. *American Journal of Kidney Diseases* **43**:796–800. DOI: https://doi.org/10.1053/j.ajkd.2003.12.043, PMID: 15112169

Langer S, Kreutz R, Eisenreich A. 2016. Metformin modulates apoptosis and cell signaling of human podocytes under high glucose conditions. *Journal of Nephrology* **29**:765–773. DOI: https://doi.org/10.1007/s40620-015-0258-1, PMID: 26733332

Langmead B, Salzberg SL. 2012. Fast gapped-read alignment with bowtie 2. *Nature Methods* **9**:357–359. DOI: https://doi.org/10.1038/nmeth.1923, PMID: 22388286

Levy D, Larson MG, Benjamin EJ, Newton-Cheh C, Wang TJ, Hwang SJ, Vasan RS, Mitchell GF. 2007. Framingham heart study 100K project: genome-wide associations for blood pressure and arterial stiffness. *BMC Medical Genetics* **8 Suppl 1**:S3. DOI: https://doi.org/10.1186/1471-2350-8-S1-S3, PMID: 17903302

HH

Li H, Durbin R. 2009. Fast and accurate short read alignment with Burrows-Wheeler transform. *Bioinformatics* **25**: 1754–1760. DOI: https://doi.org/10.1093/bioinformatics/btp324, PMID: 19451168

Lim BJ, Yang JW, Do WS, Fogo AB. 2016. Pathogenesis of focal segmental glomerulosclerosis. *Journal of Pathology and Translational Medicine* **50**:405–410. DOI: https://doi.org/10.4132/jptm.2016.09.21, PMID: 27744657

Lindsay H, Burger A, Biyong B, Felker A, Hess C, Zaugg J, Chiavacci E, Anders C, Jinek M, Mosimann C, Robinson MD. 2016. CrispRVariants charts the mutation spectrum of genome engineering experiments. *Nature Biotechnology* **34**:701–702. DOI: https://doi.org/10.1038/nbt.3628, PMID: 27404876

Liu Y, Beyer A, Aebersold R. 2016. On the dependency of cellular protein levels on mRNA abundance. *Cell* **165**: 535–550. DOI: https://doi.org/10.1016/j.cell.2016.03.014, PMID: 27104977

Love MI, Huber W, Anders S. 2014. Moderated estimation of fold change and dispersion for RNA-seq data with DESeq2. *Genome Biology* **15**:550. DOI: https://doi.org/10.1186/s13059-014-0550-8, PMID: 25516281

Lucas SR, Costa Silva VL, Miraglia SM, Zaladek Gil F. 1997. Functional and morphometric evaluation of offspring kidney after intrauterine undernutrition. *Pediatric Nephrology* **11**:719–723. DOI: https://doi.org/10.1007/s004670050374, PMID: 9438651

Lundberg E, Fagerberg L, Klevebring D, Matic I, Geiger T, Cox J, Algenäs C, Lundeberg J, Mann M, Uhlen M. 2010. Defining the transcriptome and proteome in three functionally different human cell lines. *Molecular Systems Biology* **6**:450. DOI: https://doi.org/10.1038/msb.2010.106, PMID: 21179022

Mancia G, Fagard R, Narkiewicz K, Redón J, Zanchetti A, Böhm M, Christiaens T, Cifkova R, De Backer G, Dominiczak A, Galderisi M, Grobbee DE, Jaarsma T, Kirchhof P, Kjeldsen SE, Laurent S, Manolis AJ, Nilsson PM, Ruilope LM, Schmieder RE, et al. 2013. 2013 ESH/ESC guidelines for the management of arterial hypertension: the task force for the management of arterial hypertension of the european society of hypertension (ESH) and of the european society of cardiology (ESC). *Journal of Hypertension* **31**:1281–1357. DOI: https://doi.org/10.1097/01.hjh.0000431740.32696.cc, PMID: 23817082

Martin M. 2012. Cutadapt removes adapter sequences from high-throughput sequencing reads. *Bioinformatics in Action* **17**:10–12.

McCarthy MI, Abecasis GR, Cardon LR, Goldstein DB, Little J, Ioannidis JP, Hirschhorn JN. 2008. Genome-wide association studies for complex traits: consensus, uncertainty and challenges. *Nature Reviews Genetics* **9**:356–369. DOI: https://doi.org/10.1038/nrg2344, PMID: 18398418

Miall WE, Oldham PD. 1963. The hereditary factor in arterial blood-pressure. *Bmj* **1**:75–80. DOI: https://doi.org/10.1136/bmj.1.5323.75, PMID: 13935402

Murthy SE, Dubin AE, Whitwam T, Jojoa-Cruz S, Cahalan SM, Mousavi SAR, Ward AB, Patapoutian A. 2018. OSCA/TMEM63 are an evolutionarily conserved family of mechanically activated ion channels. *eLife* **7**:e41844. DOI: https://doi.org/10.7554/eLife.41844, PMID: 30382938

Perner B, Englert C, Bollig F. 2007. The wilms tumor genes wt1a and wt1b control different steps during formation of the zebrafish pronephros. *Developmental Biology* **309**:87–96. DOI: https://doi.org/10.1016/j.ydbio.2007.06.022, PMID: 17651719

Rangel-Filho A, Lazar J, Moreno C, Geurts A, Jacob HJ. 2013. Rab38 modulates proteinuria in model of hypertension-associated renal disease. *Journal of the American Society of Nephrology* **24**:283–292. DOI: https://doi.org/10.1681/ASN.2012090927, PMID: 23291471

Remuzzi A, Puntorieri S, Alfano M, Macconi D, Abbate M, Bertani T, Remuzzi G. 1992. Pathophysiologic implications of proteinuria in a rat model of progressive glomerular injury. *Laboratory Investigation; a Journal of Technical Methods and Pathology* **67**:572–579. PMID: 1434536

Rodriguez PQ, Oddsson A, Ebarasi L, He B, Hultenby K, Wernerson A, Betsholtz C, Tryggvason K, Patrakka J. 2015. Knockdown of Tmem234 in zebrafish results in proteinuria. *American Journal of Physiology-Renal Physiology* **309**:F955–F966. DOI: https://doi.org/10.1152/ajprenal.00525.2014, PMID: 26377798

Rubattu S, Volpe M, Kreutz R, Ganten U, Ganten D, Lindpaintner K. 1996. Chromosomal mapping of quantitative trait loci contributing to stroke in a rat model of complex human disease. *Nature Genetics* **13**:429–434. DOI: https://doi.org/10.1038/ng0896-429, PMID: 8696337

Saleem MA, O'Hare MJ, Reiser J, Coward RJ, Inward CD, Farren T, Xing CY, Ni L, Mathieson PW, Mundel P. 2002. A conditionally immortalized human podocyte cell line demonstrating nephrin and podocin expression. *Journal of the American Society of Nephrology : JASN* **13**:630–638. PMID: 11856766

Schindelin J, Arganda-Carreras I, Frise E, Kaynig V, Longair M, Pietzsch T, Preibisch S, Rueden C, Saalfeld S, Schmid B, Tinevez JY, White DJ, Hartenstein V, Eliceiri K, Tomancak P, Cardona A. 2012. Fiji: an open-source platform for biological-image analysis. *Nature Methods* **9**:676–682. DOI: https://doi.org/10.1038/nmeth.2019, PMID: 22743772

Schulz A, Standke D, Kovacevic L, Mostler M, Kossmehl P, Stoll M, Kreutz R. 2003. A major gene locus links early onset albuminuria with renal interstitial fibrosis in the MWF rat with polygenetic albuminuria. *Journal of the American Society of Nephrology* **14**:3081–3089. DOI: https://doi.org/10.1097/01.ASN.0000100126.62370.25, PMID: 14638907

Schulz A, Weiss J, Schlesener M, Hänsch J, Wehland M, Wendt N, Kossmehl P, Sietmann A, Grimm D, Stoll M, Nyengaard JR, Kreutz R. 2007. Development of overt proteinuria in the Munich wistar frömter rat is suppressed by replacement of chromosome 6 in a consomic rat strain. *Journal of the American Society of Nephrology* **18**: 113–121. DOI: https://doi.org/10.1681/ASN.2006030206, PMID: 17167120

Schulz A, Schlesener M, Weiss J, Hänsch J, Wendt N, Kossmehl P, Grimm D, Vetter R, Kreutz R. 2008. Protective effect of female gender on the development of albuminuria in a polygenetic rat model is enhanced further by

replacement of a major autosomal QTL. *Clinical Science* **114**:305–311. DOI: https://doi.org/10.1042/CS20070300, PMID: 17953514

Schulz A, Schütten S, Schulte L, Kossmehl P, Nyengaard JR, Vetter R, Huber M, Kreutz R. 2010. Genetic locus on MWF rat chromosome 6 affects kidney damage in response to L-NAME treatment in spontaneously hypertensive rats. *Physiological Genomics* **42**:126–133. DOI: https://doi.org/10.1152/physiolgenomics.00036.2010, PMID: 20388842

Schulz A, Kreutz R. 2012. Mapping genetic determinants of kidney damage in rat models. *Hypertension Research* **35**:675–694. DOI: https://doi.org/10.1038/hr.2012.77, PMID: 22648060

Tajima F. 1989. Statistical method for testing the neutral mutation hypothesis by DNA polymorphism. *Genetics* **123**:585–595. PMID: 2513255

TaKaRa. 2018. *Primer Design Tool for in-Fusion HD Cloning Kit*. http://www.clontech.com/US/Support/xxclt_onlineToolsLoad.jsp?citemId=https://www.takara-bio.co.jp/infusion_primer/infusion_primer_form.php&section=162608&xxheight=1800

Teumer A, Tin A, Sorice R, Gorski M, Yeo NC, Chu AY, Li M, Li Y, Mijatovic V, Ko YA, Taliun D, Luciani A, Chen MH, Yang Q, Foster MC, Olden M, Hiraki LT, Tayo BO, Fuchsberger C, Dieffenbach AK, et al. 2016. Genome-wide association studies identify genetic loci associated with albuminuria in diabetes. *Diabetes* **65**:803–817. DOI: https://doi.org/10.2337/db15-1313, PMID: 26631737

The Human Protein Atlas. 2019. Tmem63c. http://www.proteinatlas.org/ENSG00000165548-TMEM63C/tissue/kidney [Accessed February 28, 2019].

Trapnell C, Pachter L, Salzberg SL. 2009. TopHat: discovering splice junctions with RNA-Seq. *Bioinformatics* **25**:1105–1111. DOI: https://doi.org/10.1093/bioinformatics/btp120, PMID: 19289445

Trapnell C, Williams BA, Pertea G, Mortazavi A, Kwan G, van Baren MJ, Salzberg SL, Wold BJ, Pachter L. 2010. Transcript assembly and quantification by RNA-Seq reveals unannotated transcripts and isoform switching during cell differentiation. *Nature Biotechnology* **28**:511–515. DOI: https://doi.org/10.1038/nbt.1621, PMID: 20436464

Uhlén M, Fagerberg L, Hallström BM, Lindskog C, Oksvold P, Mardinoglu A, Sivertsson Å, Kampf C, Sjöstedt E, Asplund A, Olsson I, Edlund K, Lundberg E, Navani S, Szigyarto CA, Odeberg J, Djureinovic D, Takanen JO, Hober S, Alm T, et al. 2015. Proteomics. Tissue-based map of the human proteome. *Science* **347**:1260419. DOI: https://doi.org/10.1126/science.1260419, PMID: 25613900

Van der Auwera GA, Carneiro MO, Hartl C, Poplin R, Angel Gdel, Levy-Moonshine A, Jordan T, Shakir K, Roazen D, Thibault J, Banks E, Garimella KV, Altshuler D, Gabriel S, DePristo MA, DePristo MA. 2013. From FastQ data to High-Confidence variant calls: the genome analysis toolkit best practices pipeline. *Current Protocols in Bioinformatics*:11.10.1–11.1011. DOI: https://doi.org/10.1002/0471250953.bi1110s43

van Es N, Schulz A, Ijpelaar D, van der Wal A, Kuhn K, Schütten S, Kossmehl P, Nyengaard JR, de Heer E, Kreutz R. 2011. Elimination of severe albuminuria in aging hypertensive rats by exchange of 2 chromosomes in double-consomic rats. *Hypertension* **58**:219–224. DOI: https://doi.org/10.1161/HYPERTENSIONAHA.111.170621, PMID: 21632471

Wang X, Garrett MR. 2017. Nephron number, hypertension, and CKD: physiological and genetic insight from humans and animal models. *Physiological Genomics* **49**:180–192. DOI: https://doi.org/10.1152/physiolgenomics.00098.2016, PMID: 28130427

Warren HR, Evangelou E, Cabrera CP, Gao H, Ren M, Mifsud B, Ntalla I, Surendran P, Liu C, Cook JP, Kraja AT, Drenos F, Loh M, Verweij N, Marten J, Karaman I, Lepe MP, O'Reilly PF, Knight J, Snieder H, et al. 2017. Genome-wide association analysis identifies novel blood pressure loci and offers biological insights into cardiovascular risk. *Nature Genetics* **49**:403–415. DOI: https://doi.org/10.1038/ng.3768, PMID: 28135244

Wernerson A, Duner F, Pettersson E, Widholm SM, Berg U, Ruotsalainen V, Soderberg M. 2003. Altered ultrastructural distribution of nephrin in minimal change nephrotic syndrome. *nephrology, dialysis. Transplantation* **18**:70–76.

Wieder N, Greka A. 2016. Calcium, TRPC channels, and regulation of the actin cytoskeleton in podocytes: towards a future of targeted therapies. *Pediatric Nephrology* **31**:1047–1054. DOI: https://doi.org/10.1007/s00467-015-3224-1, PMID: 26490951

Wrzesiński T, Szelag M, Cieślikowski WA, Ida A, Giles R, Zodro E, Szumska J, Poźniak J, Kwias Z, Bluyssen HA, Wesoly J. 2015. Expression of pre-selected TMEMs with predicted ER localization as potential classifiers of ccRCC tumors. *BMC Cancer* **15**:518. DOI: https://doi.org/10.1186/s12885-015-1530-4, PMID: 26169495

Yates A, Akanni W, Amode MR, Barrell D, Billis K, Carvalho-Silva D, Cummins C, Clapham P, Fitzgerald S, Gil L, Girón CG, Gordon L, Hourlier T, Hunt SE, Janacek SH, Johnson N, Juettemann T, Keenan S, Lavidas I, Martin FJ, et al. 2016. Ensembl 2016. *Nucleic Acids Research* **44**:D710–D716. DOI: https://doi.org/10.1093/nar/gkv1157, PMID: 26687719

Yeo NC, O'Meara CC, Bonomo JA, Veth KN, Tomar R, Flister MJ, Drummond IA, Bowden DW, Freedman BI, Lazar J, Link BA, Jacob HJ. 2015. Shroom3 contributes to the maintenance of the glomerular filtration barrier integrity. *Genome Research* **25**:57–65. DOI: https://doi.org/10.1101/gr.182881.114, PMID: 25273069

Yu H, Artomov M, Brähler S, Stander MC, Shamsan G, Sampson MG, White JM, Kretzler M, Miner JH, Jain S, Winkler CA, Mitra RD, Kopp JB, Daly MJ, Shaw AS. 2016. A role for genetic susceptibility in sporadic focal segmental glomerulosclerosis. *Journal of Clinical Investigation* **126**:1067–1078. DOI: https://doi.org/10.1172/JCI82592, PMID: 26901816

Zhao X, Yan X, Liu Y, Zhang P, Ni X. 2016. Co-expression of mouse TMEM63A, TMEM63B and TMEM63C confers hyperosmolarity activated ion currents in HEK293 cells. *Cell Biochemistry and Function* **34**:238–241. DOI: https://doi.org/10.1002/cbf.3185, PMID: 27045885

JJ

Zhou W, Hildebrandt F. 2012. Inducible podocyte injury and proteinuria in transgenic zebrafish. *Journal of the American Society of Nephrology* **23**:1039–1047. DOI: https://doi.org/10.1681/ASN.2011080776, PMID: 22440901

KK

eLIFE elifesciences.org

RESEARCH ARTICLE

Figures and figure supplements

Analysis of the genomic architecture of a complex trait locus in hypertensive rat models links *Tmem63c* to kidney damage

Angela Schulz *et al*

LL

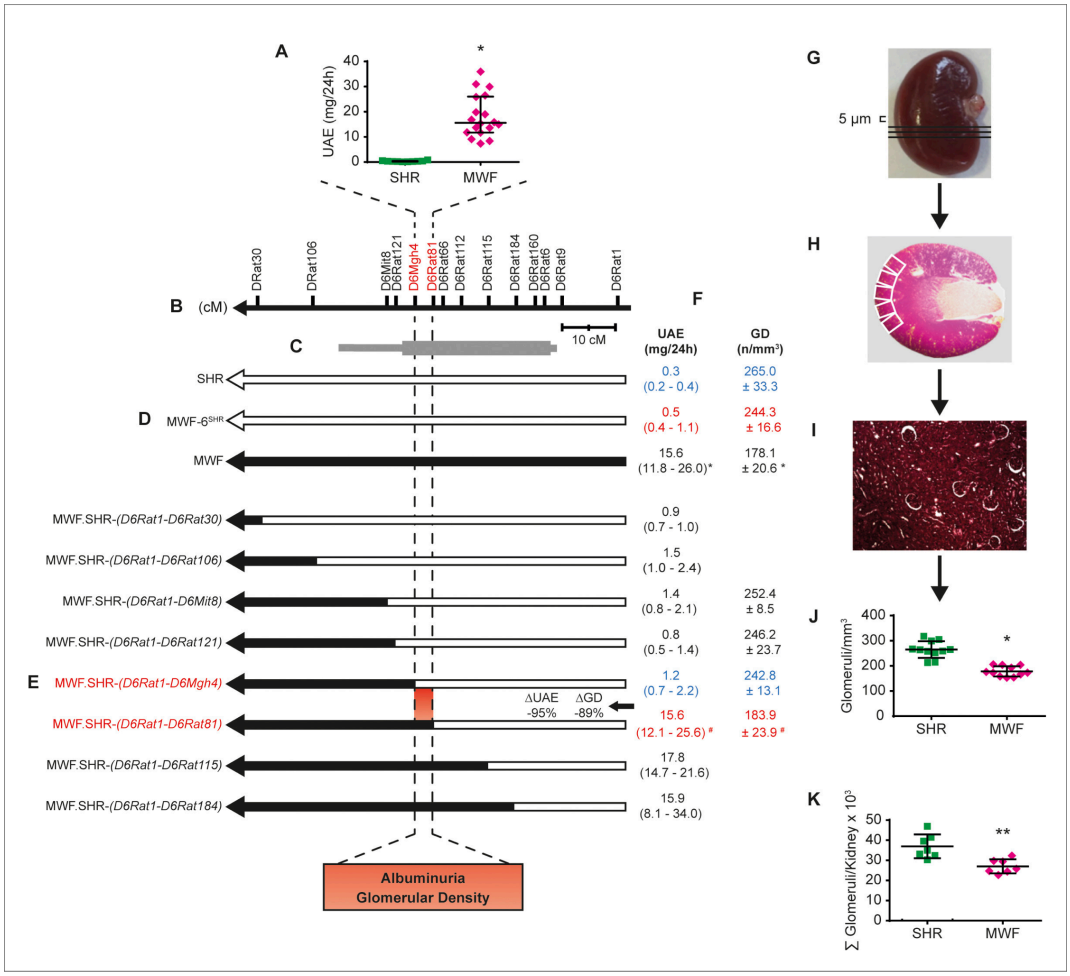

Figure 1. Congenic substitution mapping of the albuminuria and nephron deficit QTL on rat chromosome 6. (**A**) Urinary albumin excretion (UAE) in Munich Wistar Frömter (MWF) and spontaneously hypertensive rats (SHR) at 8 weeks of age. MWF (n = 18); SHR (n = 10); values plotted: median ±interquartile range (IQR); Mann-Whitney U test; *p<0.0001. (**B**) Genetic map of RNO6 with genetic markers and distance in centi Morgan (cM). (**C**) 1-LOD (thick bar) and 2-LOD (thin bar) confidence intervals for placement of the albuminuria QTL by linkage mapping. (**D**) The chromosomal fragment for the MWF (black) and SHR (white) genome are indicated for the MWF (n = 18/11[§]), consomic MWF-6^{SHR} (n = 19/11[§]), and SHR (n = 10/11[§]) strains. (**E–F**) The chromosomal fragment for congenic strains designated as MWF.SHR-(*D6Rat1-D6Rat184*) (n = 17/0[§]), MWF.SHR-(*D6Rat1-D6Rat115*) (n = 10/0[§]), MWF.SHR-(*D6Rat1-D6Rat81*) (n = 25/11[§]), MWF.SHR-(*D6Rat1-D6Mgh4*) (n = 24/11[§]), MWF.SHR-(*D6Rat1-D6Rat121*) (n = 29/6[§]), MWF.SHR-(*D6Rat1-D6Mit8*) (n = 18/6[§]), MWF.SHR-(*D6Rat1-D6Rat106*) (n = 10/0[§]), and MWF.SHR-(*D6Rat1-D6Rat30*) (n = 10/0[§]) (**E**). Corresponding phenotypes for UAE and glomerular density (GD) (**F**). Red values indicate disease phenotypes and blue values an amelioration of phenotypes for informative strains. [§] n is presented for the phenotypes in the following order UAE/GD; values shown for UAE: median ±IQR, Kruskall-Wallis test with Dunn's multiple comparisons test; *p<0.0001; values shown for GD: mean ±SD; one-way ANOVA with post hoc Bonferroni's multiple comparisons test and Mann-Whitney U test; *p<0.0001 vs. SHR, MWF-6^{SHR}, MWF.SHR-(*D6Rat1-D6Mgh4*), respectively; [#]p<0.0001 vs. MWF.SHR-(*D6Rat1-D6Mgh4*), respectively; [##]p=0.029 vs. MWF.SHR-(*D6Rat1-D6Rat30*). (**G–K**) Evaluation of nephron deficit in MWF and SHR rats by determination of GD. Right kidneys at 4 weeks of age were cut into 5 µm thick histological sections (**G**). For evaluation of glomerular diameter and glomerular number adjacent pictures were taken for

Figure 1 continued on next page

Figure 1 continued

each periodic acid-Schiff (PAS) stained histological section (white rectangles) (**H**). Calculation of GD (10x magnification) (**I**). Direct comparison of GD evaluation (**J**) vs. total glomerular number as previously estimated by the physical fractionator method (**K**). Total glomerular number (n = 7 each); GD (n = 11 each); values plotted: mean ±SD; two-tailed student's t-test; *p<0.0001 vs. SHR; **p=0.0024 vs. SHR.

DOI: https://doi.org/10.7554/eLife.42068.003

NN

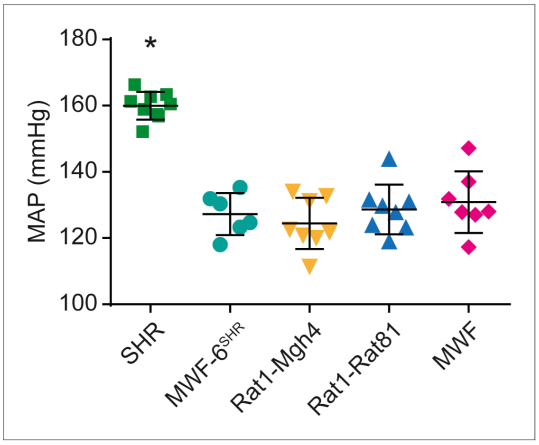

Figure 2. Mean arterial blood pressure (MAP) in consomic and congenic rat strains. Measurement of MAP is shown for SHR (n = 9), MWF-6^{SHR} (n = 6), congenic MWF.SHR-(*D6Rat1-D6Mgh4*) (Rat1-Mgh4, n = 8) and congenic MWF.SHR-(*D6Rat1-D6Rat81*) (Rat1-Rat81, n = 8) and MWF (n = 7) at week 14; values plotted: mean ±SD; one-way ANOVA with Bonferroni's post hoc analysis; *p<0.0001 vs. other strains, respectively.
DOI: https://doi.org/10.7554/eLife.42068.006

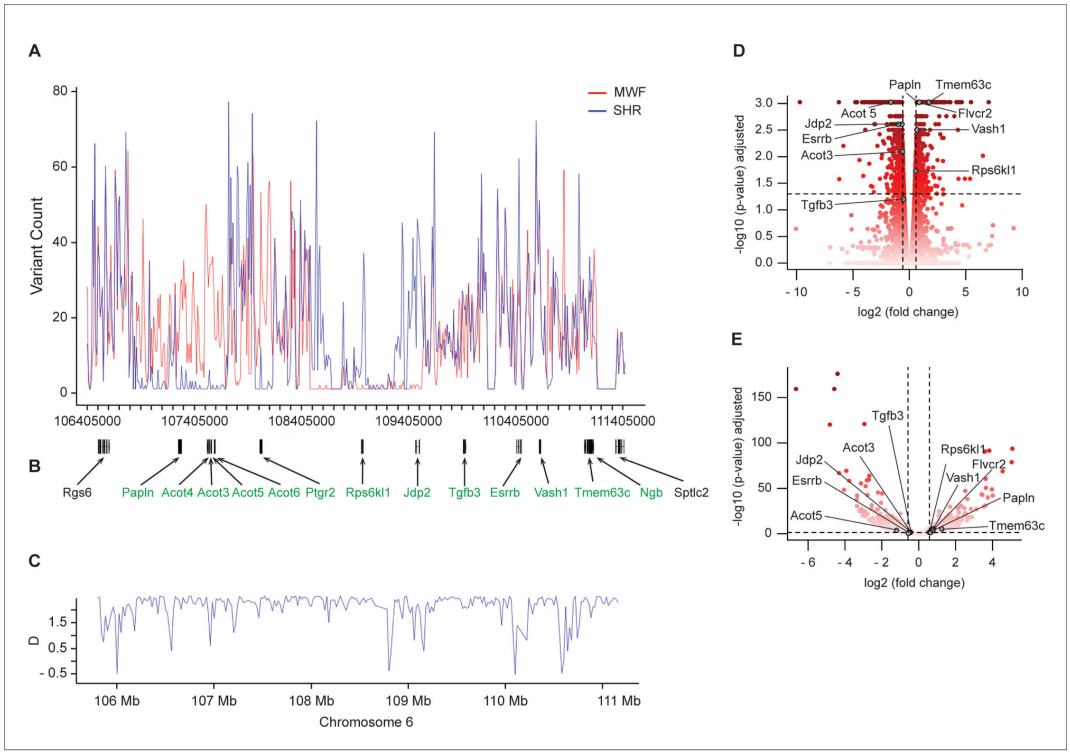

Figure 3. Next-generation sequencing (NGS) analysis of the kidney damage region on rat chromosome 6 and RNA sequencing (RNA-Seq) analysis in isolated glomeruli. (**A–B**) DNA sequencing (DNA-Seq) analysis revealed the numbers of DNA variants in comparison to the reference genome across the sequenced region for the Munich Wistar Frömter (MWF) and spontaneously hypertensive rat (SHR) strains (n = 3, each) (**A**). The physical map between nucleotide position 106,405,000 and 111,405,000 is shown together with positions of potential candidate genes (in green) (**B**); in addition, the two genes at the 5'-position and 3'-position of the candidate region are visualized in black. (**C**) The Tajima's D variation across the sequenced region. (**D–E**) Volcano plots illustrating the differential expression results (MWF vs. SHR) in RNA-Seq analysis in isolated glomeruli using the Cuffdiff (**D**) and DESeq2 (**E**) analysis tools. For each gene, the log10 transformed differential expression *P*-value adjusted for false discovery rate is plotted against the log2 transformed expression fold change. The color gradient refers to the P-values given on the y-axis. The applied significance threshold of adjusted p-value<0.05 is indicated as dashed horizontal line. Dashed vertical lines indicate fold changes > 1.5. Genes of interest are highlighted in grey and are annotated with gene symbols. (See ***Figure 3—figure supplement 1***).

DOI: https://doi.org/10.7554/eLife.42068.008

PP

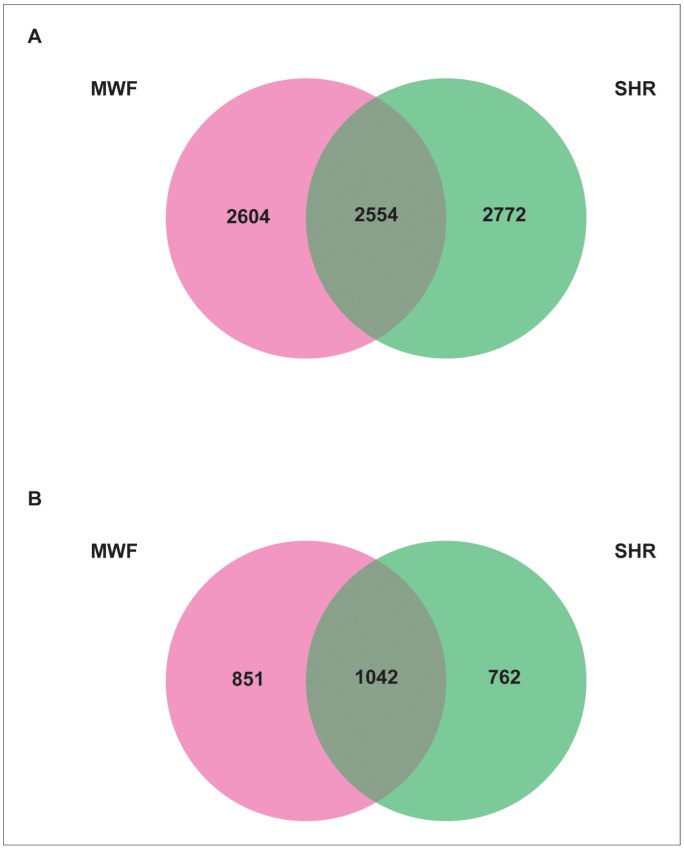

Figure 3—figure supplement 1. Venn diagram of NGS analysis. (**A–B**) The number of SNPs (**A**) and small insertions and deletions (INDELs) (**B**) are given in the Munich Wistar Frömter (MWF) and spontaneously hypertensive rat (SHR) strains (*n* = 3, each) in comparison to the reference genome. The numbers in the intersection refer to the variants that are common between MWF and SHR.
DOI: https://doi.org/10.7554/eLife.42068.009

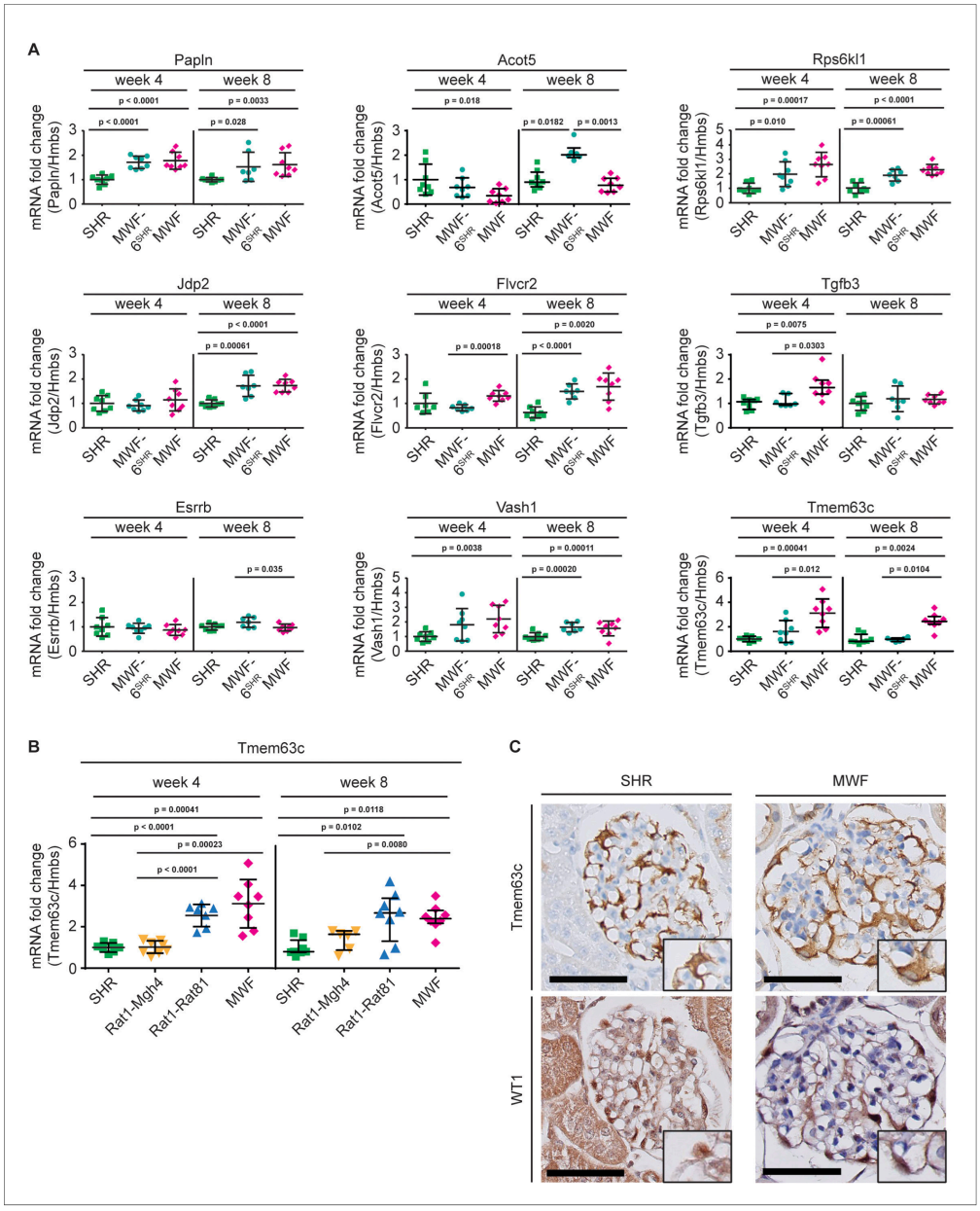

Figure 4. Validation of differentially expressed genes in isolated glomeruli by quantitative real-time PCR (qPCR) analysis. (**A**) qPCR analysis showed no consistent differential expression for eight genes from overall 10 genes identified with differential expression in RNA sequencing (RNA-Seq) analysis

Figure 4 continued on next page

Figure 4 continued

(***Table 3***) between parental Munich Wistar Frömter (MWF), spontaneously hypertensive rats (SHR), and consomic MWF-6^{SHR} during the crucial time window for onset of albuminuria between weeks 4 and 8. Only transmembrane protein 63c (*Tmem63c*) demonstrated differential mRNA expression at both time points. Acyl-CoA thioesterase 3 (*Acot3*) (***Table 3***) showed very low mRNA expression in qPCR analysis precluding quantitative analysis. Consequently, *Acot3* and the genes shown were excluded from and *Tmem63c* was included for further functional analysis. Rats per strain (n = 7–8, each); values for *Acot5* (week 8),*Tgfb3* (week 4) and *Tmem63c* (week 8) are plotted as median ±IQR, while the rest of data are plotted as mean ±SD; data for *Acot5* (week 8), *Tgfb3* (week 4) and *Tmem63c* (week 8) were analyzed using Kruskal-Wallis test with Dunn's post-hoc analysis and Mann-Whitney U test, while the rest of data was analyzed by one-way ANOVA with Bonferroni's post hoc analysis and Mann-Whitney U test. (**B**) mRNA expression analysis for *Tmem63c* in isolated glomeruli by qPCR analysis is shown for MWF, SHR, congenic MWF.SHR-(*D6Rat1-D6Mgh4*) (Rat1-Mgh4) and congenic MWF.SHR-(*D6Rat1-D6Rat81*) (Rat1-Rat81), at week 4 and week 8. Rats per strain (n = 6–8, each); data for week 8 are plotted as median ±IQR and analyzed using Kruskal-Wallis test with Dunn's post hoc analysis and Mann-Whitney U test; the other data are plotted as mean ±SD and analyzed by one-way ANOVA with Bonferroni's post hoc analysis and Mann-Whitney U test (**C**) Representative immunohistochemical stainings of TMEM63C and Wilms tumor 1 (WT1) on kidney sections from SHR and MWF at 8 weeks of age; the insert indicates expression in podocytes. Scale bar = 50 µm. Quantitative analysis of TMEM63C intensity in podocytes using one-way ANOVA revealed lower intensity in MWF (n = 7) vs. SHR (n = 6) at 8 weeks (p=0.0032).

DOI: https://doi.org/10.7554/eLife.42068.013

SS

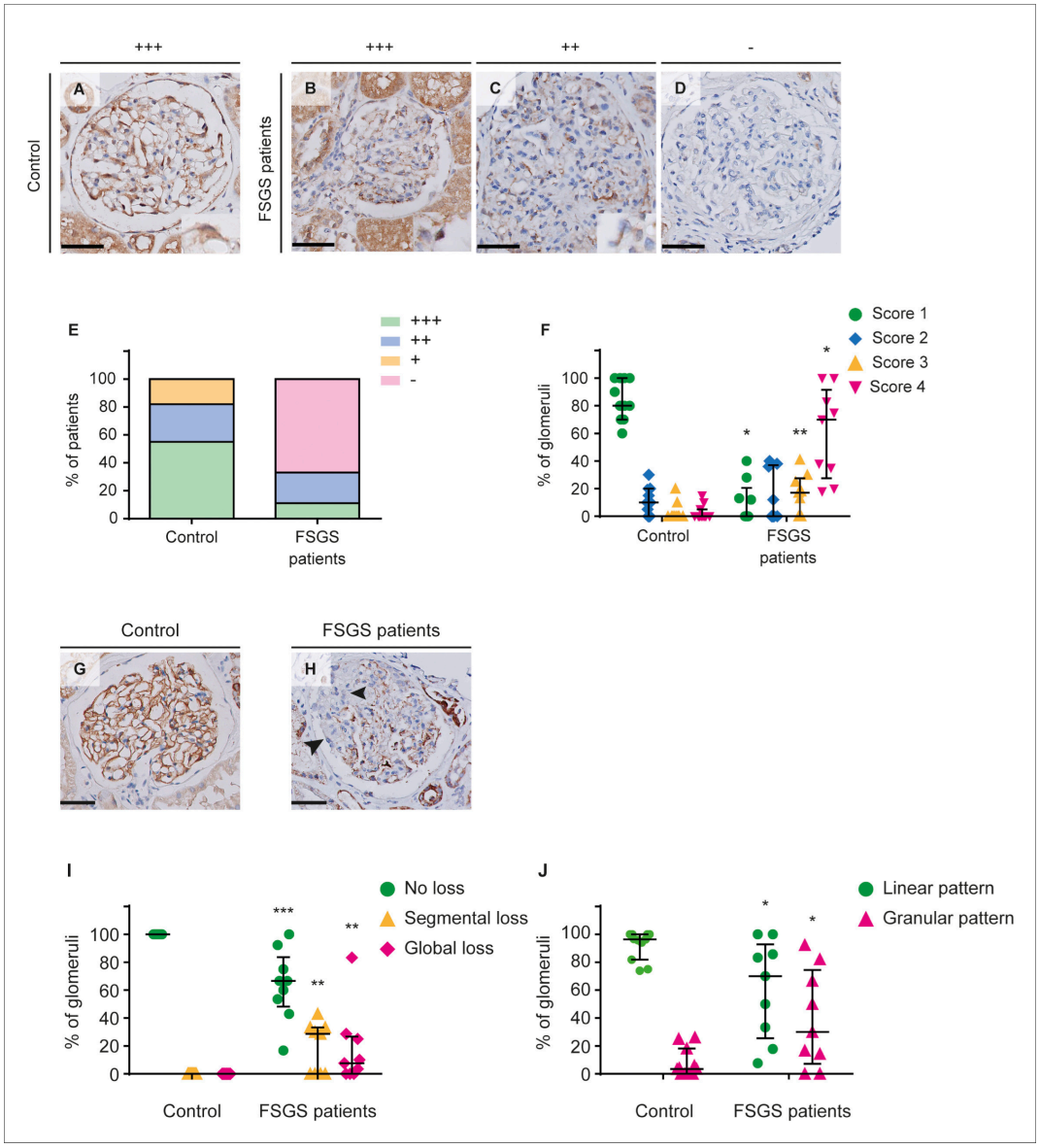

Figure 5. Transmembrane protein 63c (TMEM63C) protein and Nephrin expression deficiency in patients with focal segmental glomerulosclerosis (FSGS). (**A–D**) High-intensity TMEM63C staining in a glomerulus of a healthy human control subject (**A**) and representative glomeruli of FSGS patients with high (+++) (**B**), intermediate (+) TMEM63C staining intensity (**C**), or loss (-) of TMEM63C protein expression (**D**). The inserts indicate TMEM63C-positive podocytes. Scale bar = 50 µm. (**E**) Scoring of the TMEM63C staining intensity in controls (n = 11) and FSGS patients (n = 9). Percentage of

Figure 5 continued on next page

TT

Figure 5 continued

cases with high intensity (green); intermediate intensity (blue); low intensity (yellow) and no TMEM63C staining (magenta). Linear-by-Linear association; p=0.005. (**F**) Scoring of the percentage of TMEM63C positivity in glomeruli. Green: no loss; blue:<25% loss; yellow: 25–50% loss; magenta:>50% loss of TMEM63C expression. Controls (n = 11) and FSGS patients (n = 9); values plotted: median ±IQR; Mann-Whitney U test; *p<0.0001 vs. control; **p=0.021 vs. control. (**G–J**) Linear nephrin staining in a glomerulus of a healthy human control subject (**G**) and segmental loss of nephrin staining in a glomerulus of a patient with FSGS (**H**), indicated by arrowheads. Nephrin expression was significantly reduced in patients with FSGS compared to healthy controls (**I**). Moreover, we observed a shift from a normal linear staining pattern, following the glomerular capillary wall, to a granular staining pattern (**H and J**). values plotted: median ±IQR; Mann-Whitney U test; *p=0.05 vs. control; **p<*0.01* vs. control; ***p<0.001 vs. controls.

DOI: https://doi.org/10.7554/eLife.42068.017

UU

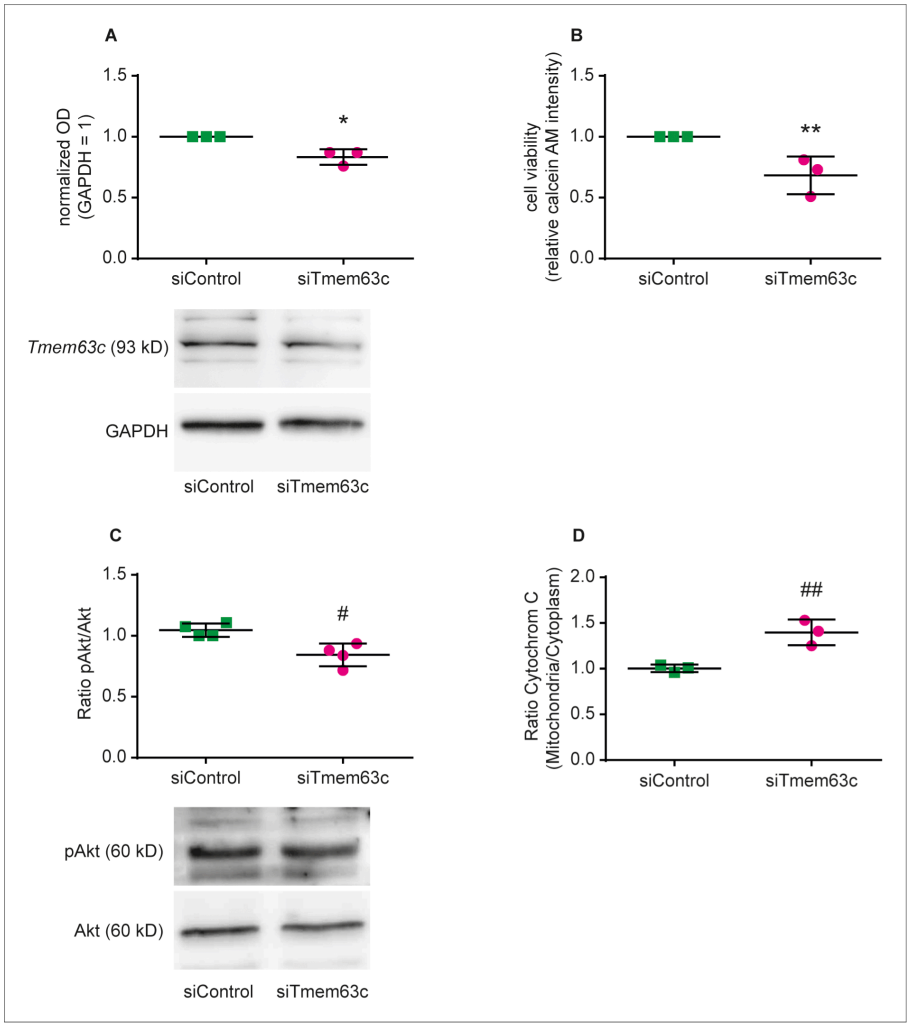

Figure 6. Functional role of TMEM63C in human podocytes (hPC) in vitro. Shown is the impact of siRNA-mediated inhibition of TMEM63C (siTMEM63C) or treatment of hPC with a corresponding nonsense negative control (siControl). (**A**) TMEM63C protein expression normalized against GAPDH as a loading control (*p=0.011). Shown is a representative Western blot. (**B**) Cell viability determined via measurement of calcein acetoxymethyl (AM) fluorescence intensity in hPC (**p=0.024). (**C**) Phosphorylation state of protein kinase B (pAKT) normalized against the expression of total AKT (AKT) ($^{\#}$p=0.0094). Shown is a representative Western blot, GAPDH is used as a loading control. (**D**) Pro-apoptotic cytochrome C transition from mitochondria to the cytoplasm of hPC ($^{\#\#}$p=0.0096). The mean ±SD of at least three independent experiments is shown, respectively. Two-tailed Student's *t*-test was performed for all experiments.

DOI: https://doi.org/10.7554/eLife.42068.020

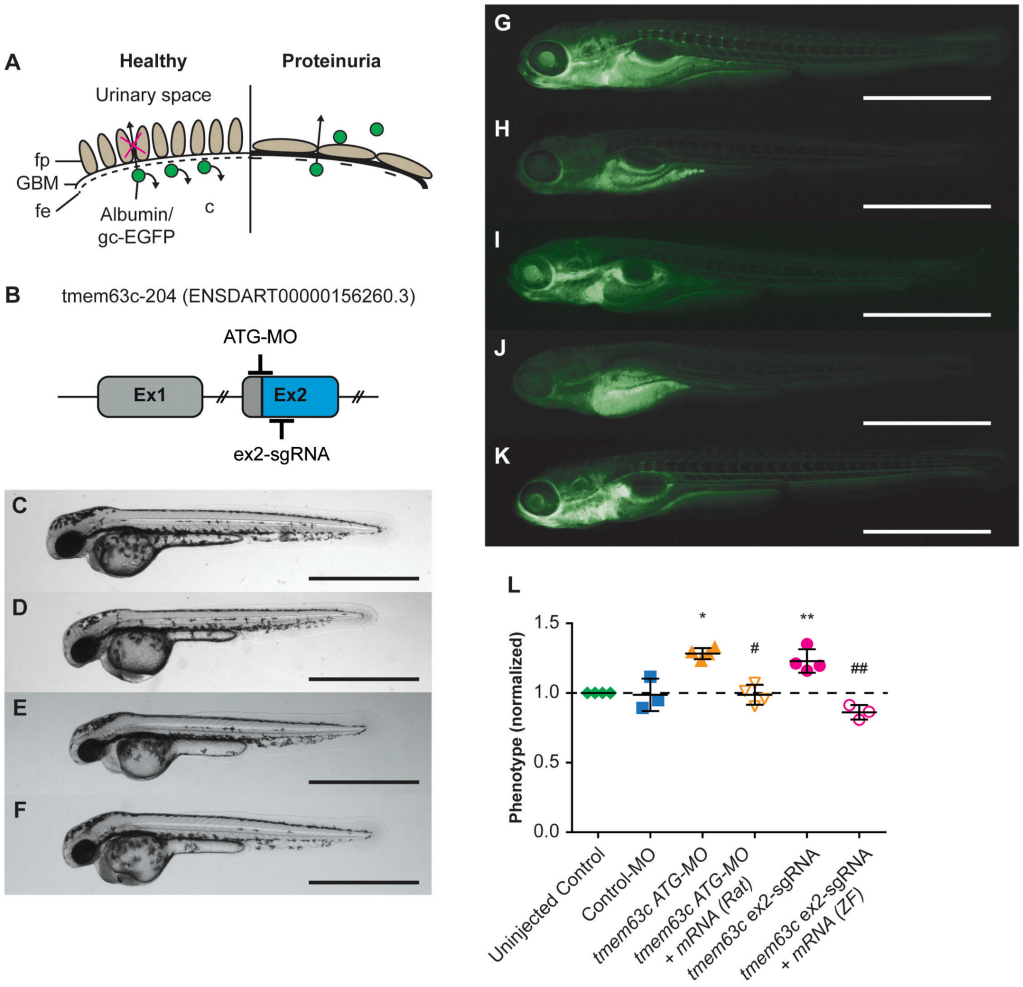

Figure 7. Functional assessment of the glomerular filtration barrier (GFB) after loss of transmembrane protein 63c (*tmem63c*) in zebrafish. (**A**) Scheme of the GFB in healthy and albuminuric zebrafish embryos. Green fluorescent protein (gc-EGFP) represents an albumin surrogate and is filtrated after impairment of the GFB. fe, fenestrated endothelium; fp, foot processes of podocytes; GBM, glomerular basement membrane. (**B**) Schematic of *tmem63c* showing the target regions in Exon 2 (ex2) used for Morpholino (MO)- and CRISPR/Cas9-mediated somatic mutagenesis. (**C–F**) Bright field view of wildtype embryos at 48 hr post-fertilization (hpf) in uninjected controls (**C**), ATG-MO injected (**D**), 159.6 ng/µl ex2-sgRNA injected (**E**), and 250 ng/µl ex2-sgRNA injected embryos (**F**). Scale bar = 1 mm. (**G–K**) Fluorescence microscopy of *Tg[fabp10a:gc-EGFP]* embryos at 120 hpf. Uninjected control with clearly visible gc-EGFP fluorescence in the trunk vasculature ('fluorescent') (**G**). *tmem63c* ATG-MO-injected embryo with partial or a complete loss of trunk fluorescence ('deficient-fluorescent') (**H**) and *tmem63c* ATG-MO +*Tmem63c* mRNA (Rat) co-injected embryo (**I**) showing rescue of the phenotype. *Tmem63c* ex2-sgRNA-injected embryo with partial or a complete loss of trunk fluorescence ('deficient-fluorescent') (**J**) and *tmem63c* ex2-sgRNA + *tmem63c* mRNA (ZF) co-injected embryo (**K**) showing rescue of the phenotype. Scale bar = 1 mm. (**L**) Analysis of gc-EGFP in the trunk vasculature. Shown are embryos categorized as 'deficient-fluorescent' (df), see Materials and method section and ***Figure 7—figure supplement 2*** for

Figure 7 continued on next page

Figure 7 continued

details. Experimental groups are normalized to the corresponding uninjected control group per experiment. Uninjected Control (*n* = 1198); Control-MO (*n* = 189); *tmem63c* ATG-MO (*n* = 227); tmem63c ATG-MO +Tmem63c mRNA (Rat) (*n* = 230); *tmem63c* ex2-sgRNA (*n* = 371); *tmem63c* ex2-sgRNA + *tmem63c* mRNA (ZF) (*n* = 126); One-way ANOVA with Bonferroni's multiple comparisons test. Values plottet: mean ±SD, dashed line at y = 1 indicates the uninjected control level; *p=0.0002 vs. uninjected Control, $^{\#}$p<0.0001 vs. *tmem63c* ATG-MO. **p=0.0014 vs. uninjected Control, $^{\#\#}$p<0.0001 vs. *tmem63c* ex2-sgRNA. Data points in the graph represent the ratio per independent experiment, %(Uninjected Control (df)) / % (experimental group (df)), N ≥ 3. (See ***Figure 7—figure supplement 1*** and ***Figure 7—figure supplement 2***).

DOI: https://doi.org/10.7554/eLife.42068.022

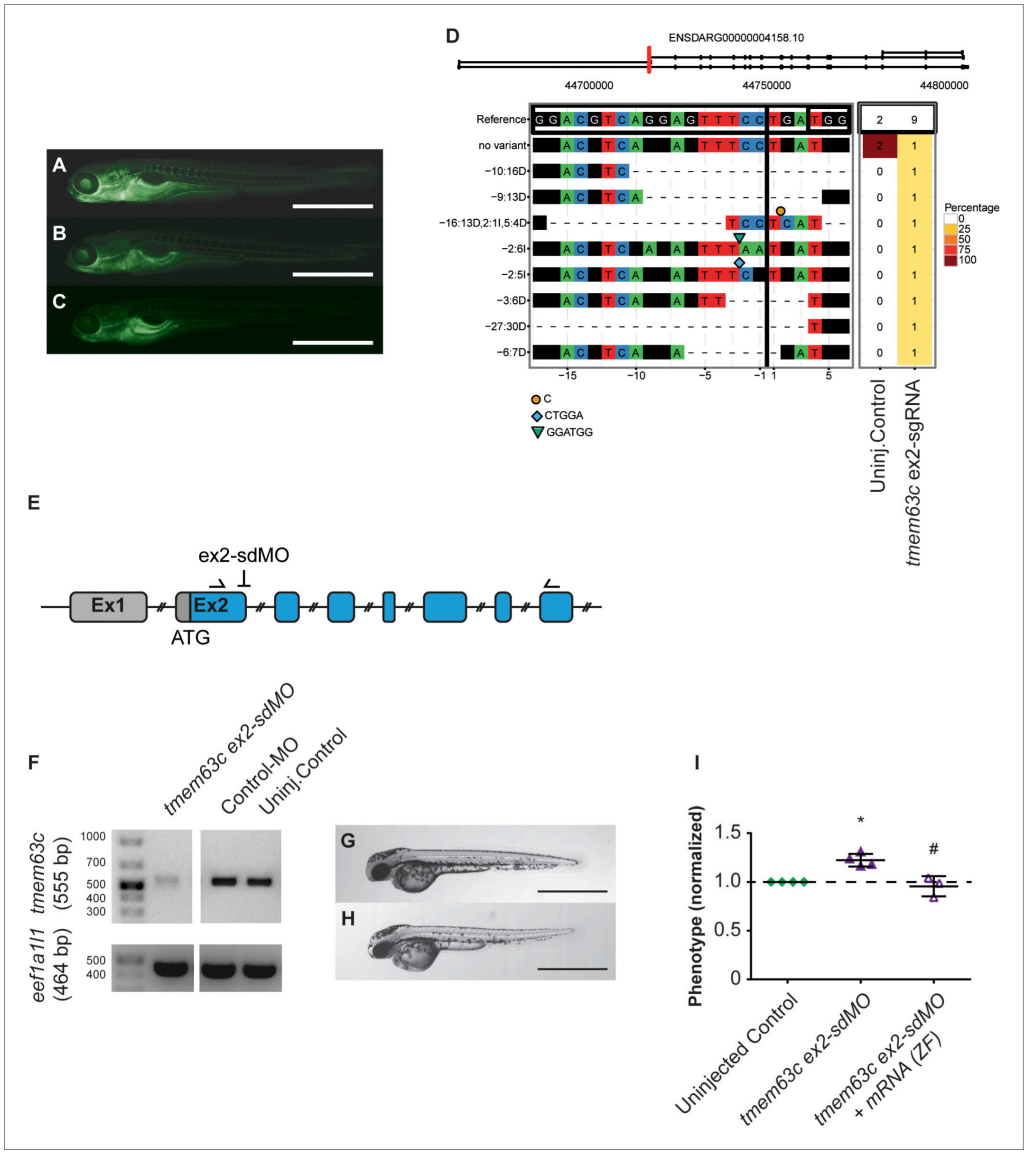

Figure 7—figure supplement 1. Functional assessment of the glomerular filtration barrier (GFB) in *Tg[fabp10a:gc-EGFP]* zebrafish embryos. (**A–C**) Representative fluorescence microscopy pictures of *Tg[fabp10a:gc-EGFP]* zebrafish embryos categorized as 'fluorescent' or 'deficient-fluorescent', respectively to assess functionality of the GBM. An embryo of the 'fluorescent group' (**A**) shows clearly visible fluorescence in the trunk vasculature. (**B–C**) Embryos of different fluorescence intensities both characterized as 'deficient-fluorescent' with marked decrease in the fluorescence in the trunk vasculature. (**D**) Plot of mutagenesis output in transmembrane protein 63 c (*tmem63c*) crispants as created by CrispR Variants Lite analysis of the sequencing data from individual embryos. The gene schematic at the top illustrates the location of the sgRNA in red with respect to all overlapping

Figure 7—figure supplement 1 continued on next page

Figure 7—figure supplement 1 continued

transcripts on the reference strand in the Ensembl database (***Yates et al., 2016***). The panel below shows the pairwise alignment of each variant to the reference genome. The 20 bp sgRNA and the 3 bp PAM sequences are indicated in boxes in the reference sequence, the cutting site is indicated by a vertical line. Deletions are given by "- "and insertions by symbols with the inserted sequences shown underneath the plot with respect to the cutting site. The right panel demonstrates the frequency of the variants in the embryos analyzed with colors corresponding to variant frequencies as shown. The header displays the total number of embryos sequenced. (**E–I**) Functional assessment of the GFB after *tmem63c*-knockdown using *tmem63c* ex2-sdMO. (**E**) Schematic of *tmem63c* showing the region in Exon 2 (ex2) targeted by ex2-sdMO. Arrows indicate the positions of primers used for RT-PCR. (**F**) RT-PCR showing *tmem63c*-deficiency after injection of *tmem63c* ex2-sdMO, but not in Control-MO injected embryos or uninjected Controls, respectively. Eukaryotic translation elongation factor 1 alpha 1, like 1 (*eef1a1l1*) is used as a loading control. (**F–G**) Bright-field view of wildtype embryos at 48 hr post-fertilization (hpf) in uninjected controls (**F**) and *tmem63c* ex2-sdMO injected embryos (**G**). Scale bar = 1 mm. (**H**) Analysis of gc-EGFP in the trunk vasculature. Shown are embryos categorized as 'deficient-fluorescent' (df). Experimental groups are normalized to the corresponding uninjected control group per experiment. Uninjected Control (n = 457); *tmem63c* ex2-sdMO (n = 297); *tmem63c* ex2-sdMO + *tmem63* c mRNA (ZF) (n = 246); One-way ANOVA with Bonferroni's multiple comparisons test. Values plottet: mean ±SD, dashed line at y = 1 indicates the uninjected control level; *p=0.0039 vs. uninjected Control, # p=0.0021 vs. *tmem63c* ex2-sdMO. ZF = zebrafish. Data points in the graph represent the ratio per independent experiment, %(Uninjected Control (df)) / %(experimental group (df)), $N \geq 3$.

DOI: https://doi.org/10.7554/eLife.42068.023

ZZ

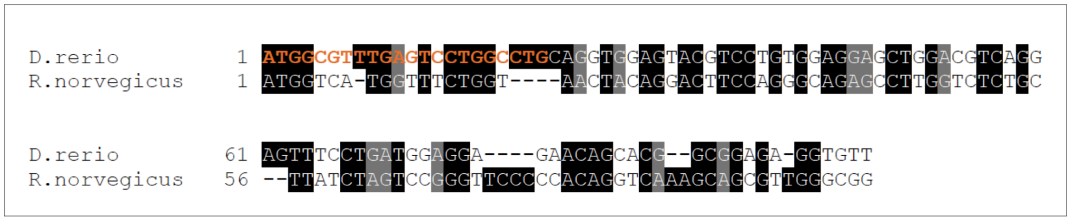

Figure 7—figure supplement 2. Excerpt from sequence alignment of *tmem63c* mRNA zebrafish (NM_001159836) vs *Tmem63c* mRNA rat (NM_001108045.1). Sequence alignment shows the first 100 bp of *tmem63c* mRNA zebrafish vs. *Tmem63c* mRNA rat following ATG. Orange bases indicate the zebrafish sequence following ATG targeted by *tmem63c* ATG-MO to prove no targeting of rat mRNA by the used *tmem63c* ATG-MO. Sequence identity is 65,82% (Clustal 2.1) for mRNA sequences or 53,52% (Clustal 2.1) for protein sequences, respectively. D., Danio; R., Rattus.
DOI: https://doi.org/10.7554/eLife.42068.025

AAA

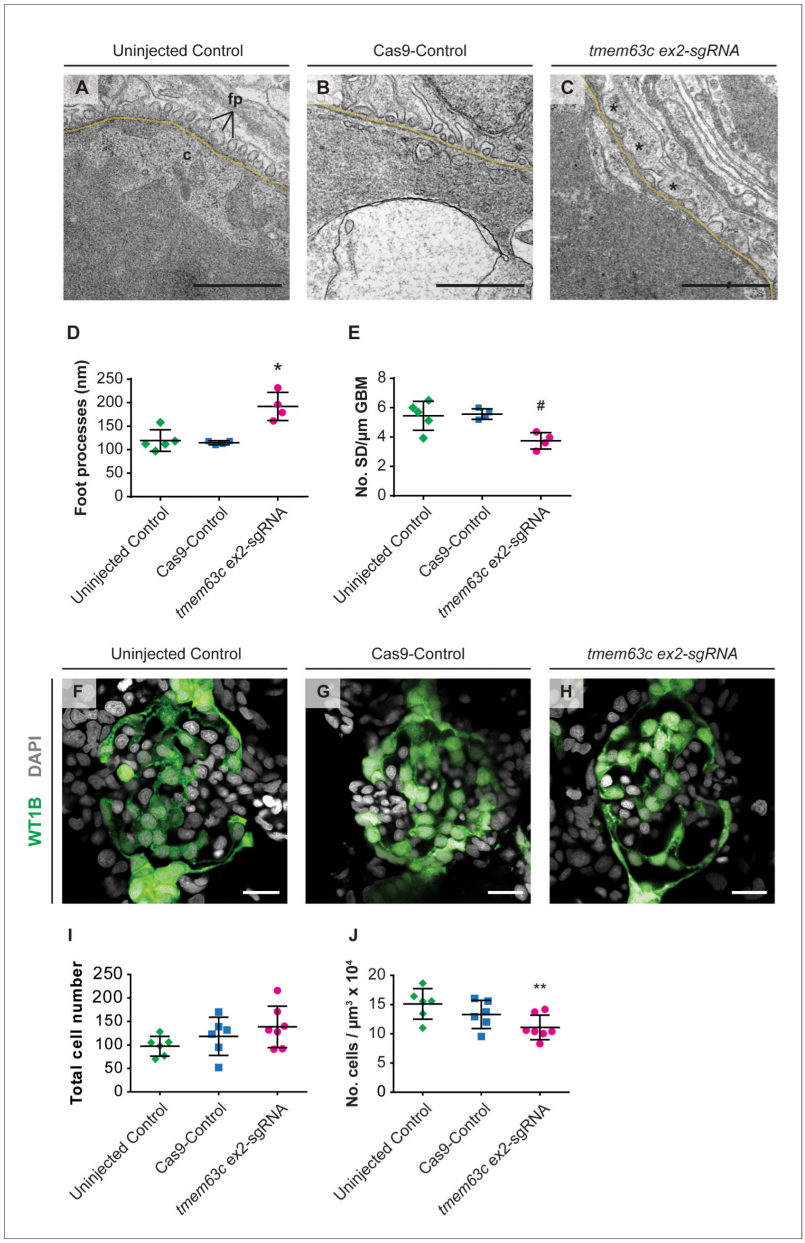

Figure 8. Ultrastructural and morphological analysis of glomerular structures after loss of *tmem63c* in zebrafish. (**A–E**) Electron microscopy and quantitative assessment of GFB ultrastructure. Representative electron microscopy pictures of the GFB in uninjected Controls (**A**), Cas9-Controls (**B**) and

Figure 8 continued on next page

Figure 8 continued

after *tmem63c* knockdown (**C**), asterisks indicate effaced podocyte foot processes). Quantitative analysis of podocyte foot process width (**D**) and number of slit diaphragms per µm GBM (**E**). Uninjected Control (n = 5); Cas9-Control (n = 4); *tmem63c* ex2-sgRNA (n = 4); Scale bar = 1 µm; values plottet: mean ±SD; One-way ANOVA with Bonferroni's multiple comparisons test; *p=0.0019 vs. uninjected Control, *p=0.0017 vs Cas9-Control; # p=0.0171 vs. uninjected Control, # p=0.0148 vs. Cas9-Control. (**F–J**) Confocal microscopy and analysis of absolute and relative podocyte cell number in *Tg(wt1b:EGFP)* at 96 hpf. Representative confocal microscopy pictures of glomeruli in uninjected Controls (**F**), Cas9-Controls (**G**) and after *tmem63c* knockdown (**H**). Quantitative analysis of absolute (**I**) and relative (**J**) podocyte cell number. Relative podocyte cell number has been obtained after normalization to the glomerular volume. Uninjected Control (n = 6); Cas9-Control (n = 6); tmem63c ex2-sgRNA (n = 7); Scale bar = 15 µm; values plottet: mean ±SD; One-way ANOVA with Bonferroni's multiple comparisons test; **p=0.0421 vs. uninjected Control.

DOI: https://doi.org/10.7554/eLife.42068.027

CCC

Lebenslauf

Mein Lebenslauf wird aus datenschutzrechtlichen Gründen in der elektronischen Version meiner Arbeit nicht veröffentlicht.

Komplette Publikationsliste

1) Originalarbeiten

Merks AM*, Swinarski M*, Meyer AM, **Müller NV**, Ozcan I, Donat S, Burger A, Gilbert S, Mosimann C, Abdelilah-Seyfried S, Panakova D. Planar cell polarity signalling coordinates heart tube remodelling through tissue-scale polarisation of actomyosin activity. Nat Commun. 2018;9(1):2161. * equal contribution

Schulz A*, **Müller NV***, van de Lest NA, Eisenreich A, Schmidbauer M, Barysenka A, Purfurst B, Sporbert A, Lorenzen T, Meyer AM, Herlan L, Witten A, Ruhle F, Zhou W, de Heer E, Scharpfenecker M, Panakova D, Stoll M**, Kreutz R**. Analysis of the genomic architecture of a complex trait locus in hypertensive rat models links *Tmem63c* to kidney damage. Elife. 2019;8. * equal contribution, ** equal contribution

2) Abstracts-Poster

Nicola Müller, Christian Frätzer, Theodor Lorenzen, Alexander M. Meyer, Daniela Panáková, Reinhold Kreutz, Angela Schulz, „Funktionelle Analysen im Zebrafisch bestätigen *ptgr2* als neues Kandidatengen für die Entwicklung einer Albuminurie und chronischer Nierenerkrankungen“, Kongress der Deutschen Hochdruckliga e.V. DHL , Berlin, veröffentlicht in Med Welt, Vol.6, 2016

3) Abstracts-Vorträge

Nicola Müller, Angela Schulz, Alexander M. Meyer, Monika Stoll, Daniela Panáková, Reinhold Kreutz, “Functional analysis of a novel candidate gene in zebrafish reveals a role of prostaglandins for albuminuria development and hypertensive kidney damage”, Kongress des European Council of Cardiovascular Research, veröffentlicht in High Blood Pressure & Cardiovascular Prevention, 2017

Nicola Müller, Angela Schulz, Daniela Panáková, Reinhold Kreutz, “Loss of *tmem63c*, a novel candidate for albuminuria in hypertension, affects glomerular function and morphology in zebrafish”, Vortrag als Repräsentatin des European Council for Cardiovascular Research beim Kongress der International Society of Hypertension, Peking, 2018

Nicola Müller, Angela Schulz, Monika Stoll, Daniela Panáková, Reinhold Kreutz, “Loss of *transmembrane protein 63c* results in damage of podocytes and glomerular structure supporting its role in hypertension mediated organ damage in the kidney”, Kongress der European Society of Hypertension, Mailand, veröffentlicht in Journal of Hypertension, 2019

Danksagung

Zuallererst danke ich meinem Doktorvater Herrn Professor Reinhold Kreutz für die Überlassung meines Promotionsthemas, seine jederzeit gute Betreuung und Gesprächsbereitschaft und unermüdliche Förderung und Unterstützung meiner Arbeit.

Dr. Daniela Panáková, meiner Betreuerin am Max-Delbrück-Centrum für Molekulare Medizin, danke ich für die herzliche Aufnahme in ihre Arbeitsgruppe zur Durchführung der Zebrafischarbeiten und die stete Betreuung meines Projektes. Ich habe mich am MDC immer willkommen gefühlt und danke besonders für inspirierende wissenschaftliche Diskussionen, ein immer offenes Ohr und allgegenwärtige Motivation und Optimismus, aber auch ehrliches Feedback und angebrachte Kritik.

Meiner Betreuerin Dr. Angela Schulz danke ich für ihre hervorragende Betreuung und unsere immer hilfreichen, motivierenden und aufbauenden Gespräche und Diskussionen auf wissenschaftlicher und privater Ebene.

Der Nachwuchskommission der Charite-Universitätsmedizin Berlin danke ich für die Gewährung des Promotionsabschlussstipendiums und dem mir und meinem Projekt entgegengebrachten Vertrauen.

Ich danke Robby Fechner und Björn Fiege als verantwortliche Tierpfleger der Zebrafischanlage für ihre immer exzellente Pflege der Fische und der Anlage sowie ihre fachliche Unterstützung bei der Zebrafischzucht und -haltung.

Des Weiteren danke ich Dr. Anje Sporbert von der MDC Advanced Light Microscopy-Plattform sowie Dr. Bettina Purfürst und Christina Schiel von der MDC Elektronenmikroskopie-Plattform für ihren großen Einsatz und die methodische Hilfe bei der Etablierung und Durchführung der Konfokal- bzw. Elektronenmikroskopie.

Ein besonderer Dank gilt meinen Kollegen und Freunden der AG Panáková, Anne Merks, Sara Lelek, Laura Bartolini, Kevin Manuel Méndez-Acevedo, Mai Phan, Motahareh Moghtadaei, Kitti D. Csályi, Mariana Guedes-Simões und Ismail Özcan für lebhafte wissenschaftliche und private Diskussionen sowie Rat, Tat, aufbauende Worte und Kaffee mit Milchschaum in allen Lebenslagen. Alexander Meyer danke ich für die methodische Einarbeitung, ständige Unterstützung und kollegiale Zusammenarbeit.

Mein größter Dank gilt meinen Eltern, meinem Bruder und meinem Freund Boris, die nicht nur während der Zeit meiner Doktorarbeit all meine Launen ertragen, mir immer den Rücken gestärkt und mich so oft auf den Boden der Tatsachen zurückgeholt haben.

FFF